# DESIGN AND CONSTRUCTION OF BIOSENSING PLATFORMS FOR THE DETECTION OF BIOMARKERS

**DENG HUIMIN**

*(B. Sc., SICHUAN UNIVERSITY)*

**A THESIS SUBMITTED**

**FOR THE DEGREE OF DOCTOR OF PHILOSOPHY**

**DEPARTMENT OF CHEMISTRY**

**NATIONAL UNIVERSITY OF SINGAPORE**

**2015**

# Declaration

I hereby declare that this thesis is my original work and it has been written by me in its entirety, under the supervision of Assoc. Prof. Gao Zhiqiang, (in the Biosensors and Electroanalytical Laboratory located at S5-02-03), Chemistry Department, National University of Singapore, between August 2011 and April 2015. I have duly acknowledged all the sources of information which have been used in the thesis. This thesis has also not been submitted for any degree in any university previously.

The content of the thesis has been partially published in:

1. H. M. Deng, W. Shen, Z. Q. Gao, *Chemphyschem.* 2013, 14, 2343-2347.
2. H. M. Deng, A. K. L. Teo, Z. Q. Gao, *Sensor. Actuat. B-Chem.* 2014, 191, 522-528.
3. H. M. Deng, X. J. Yang, S. P. X. Yeo, Z. Q. Gao, *Anal. Chem.* 2014, 86, 2117-2123.
4. H. M. Deng, X. J. Yang, Z. Q. Gao, *Analyst* 2015, 140, 3210-3215.
5. X. M. Guo, H. M. Deng, H. Zhou, T. X. Fan, Z. Q. Gao, *Sensor. Actuat. B-Chem.* 2015, 206, 721-727.

| Deng Huimin | Deng Huimin | April, 2015 |
|---|---|---|
| Name | Signature | Date |

# Acknowledgements

First and foremost, I would like to thank my supervisor, Assoc. Prof. Gao Zhiqiang, for his guidance, help, and timely advice during my PhD study. His efficiency, immense knowledge, and critical thinking in scientific research have inspired me a lot. I really appreciate his patience in guiding me on the academic writing and revising my manuscripts.

I would also like to thank the research fellow in our laboratory, Dr. Yang Xinjian, for his useful suggestions on the design of my experiments and the discussion on the experimental results.

I would like to express my gratitude to the honors students Mr. Teo Kay Liang Alan, Ms. Yeo Pei Xing Stephanie, and Ms. Png Si Ying for their cooperation in the final year projects which have been included partially in my thesis. I am also grateful to my other lab mates Ms. Shen Wei, Dr. Li Ying, Dr. Shnamuga Sundaram Komathi, Ms. Ren Yuqian, Ms. Zhang Yanmei, Ms. Guo Xingmei, Mr. Chen Chengbo, and Ms. Guo Yuwenxi for their help.

I really appreciate my family and friends for their support and encouragements. I especially thank my parents, Mr. Deng Xianshun and Mdm. Tan Meirong, for their endless love and being a pillar of strength during my frustration period during my PhD study.

Financial support from National University of Singapore is gratefully acknowledged.

# Table of Contents

# Summary

Biosensors can provide cost-effective, easy-to-use, sensitive and highly accurate detection devices in a variety of research and commercial applications. This thesis focuses on the development of novel biosensing platforms for glucose and deoxyribonucleic acid (DNA) methyltransferase (MTase) activity detection.

Firstly, two different types of mediators are employed to construct highly sensitive and selective electrochemical glucose biosensors with excellent anti-interference characteristics. One is an osmium-bipyridine complex ($Os(bpy)_2$) -based anionic redox polymer (Os-RP), and the other is a novel ruthenium complex-tethered redox polymer (Ru-RP). The biosensing membranes are formed through the co-immobilization of glucose oxidase (GOx) and the mediators on the surfaces of glassy carbon electrodes (GCE) in a simple one-step chemical crosslinking process. Both the fabricated Os-RP/GOx and the Ru-RP/GOx biosensors show excellent electrocatalytic activity toward the oxidation of glucose and exhibit good linear correlations between the oxidation current and the glucose concentration up to 10 mM with a sensitivity of 16.5 and 24.3 $\mu A\ mM^{-1}\ cm^{-2}$, respectively. Moreover, both glucose biosensors display outstanding anti-interference capabilities resulting from the presence of anionic sulfonic acid groups in the backbones of the Os-RP and the ultralow working potential (-0.15 V) of the Ru-RP, respectively. In addition, a novel lamellar-ridge architectured gold (*lamellar ridge*-Au) material is prepared using blue scales of *Morph* butterfly as templates.

Prominent performance in the nonenzymatic detection of glucose using a *lamellar ridge*-Au modified electrode is achieved with a wide linear range from 2 μM to 23 mM with a sensitivity of 29.0 μA $mM^{-1}$ $cm^{-2}$. This is attributed to the synergistic effect of increased surface area and efficient mass transport of the architectured *lamellar ridge*-Au.

Secondly, three types of DNA MTase activity biosensors are established coupling with the methylation sensitive restriction endonuclease. In general, the principle of these biosensors depends on the changes in signal producers bound or labeled to the substrate DNA of MTase, which result from the methylation-cleavage events catalyzed by the MTase and endonuclease. In the first MTase biosensor, a synthetic threading intercalator, N,N'-bis(3-propylimidazole)-1,4,5,8-naphthalene diimide (PIND) functionalized with electrocatalytic redox $Os(bpy)_2Cl^+$ moieties (PIND-Os), which strongly and selectively binds to double-stranded DNA (ds-DNA) and catalyzes the oxidation of ascorbic acid (AA), is employed to reflect the DNA methylation level and to provide a highly sensitive electrochemical signal. A linear correlation between the catalytic oxidation current of AA and the activity of M.SssI MTase ranged from 0 to 120 U/mL with a current sensitivity of 0.046 μA mL $U^{-1}$ is obtained. In the second MTase biosensor, layered transition metal dichalcogenides – $MoS_2$ nanosheets are used as a fluorescence quencher for the construction of a simple signal-on fluorescent MTase sensor. The fluorescence signal mainly relies on the restored fluorescence which results from the affinity difference of fluorophore labeled long (>10 bases) and short (5 bases) DNA strands produced before and after the methylation process. Based on this principle, a linear correlation between the restored fluorescence

intensity and the Dam MTase activity ranged from 0.2 to 20 U/mL is achieved. In the third MTase biosensor, invertase which catalyzes the hydrolysis of sucrose into glucose and fructose is conjugated with the substrate DNA to act as the signal producer. The resulting glucose is then monitored by a personal glucose meter (PGM). Taking advantage of the ease of operation, low cost, and readily accessibility characteristics of the PGM, a linear relationship between the glucose reading and the Dam MTase activity from 0.5 to 80 U/mL is achieved, offering a good opportunity for the development of simple and robust MTase activity detection tool for uses at point-of-care. Excellent sensitivity and selectivity for MTase activity measurements are attained in these three biosensors.

# List of Tables

# List of Figures

# List of Schemes

# List of Abbreviations

| | |
|---|---|
| DNA | deoxyribonucleic acid |
| MTase | methyltransferase |
| $Os(bpy)_2$ | Osmium-bipyridine complex |
| Os-RP | $Os(bpy)_2$ complex-based redox polymer |
| Ru-RP | ruthenium complex-tethered redox polymer |
| GOx | glucose oxidase |
| GCE | glassy carbon electrode |
| *lamellar ridge*-Au | lamellar-ridge architectured gold |
| PIND | N,N'-bis(3-propylimidazole)-1,4,5,8-naphthalene diimide |
| PIND-Os | PIND functionalized with electrocatalytic redox $Os(bpy)_2Cl^+$ moieties |
| ds-DNA | double-stranded DNA |
| ss-DNA | single-stranded DNA |
| AA | ascorbic acid |
| PGM | personal glucose meter |
| MTases | methyltransferases |
| SAM | S-adenosyl-L-methionine |
| IUPAC | International Union of Pure and Applied Chemistry |
| GDH | glucose dehydrogenase |
| FAD | Flavin adenine dinucleotide |
| DA | dopamine |
| UA | uric acid |
| AMP | acetaminophen |
| $^3$H-SAM | S-adenosyl-L-[$^3$H-methyl] methionine |
| SAH | S-adenosyl-L-homocysteine |

| | |
|---|---|
| HRP | horseradish peroxidase |
| GFP | green fluorescent protein |
| 2D | two dimensional |
| EIS | electrochemical impedance spectroscopy |
| DPV | differential pulse voltammetry |
| AFM | atomic force microscopy |
| PBS | phosphate-buffered saline solution |
| GPC | gel permeation chromatography |
| PVPAA | poly (vinylpyridine-co-acrylamide) |
| GA | glutaraldehyde |
| $M_w$ | weight-average molecular weight |
| PDI | polydispersity index |
| MLCT | metal-to-ligand charge-transfer |
| $R_{ct}$ | charge transfer resistance |
| $K_m$ | Michaelis-Menten constant |
| LOD | limit of detection |
| *flat*-Au | flat gold |
| FESEM | filed emission scanning electron microscopy |
| XRD | X-ray diffraction |
| XPS | X-ray photoelectron spectroscopy |
| TGA | thermal gravimetric analysis |
| EASA | electrochemical active surface area |
| CNT | carbon nanotube |
| 5-Aza | 5-azacytidine |
| 5-Aza-dC | 5-aza-2’-deoxycytidine |
| MCH | 6-mercapto-1-hexanol |
| Tris | tris(hydroxymethyl)aminomethane |
| TCEP | tris(2-carboxyethyl)phosphine hydrochloride |
| Oligo | oligonucleotide |

| | |
|---|---|
| CV | cyclic voltammetry |
| $E_p$ | peak potential |
| $I_p$ | peak potential |
| $IC_{50}$ | half maximal inhibitory concentration |
| IGAs | inorganic graphene analogues |
| TMDCs | transition metal dichalcogenides |
| TCSPC | time-correlated single photon counting |
| GO | graphene oxide |
| sulfo-SMCC | 4-(N-Maleimidomethyl) cyclohexane-1-carboxylic acid 3-sulfo-N-hydroxysuccinimide ester sodium salt |
| PAGE | polyacrylamide gel electrophoresis |

# Chapter 1. Introduction

Diabetes mellitus, a kind of metabolic disease characterized by high blood sugar (glucose) levels, has long been a worldwide public health problem. In 2013, 382 million people had diabetes; this number is expected to rise to 592 million by 2035.[1] Patients with diabetes risk serious complications from heart disease, kidney failure, nerve degradation, blindness, and amputations.[2] Highly sensitive, selective, and reliable detection of glucose is of great importance for diabetes mellitus diagnosis and management.

DNA methyltransferases (MTases) are a family of enzymes that catalyze the transfer of a methyl group from S-adenosyl-L-methionine (SAM) to adenine or cytosine residues in the specific sites of DNA during the biological DNA methylation process.[3] In mammals, abnormal DNA methylation patterns caused by altered DNA MTase activity have been demonstrated to be closely associated with human diseases including cancer.[4, 5] Consequently, DNA MTases have been recognized as potential targets for early disease diagnosis. Therefore, the development of DNA MTase activity biosensors is critical for both scientific research and clinical applications.

My research is mainly focused on the development of novel glucose and DNA MTase activity biosensors. In this chapter, a brief introduction on biosensors will be presented followed by two parallel reviews on glucose biosensor and DNA MTase biosensors and the objectives and scope of this thesis.

## 1.1 Biosensors

### 1.1.1 Definition of a biosensor

According to the International Union of Pure and Applied Chemistry (IUPAC) nomenclature, a biosensor is defined as an analytical device that is capable of providing quantitative or semi-quantitative information using specific biochemical reactions with a physicochemical detector.[6] As illustrated in Figure 1.1, it typically consists of two components, a biological recognition element (bioreceptor) and a transduction element (transducer). The role of the bioreceptor is to interact specifically with the target analyte, and the bioreceptor element can be an enzyme, antibody, nucleic acid, cell structure, organelles, microorganisms, or tissue. A comprehensive overview of various kinds of recognition receptors used in biosensors is available.[7] On the other hand, the role of the transducer is to transform the biorecognition event resulting from the interaction of the analyte with the biological element into a detectable signal that can be more easily measured and quantified. The transducer usually works in a physicochemical way, for example, the electrochemical technique, the optical technique, the piezoelectric technique, etc.

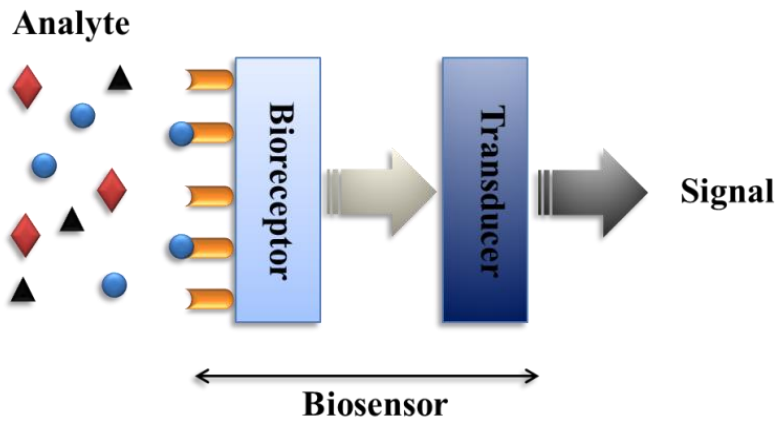

**Figure 1.1.** Schematic illustration of a biosensor.

### 1.1.2 Applications of biosensors

Comparing with conventional analytical methods based on techniques such as spectrometry, chromatography, biochemical or microbiological techniques, biosensors are cost-effective, time-saving, easy-to-use, sensitive and highly accurate detection devices in a variety of research and commercial applications. To date, biosensors have found a broad range of applications in environmental pollution control, industrial processing and monitoring, defense, healthcare, and so forth.

Environmental applications of biosensors mainly focus on the detection and monitoring of pollutants in soil, water, and air.[8, 9] The most intensively investigated environmental biosensors are based on the detection of pesticides,[10] heavy metal (e.g. mercury, lead, cadmium, etc.) ions,[11] microorganisms,[12] and toxic gases (sulfur, nitrogen, and carbon oxides, hydrogen cyanide, etc.).[13] In addition, various biosensors have been developed in order to assess the quality of foodstuff and beverage and to monitor industrial processes in the food and beverage industries.[14] The majority of biosensor research for food industry is focused on the verification of maximum pesticide residues and monitoring of analyte concentrations, such as carbohydrates, alcohols, and acids, which may be indicators of food acceptability and quality. Defense in general, and defense against terror attacks in particular, is currently a matter of great concern that has prompted the development of biosensors for explosives and warfare agents.[15, 16] Various types of biosensors for the detection of biological warfare agents have been

developed using various recognition components, such as antibodies, enzymes, biologically-inspired synthetic ligands, whole-cell, etc. Moreover, one of the main fields of biosensor applications is healthcare in which biosensors are utilized for in vitro or in vivo determination of chemical species of physiological relevance.[17] It is noteworthy that glucose meters for self-monitoring of blood glucose levels for people with diabetes are commercially available, and accounts for about 85% of the total biosensor market.[18] Besides, biosensors for different biomarkers have been developed for the clinical diagnosis of many types of cancer, cardiovascular diseases, and hormone-related health problems.[19]

### 1.1.3 Classification of biosensors

Biosensors may be classified according to the biological specificity-conferring mechanism or, alternatively, to the mode of physicochemical signal transduction.[8] The bioreceptor may be based on a chemical reaction catalyzed by, or on an equilibrium reaction with macromolecules that have been isolated, engineered or present in their original biological environment. In the latter case, equilibrium is generally reached and there is no further, if any, net consumption of analyte by the immobilized biorecognition agent incorporated into the biosensors. Most commonly, according to the transducing mechanism, biosensors are categorized as electrochemical, optical, thermometric, and piezoelectric biosensors (Figure 1.2).

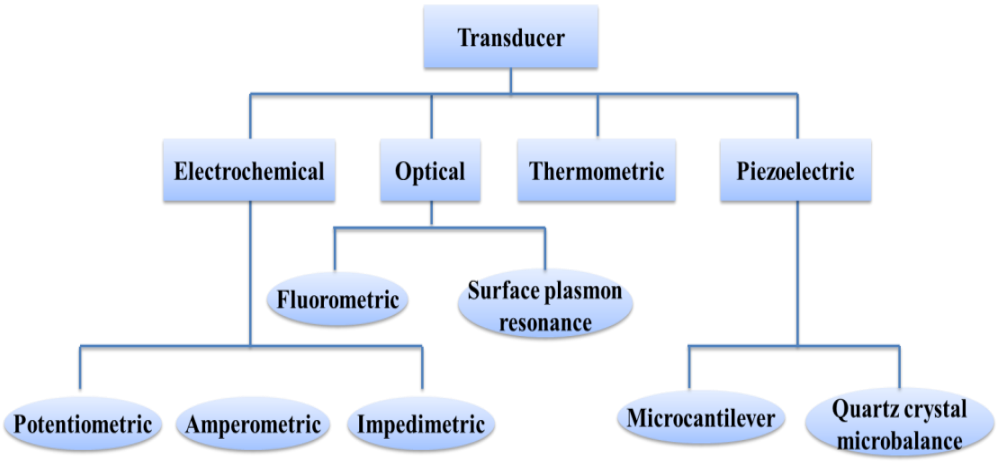


**Figure 1.2.** Classification of biosensors based on transducers.

The basic principle of electrochemical biosensors is that the chemical reactions between the bioreceptor and target analyte produce or consume ions or electrons, which affects measurable electrical properties of the solution.[20] Electrochemical biosensors can be further classified as potentiometric, amperometric, and impedimetric biosensors. Potentiometric biosensors deal with the potential difference either between an indicator and a reference electrode, or two reference electrodes separated by a permselective membrane. Amperometric biosensors are based on the measurement of the current resulting from the electrochemical oxidation or reduction of an electroactive species. Additionally, a series of electrochemical transduction methods are based on the concept of electrochemical impedance. The electrochemical impedance indicates the opposition to the flow of an alternating current through an electrochemical cell. Optical biosensors can be based on light emission or light absorption by the sensing element. Such processes are associated with transitions between energy levels of certain species (molecules or nanoparticles) included in the sensing element. Biosensors depending on

optical transducers may detect changes in the absorbance, fluorescence/phosphorescence, chemiluminescence, reflectance, light scattering, or refractive index.[21] Thermometric biosensors exploit the fundamental property of biological reactions, i.e. absorption or evolution of heat, which is reflected as a change in the temperature within the reaction medium.[22] The total heat evolution or absorption is proportional to the molar enthalpy and to the total number of product molecules created in the biochemical reaction. Piezoelectric biosensors rely on the mass-sensitive sensing technique. The mass change resulting from the recognition between the analyte and the sensing element is measured. They usually involve the utilization of materials that exhibit the piezoelectric effect, such as quartz crystals or cantilever.[23, 24]

In addition to the transducer-based categories described above, biosensors may be further classified according to the analytes or reactions that they monitor: direct monitoring of analyte concentration or of reactions producing or consuming such analytes; alternatively, an indirect monitoring of inhibitor or activator of the biological recognition element (biochemical receptor) may be achieved. My research interest is focused on two aspects, one is the monitoring of glucose which is of great importance for diabetes mellitus diagnosis and control; the other is the monitoring of DNA MTase activity which plays an essential role in DNA methylation related biological processes like gene expression, genomic imprinting, etc. In terms of these two types of analytes of interest, two parallel reviews on glucose biosensors and DNA MTase biosensors will be given in the following sections.

## 1.2 Glucose biosensors

### 1.2.1 Diabetes mellitus and glucose sensing

Glucose is the primary source of energy for most cells of the body. In medicine and animal physiology, "blood sugar" refers to glucose in the blood. Glucose in bloodstream is regulated by hormones produced by the body. The human body regulates blood glucose levels at a concentration of 4-8 mM (70-120 mg $dL^{-1}$). In the presence of physiopathological conditions, blood glucose levels could vary in the range of 2-30 mM (30-500 mg $dL^{-1}$).[25] A persistent high glucose level is present in patients with diabetes mellitus, since they are unable to effectively regulate blood glucose levels.

Diabetes mellitus is a group of metabolic diseases characterized by hyperglycemia resulting from defects in insulin secretion, insulin action, or both.[26] It is a leading cause of morbidity and mortality, and a major health problem in most developed societies. The International Diabetes Federation has produced estimates of diabetes prevalence since the year 2000. As of 2013, the latest study estimated that 382 million people had diabetes worldwide and this number is expected to rise to 592 million by 2035.[1] Diabetes mellitus can be classified into two broad etiopathogenetic categories: type 1 and type 2 diabetes. The former type of diabetes, which accounts for only 5-10% of the diabetic population, is caused by an absolute deficiency of insulin secretion, which resulting from a cellular-mediated autoimmune destruction of the β-cells of the pancreas. The later type of diabetes, type 2 diabetes, is much more prevalent, and accounts for ~90-95% of the diabetic population. It is caused by

a combination of resistance to insulin action and an inadequate compensatory insulin secretory response.

The chronic hyperglycemia of diabetes is associated with long-term damage, dysfunction, and failure of different organs. Long-term complications of diabetes mellitus include retinopathy with potential loss of vision; nephropathy leading to renal failure; peripheral neuropathy with risk of foot ulcers, amputations, and Charcot joints; and autonomic neuropathy causing gastrointestinal, genitourinary, and cardiovascular symptoms, and sexual dysfunction.[27] The monitoring of blood glucose concentration is of great importance for the diagnosis and management of patients with diabetes. Self-monitoring of blood glucose helps the patient achieve and maintain normal blood glucose concentrations in order to delay or even prevent the progression of microvascular (retinopathy, nephropathy, and neuropathy) and macrovascular complications.[28] Thus, this demand greatly promoted the intensive research on the development of glucose biosensors.

To date, various glucose biosensors based on different sensing mechanism, such as electrochemical[29-31] and optical,[32, 33] have been reported and reviewed by several experts. More recently, due to the rapid development of nanotechnology, many glucose biosensors that utilize a number of nanomaterials (nanoparticles, nanofilms, nanotubes, and nanocomposites) have been surveyed.[25, 34, 35] Electrochemical biosensors can provide the advantages of cost-effective, ease of operation, fast response, and ease of miniaturization, glucose biosensors based on this type of transduction dominate the biosensor market. The following section will review the brief

history of electrochemical glucose biosensors and their basic operation principle.

### 1.2.2 History of electrochemical glucose biosensors

Since the conception of glucose enzyme electrode proposed by Clark and Lyons in 1962,[36] numerous efforts have been made toward the development of electrochemical glucose biosensors for reliable determination of glucose in the past 50 years. Up to now, different methodologies, such as amperometric,[37-39] potentiometric,[40, 41] and impedimetric[42, 43] transductions have been established for electrochemical glucose detection. Among them, enzymatic amperometric glucose biosensors are the most common devices commercially available, and have been widely studied over the last few decades. Generally, glucose measurements are based on the catalytic oxidation by the immobilized glucose dehydrogenase (GDH) or glucose oxidase (GOx).[44, 45] Although glucose biosensors based on GDH have been constructed, the lack of specificity and stability rule out the widespread use of this enzyme in glucose biosensors.[45] In comparison, GOx is easy to obtain, cheap, and can withstand greater extremes of pH, ionic strength, and temperature, thus allowing less stringent conditions during the manufacturing process.[46] General milestones and achievements relevant to electrochemical glucose biosensors are summarized in Table 1.1. More specifically, there are three generations of glucose biosensors, detailed reviews of each generation will be presented in the following sections.

**Table 1.1.** Historical landmarks of electrochemical glucose biosensors.

| Year | Event | References |
|---|---|---|
| 1962 | First glucose enzyme electrode | [36] |
| 1967 | First practical enzyme electrode | [47] |
| 1973 | Glucose enzyme electrode based on peroxide detection | [48] |
| 1975 | Relaunch of first commercial glucose sensor system, YSI analyzer | YSI Inc. |
| 1982 | First needle-type enzyme electrode for in vivo glucose monitoring | [49] |
| 1984 | First ferrocene mediated amperometric glucose biosensor | [50] |
| 1987 | Launch of the MediSense ExacTech blood glucose biosensor | Medisense Inc. |
| 1988 | Electrical wiring of redox centers of enzymes to electrodes | [51, 52] |
| 1999 | Launch of a commercial in vivo glucose sensor | MiniMed Inc. |
| 2000 | Introduction of a wearable noninvasive glucose monitor | Cygnus Inc. |
| 2002 | Electrodeposition paints as immobilization matrices for biosensors | [53] |
| 2007 | An implanted glucose biosensor operated for five days | [54] |

*1.2.2.1 First generation of glucose biosensors*

The first generation of glucose biosensors mainly rely on the biocatalytic reaction involving the reduction of flavin adenine dinucleotide (FAD) in the glucose oxidase (GOx) by glucose, followed by the reoxidation of the reduced form of FAD ($FADH_2$) by molecular oxygen (equation 1 and 2).

$$GOx\ (FAD) + glucose \rightarrow GOx\ (FADH_2) + gluconolactone \quad (1)$$

$$GOx\ (FADH_2) + O_2 \rightarrow GOx\ (FAD) + H_2O_2 \quad (2)$$

In this case, glucose concentration is indirectly monitored by either the consumption of molecular oxygen using an oxygen electrode[36] or the production of $H_2O_2$ through amperometric measurement.[48] However, this indirect glucose detection strategy is limited by two major drawbacks. The first limitation factor, known as the "oxygen deficit", is the co-substrate molecular oxygen, due to its much lower level than glucose in blood, the development of highly sensitive glucose biosensors is severely affected. The other limitation is caused by the amperometric measurement of the produced $H_2O_2$, the requirement of a relatively high working potential (+ 0.6 V, vs. Ag/AgCl) results in the interference caused by readily oxidizable species that coexist in blood.

*1.2.2.2 Second generation of glucose biosensors*

In order to overcome the drawbacks of the first generation of glucose biosensors, further improvements have been obtained by replacing the natural molecular oxygen with mediators. Mediators are artificial electron transferring agents that can readily participate in the redox reaction with the biological component and thus help in the rapid electron transfer.[55] The direct electron transfer between the FAD redox center of GOx and the electrode surface is impeded by the intrinsic barrier of the thick glycoprotein shell surrounding the active sites. The electron mediators, such as ferrocene and its derivatives, ferricyanide, quinine compounds, methylene blue, etc. have been widely used

to construct mediated glucose biosensors to help shuttling electrons between the redox centers of GOx and the substrate electrode.[50, 56-59]

The operating principle of the mediated glucose biosensors is illustrated in Figure 1.3. Electrons are rapidly shuttled through a nondiffusional routine and the subsequent reoxidation of the mediator at the electrode surface produce the current signal which is proportional to the concentration of glucose.

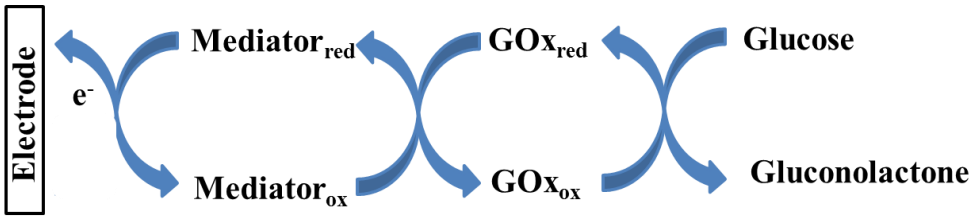


**Figure 1.3.** Working principle of mediated glucose biosensors.

In addition, various strategies to facilitate electron transfer between the redox centers of GOx and the electrode surface have been employed, such as enzyme wiring of GOx by electron-conducting redox hydrogels, the chemical modification of GOx with electron-relay groups, and the application of nanomaterial as electrical connectors.[60-62]

*1.2.2.3 Third generation of glucose biosensors*

Some electrodes which are prepared by the coating of the electronic conductors (conducting salts) have been developed. The reduced enzyme can be directly oxidized on these electrodes (equation 3 and 4). Glucose biosensors using these electrodes have been classified as the third generation of glucose biosensors. Several studies for other direct electron transfer approaches on the

third-generation glucose biosensors have been reported, including TTF-TCNQ that has a tree-like crystal structure, the GOx/polypyrrole system, and oxidized boron-doped diamond electrodes.[63-65]

$$GOx\ (FAD) + glucose \rightarrow GOx\ (FADH_2) + gluconolactone \quad (3)$$

$$Electrode:\ GOx\ (FADH_2) \rightarrow GOx\ (FAD) + 2H^+ + 2e^- \quad (4)$$

### 1.2.3 Interference issue in electrochemical glucose biosensors

The analytical performance of glucose biosensors is usually evaluated in terms of precision, accuracy, linearity, and anti-interference capability. In this section, interference which is still a big issue in electrochemical glucose biosensors will be addressed.

Although enzymes are generally very efficient and very selective, the amperometric glucose biosensors which operate at relatively high potentials often lose their selectivity due to the contribution of the electrochemical responses from biologically electroactive interferences. The commonly encountered interferences in blood fluids are ascorbic acid (AA), dopamine (DA), uric acid (UA), as well as one of the common drugs-acetaminophen (AMP).[30, 66, 67]

#### *1.2.3.1 Permselective membrane covering*

To alleviate the interference problem and improve the anti-interference ability of the electrochemical glucose biosensors, permselective coatings with

transport properties based on charge or size exclusion principle have been utilized in the construction of glucose biosensors toward the regulation of the coexisting substances. For example, Nafion, which is a negatively-charged perfluorinated ionomer can prevent the diffusion of anionic species, such as AA and UA, toward the electrode, is frequently employed in the construction of glucose biosensors.[68-70] Besides, polymer films (i.e. polyphenylenediamine, polypyrrole, polymeric mercaptosilane, etc.) and cellulose acetate membranes are the commonly reported coatings based on size exclusion for minimizing the interference.[71-74]

The approach of coating a permselective membrane on a biosensing layer provides a simple, fast way to block interferants from accessing the electrode. However, Nafion or other polymeric films in these methods were dispersed over the electrode surface by dipping or spin coating. As a result, the membrane thickness was hard to control. More importantly, these methods face the limitations of poor repeatability, non-uniformity of coating and poor adhesion.

*1.2.3.2 Operation potential lowering*

Mediated amperometric glucose biosensors are known to be less susceptible to interferences when they are operated at very low applied potentials. Therefore, paramount works have been done on the exploring of various mediators that pose low redox potentials. Jiang and co-workers proposed an osmium complex-based glucose biosensor which has a working potential of 0 mV (vs. Ag/AgCl).[75] Similarly, Nam and co-workers showed that when

$[Ru(NH_3)_6]^{3+}$ was used as the mediator, it allowed the use of a relatively low applied potential of 0 mV (vs. Ag/AgCl).[76] The adoption of these low working potential mediators could effectively eliminate interference from AA, DA, and UA.

Although a number of mediators which operate at relatively low working potentials have been developed, it is still of great significance to explore novel structured mediators with even lower working potentials for practically completely eliminating interference.

## 1.3 DNA MTase activity biosensors

### 1.3.1 DNA methylation

Epigenetics is defined as heritable changes in gene expression that are not due to any alteration in the DNA sequence.[77] There are three main, inter-related types of epigenetics: DNA methylation, genomic imprinting, and histone modification.[78] Among them, DNA methylation is the best known epigenetic marker, and it is the first epigenetic modification to be characterized at the molecular level.[79, 80] DNA methylation is a biochemical process which refers to a covalent chemical modification resulting in the transfer of a methyl group from S-adenosyl-L-methionine (SAM) to the cytosine ($C^5$ or $N^4$ position) or adenine ($N^6$ position) nucleotide (Figure 1.4). This process is brought out enzymatically by DNA MTases after DNA replication in a sequence-specific manner, usually at palindromic sites.[81] Examples of typical DNA MTases (from both prokaryotes and eukaryotes) involved in DNA methylation machinery are summarized in Table 1.2. DNA

methylation does not affect the Watson/Crick pairing properties of cytosine and adenine, the methyl group is positioned in the major groove of the DNA, where it can easily be detected by proteins interacting with the DNA.

**Table 1.2.** Examples of DNA MTase.

| MTase | Recognition site (5'-3') | Classification | Source |
|---|---|---|---|
| AluI | AG<u>C</u>T | $C^5$-cytosine | *Arthrobacter luteus* |
| Dam | G<u>A</u>TC | $N^6$-adenine | *E. coli* |
| Dnmt1 | Hemimethylated <u>C</u>G | $C^5$-cytosine | *human Dnmt1 cDNA* |
| HaeIII | GG<u>C</u>C | $C^5$-cytosine | *Haemophilus aegyptius* |
| Met1 | <u>C</u>G | $C^5$-cytosine | *A. thaliana* |
| M.SssI | <u>C</u>G | $C^5$-cytosine | *Spiroplasma sp.* |
| M.PvuII | CAG<u>C</u>TG | $N^4$-cytosine | *Proteus vulgaris* |

DNA methylation in prokaryotes includes all three types of methylation illustrated in Figure 1.4. The major role of DNA methylation in prokaryotes is a host mechanism against foreign DNA as part of restriction modification systems.[82] In higher eukaryotes, only $C^5$-cytosine methylation has been found at the CpG dinucleotide sequence, and about 60%-90% CpG sites are methylated in mammals.[83] In mammals, studies have revealed that DNA methylation plays an essential role in many biological processes, such as genomic imprinting, X-chromosome inactivation, and transcriptional gene silencing.[84-86]

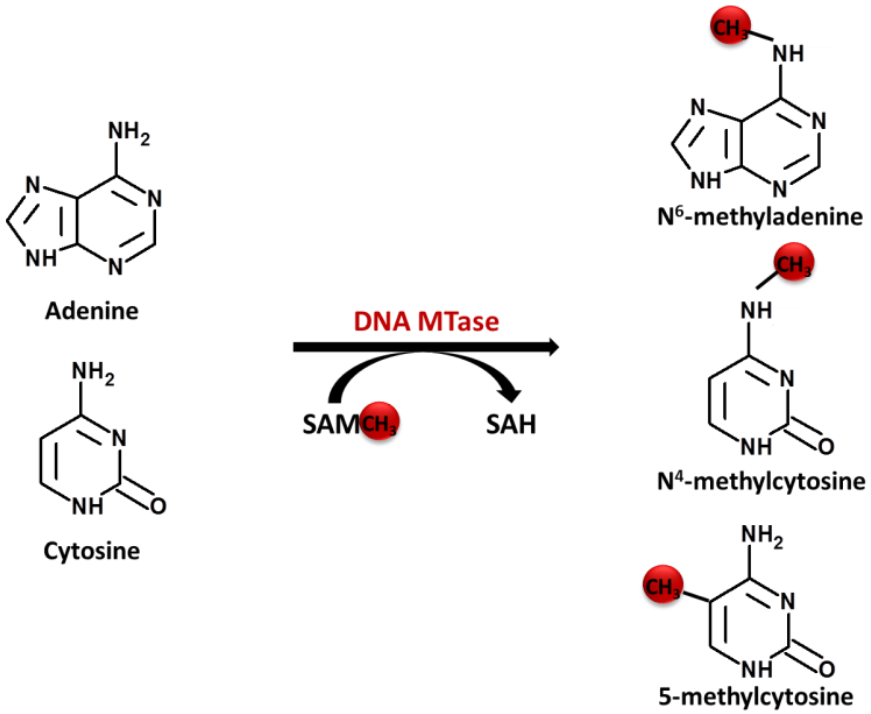


**Figure 1.4.** DNA MTase catalyzed adenine and cytosine methylation.

### 1.3.2 DNA MTase biomarker in cancer

Aberrant DNA methylation resulting in transcriptional repression has been documented in several types of human cancer,[87-90] such as colon cancer, breast cancer, lung cancer, kidney cancer, prostate cancer, liver cancer, ovarian cancer, etc. As the catalytic enzymes in the DNA methylation process, alterations of DNA MTases activity have been confirmed to be closely related to the aberrant DNA methylation level in several diseases. Issa and co-workers have demonstrated that an increased DNA methylation capacity accompanies the increase in DNA MTase transcripts were observed during progressive stages of colon cancer, the cytosine DNA MTase activity was 5.4-fold in the cancer specimens compared with normal control subjects.[91] Belinsky et al. has revealed that DNA MTase activity increased incrementally during lung

cancer progression and coincided with increased expression of the DNA MTase gene in hyperplasias, adenomas, and carcinomas.[92] Patra et al. carried out the studies on methylation-demethylation enzymes activities in human prostate cancer for the first time.[93] Their experimental results clearly demonstrated that the Dnmt1 MTase activity is upregulated, whereas the DNA demethylase, MBD2, is repressed at the level of translation in human prostate cancer.

In addition, DNA MTases have been used as potential targets for therapy of epigenetic cancer.[94] For example, researchers examined the prognostic and predictive impact of Dnmt1 and Dnmt3b expression in gastric carcinomas treated by neoadjuvant chemotherapy.[95] Low Dnmt1 expression was observed for the patients treated with (platinum/5-fluorouracil)-based neoadjuvant chemotherapy. Recently, increased Dnmt1 MTase activity and elevated methylation induced by epidermal growth factor receptor activation were investigated in ovarian cancer by Samudio-Ruiz.[96] Treatment with the Dnmt1 inhibitor agent 5-Aza-2'-deoxycytidine inhibited the epidermal growth factor induced increase of both DNMT activity and global methylation. These data support a role for epidermal growth factor receptor in the process of accumulated DNA methylation during ovarian cancer progression and suggest that epigenetic therapy may be beneficial for the treatment of ovarian cancer.

In view of the essential roles of DNA methylation and DNA MTase in gene regulation, as well as their potentials to act as targets for cancer diagnosis and therapy, the development of DNA MTase activity biosensors is of paramount significance for both scientific research and clinical applications. Over the past decades, a number of methods have been reported for DNA MTase activity

measurement. The development history of various DNA MTase activity biosensors will be reviewed in the following section.

### 1.3.3 Methods for the detection of DNA MTase activity

In 1992, Boye et al. reported the direct quantitation of Dam MTase in *Escherichia coli* by gel electrophoresis.[97] After polyacrylamide gel electrophoresis, the amounts of Dam MTase in extracts of wild-type cells were measured by immunoblotting. Later on, various indirect detection methods based on tritium labeled S-adenosyl-L-[$^3$H-methyl] methionine ($^3$H-SAM) were established. The DNA MTase activity was reflected on the radioactivity of the $^3$H incorporation into substrate DNA after methylation catalyzed by MTase. Before the radioactivity measurement by scintillation counting, various separation approaches of the methylated $^3$H incorporated substrate DNA from $^3$H-SAM cocktails were reported, such as direct filtration,[98] gel electrophoresis,[99] column chromatography,[100] biotin-avidin microplate,[101] magnetic beads,[102] etc. Alternatively, an indirect method that monitors the conversion of SAM to S-adenosyl-L-homocysteine (SAH) using liquid chromatography/mass spectrometry was applied to detect MTase activity.[103] These methods depend either on multiple-step protocols, radioisotopes, and/or expensive and demanding equipment. Thus, the development of simple, cost-effective, robust biosensors for quantifying the activity of DNA MTase has drawn intensive attention in the past few years. The following two subsections review the reported MTase activity biosensors based on electrochemical and optical platforms which are the most commonly employed techniques in recently developed DNA MTase activity biosensors.

*1.3.3.1 Electrochemical DNA MTase biosensors*

Most of the reported electrochemical DNA MTase biosensors use the restriction/modification system. Namely, the DNA MTase and methylation sensitive restriction endonuclease couples (Table 1.3) are employed. Generally, in these biosensors, the substrate DNA is firstly immobilized onto the electrode surface, the immobilized DNA is subsequently methylated by MTase, then the introduction of the endonuclease results in the amount changes of the electrochemical signal producer conjugated or absorbed onto the substrate DNA.

**Table 1.3.** Typical DNA MTase and methylation sensitive restriction endonuclease couples.

| MTase | Recognition site (5'-3') | Endonuclease | Cleavage site |
|---|---|---|---|
| Dam | G<u>A</u>TC | DpnI | $^{CH_3}$<br>5'... G A T C ...3'<br>3'... C T A G ...5'<br>$_{CH_3}$ |
| Dnmt1 | Hemimethylated <u>C</u>G | BstUI | 5'... C G C G ...3'<br>3'... G C G C ...5' |
| M.SssI | <u>C</u>G | HpaII | 5'... C C G G ...3'<br>3'... G G C C ...5' |

Methylene blue is one of the most commonly used electroactive species for signal production.[104-107] For example, Su et al. reported a signal-on electrochemical Dam MTase biosensor which was composed of a methylene blue modified signaling DNA probes and capture DNA probes tethered methylation-responsive hairpin DNA (hairpin-capture DNA probe). As illustrated in Figure 1.5, thiol-modified hairpin-capture DNA probes were firstly self-assembled on a gold electrode. Methylation induced scission of hairpin-capture DNA probes would displace the hairpin section and remain the

capture DNA probe section on the gold electrode. Subsequently, the remained capture DNA probes on the gold electrode can hybridize with the methylene blue modified signaling DNA probes, mediating methylene blue onto the gold electrode surface to a generate redox current. Apart from methylene blue, similar approaches were proposed by using other electroactive signal producers such as ferrocenecarboxylic acid,[108, 109] $[Ru(NH_3)_6]^{3+}$,[110] thionine,[111] and quantum dots.[112, 113] Moreover, Wu and co-workers developed an electrochemical Dam MTase biosensor based on methylation sensitive cleavage using terminal transferase (TdTase)-mediated extension.[114] In this biosensor, streptavidin-alkaline phosphatase, which catalyzes the conversion of electrochemically inactive 1-naphthyl phosphate into an electrochemically active phenol, was employed for the generation of an amplified electrochemical signal.

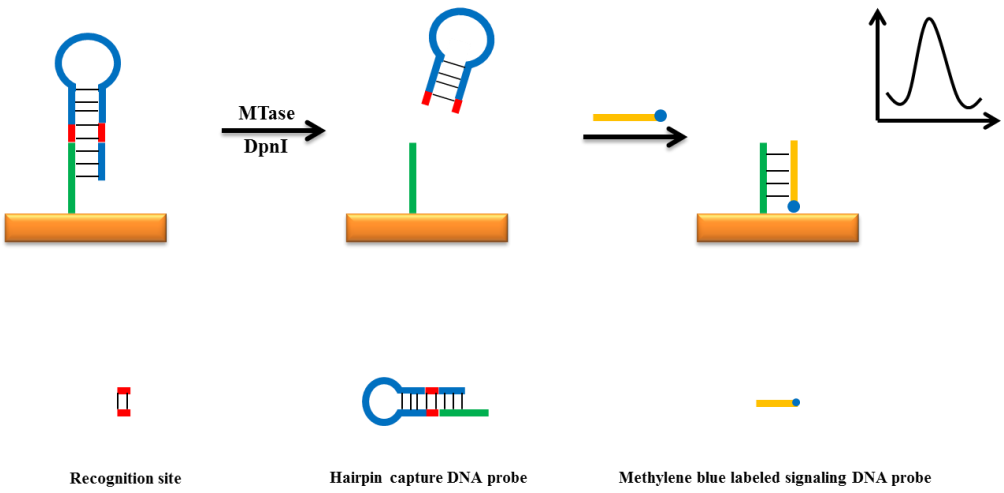


**Figure 1.5.** Schematic representation of the electrochemical MTase sensor. Reproduced from reference 104 with permission.

In addition to the above described methylation sensitive restriction endonuclease based MTase biosensors, Ai's group investigated the

electrochemical immunosensors for MTase activity analysis.[115-119] In their studies, either methyl binding domain proteins (MeCP2 and MBD) or anti-5-methylcytosine antibody was used to recognize the methylated CpG sites in substrate DNA.

*1.3.3.2 Optical DNA MTase activity biosensors*

In 2005, Woo et al. proposed a nonradioactive optical biosensor for DNA MTase activity detection for the first time.[120] In this biosnesor, double stranded-DNA (ds-DNA) substrates which were labeled with digoxigenin at one 3' end and biotin at the other 3' end were immobilized into a streptavidin coated microplate. After a subsequent treatment with MTase and restriction endonuclease, anti-digoxigenin-alkaline-phosphatase was introduced. Finally, alkaline-phosphate catalyzed the conversion of 1-nitrophenyl phosphate to phenol, and the absorbance was measured at 405 nm. Later on, new approaches based on DNA methylation induced aggregation-dispersion of DNA linked gold nanoparticles were established by several researchers.[121-123] Additionally, catalytic nucleic acids of DNAzyme which exhibit horseradish peroxidase (HRP) mimicking properties were incorporated into DNA substrates for DNA MTase activity monitoring.[124-126] The MTase methylation/endonuclease cleavage events were correlated with the DNAzymes formed after dissociation from the substrate DNAs. DNAzyme can catalyze the oxidation of 2,2'-azino-bis(3-ethylbenzothiazoline)-6-sulfonate disodium salt by $H_2O_2$ to produce colored radical ions, thereby causing a detectable color change.

On the other hand, Leonhardt's group developed fluorescence-based trapping biosensors for Dnmt1 activity analysis.[127, 128] Both biosensors used transiently expressed green fluorescent protein fused Dnmt1 (GFP-Dnmt1) and MTase inhibitors such as 5-azacytidine and 5-aza-2'-deoxycytidine. These nucleotide analogues were incorporated into the newly synthesized DNA at nuclear replication sites and caused irreversible immobilization, namely, trapping of GFP-Dnmt1 fusions at these sites. Although these biosensors allowed direct visualization of Dnmt1 activity in living cells in high throughput, the GFP-Dnmt1 and synthetic oligonucleotides preparation processes were very rigorous and tedious.

Recently, various novel strategies based on simply fluorophore-labeled DNAs have been developed. For example, a hairpin substrate DNA was modified with a fluorophore and a quencher at its 5' and 3' end, respectively. DNA methylation and cleavage by the MTase/endonuclease couple would cause the separation of the fluorophore and the quencher, resulting in the restoration of the fluorescence.[129, 130] Alternatively, other than the direct modification of substrate DNA, fluorophore and quencher linked molecular beacons were utilized for signal amplification.[131-135] In those biosensors, the nucleic acid strands dissociated from MTase substrate DNAs after methylation/cleavage would hybridize with the molecular beacons, then the following cleavage or opening the hairpin structure of the molecular beacons resulted the restoration of their fluorescence. In addition, due to the rapid development of nanotechnology, some nanomaterials such as graphene oxide,[136, 137] carbon nanoparticles,[138] and gold nanorods[139] were employed as fluorescence quenchers for MTase activity detection.

As can be seen from the review of MTase activity biosensors described above, the development of various MTase activity biosensors are mainly reported in the last ten years, indicating that it is a relatively new biosensing area targeted at MTases. Thus, further attempts to establish novel MTase activity biosensors are highly desired.

## 1.4 Objectives and significance of the studies

The purposes of the studies involved in this thesis are:

- To synthesize an anionic Os-based redox polymer and use it as an electron mediator for interference-free glucose detection.
- To synthesize a low working potential Ru-based redox polymer and use it as an electron mediator for interference-free glucose detection.
- To prepare lamellar-ridge architectured gold by using butterfly wings as the template and use it for nonenzymatic glucose detection.
- To synthesize a PIND-Os duplex DNA intercalator and use its elecrocatalytic oxidation of ascorbic acid as the signal producer and amplifier for sensitive DNA MTase activity detection.
- To prepare two dimensional (2D) $MoS_2$ nanosheets and extend their application in a fluorescent DNA MTase activity biosensor as an efficient fluorescence quencher.
- To adopt personal glucose meter as signal readout for DNA MTase activity detection.

Through these studies, we have obtained the following achievements successfully:

- By using the two kinds of redox polymers listed above, the interference problems resulting from the commonly encountered coexisting species in blood in electrochemical glucose biosensors have been successfully avoided. The excellent anti-interference capability of the two proposed glucose biosensors are attributed to the unique properties of the redox polymers. This may give more options for mediators used for reliable glucose biosensing.
- By using the gold samples with lamellar-ridge architecture templated by butterfly wings, a nonenzymatic glucose biosensor with outstanding performance has been fabricated. This presents an exemplary strategy of using the vast configuration pool from nature to blueprint the structural design of efficient electrochemical biosensors.
- By using the PIND-Os intercalator, $MoS_2$ nanosheets, and the PGM, three novel DNA MTase activity biosensors have been successfully developed. This may serve as potential DNA MTase activity biosensor candidates in clinical diagnosis applications.

## 1.5 Scope and overview of the thesis

Due to the restriction of accessing real blood samples in Singapore, a commercially available control solution (synthetic blood from Roche Diagnostics) for glucose meters which essentially contains the basic components that mimic human blood was employed to verify the reliability of

the newly developed glucose biosensor for routine analysis. The MTase models chosen in the studies on MTase activity biosensors are restricted to those MTases from bacteria since they are easy to obtain and there is no need of hemi-methylation modification of their substrate DNA. Subsequently, there is no real sample analysis performed for the MTase activity biosensors developed in the thesis.

This thesis centers on two targets, glucose and DNA MTase. The studies presented in Chapter 2, Chapter 3, and Chapter 4 aim on the glucose detection. The studies presented in Chapter 5 and Chapter 6 aim on the DNA MTase activity biosensors. Chapter 7 links glucose with DNA MTase by employing a personal glucose meter as the signal readout for the detection of DNA MTase activity. The diagrammatic representation of the outline of this dissertation is illustrated in Figure 1.6.

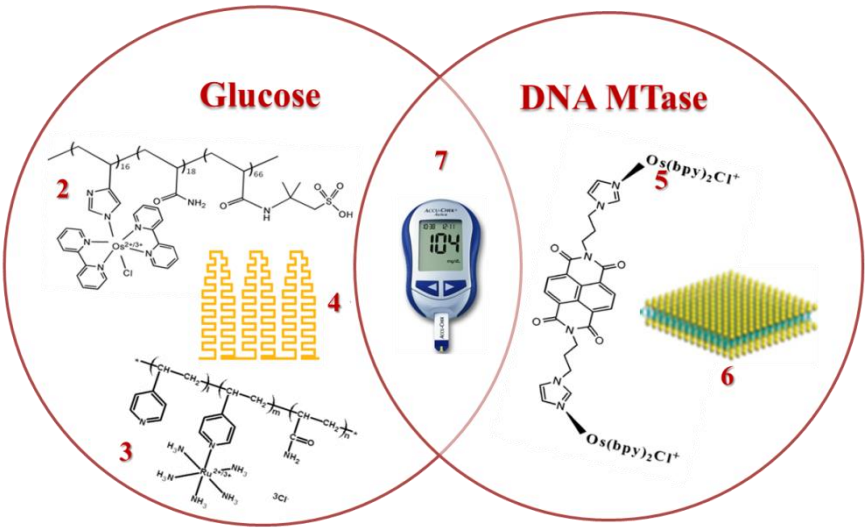


**Figure 1.6.** Diagrammatic representation of the outline of this dissertation.

The details of each study involved in the thesis, such as experimental methods, results and discussion, and conclusions, are presented separately in the following six chapters. Chapter 2 describes the glucose biosensor using a synthetic anionic Os-based redox polymer as the mediator to eliminate interference based on the electrostatic repulsion between the mediator and the interferants.

In Chapter 3, a ruthenium complex-based low-potential redox polymer (Ru-RP) was prepared and characterized by FT-IR, UV-vis spectrometry and gel permeation chromatography. Then the experimental conditions were optimized for the Ru-RP mediated glucose biosensor. Under the optimal experimental conditions, the developed biosensor showed good analytical performance and excellent anti-interference ability toward AA, UA, and DA due mainly to its very low operation potential. Finally, real sample analyses were performed to verify the reliability of the biosensor.

In Chapter 4, gold samples with lamellar-ridge architecture templated by blue scales from *Morph* butterfly wings were prepared by using an electroless deposition method. The as-prepared gold samples were characterized by SEM, XRD, XPS, and TGA. Then the gold material was used to construct an amperometric glucose biosensor. The excellent analytical performance of the biosensor, which was originated from the unique architecture of the gold samples, was demonstrated.

Chapter 5 explores an electrochemical M.SssI MTase activity biosensor, which employed a synthetic intercalator PIND-Os catalyzed ascorbic acid electro-oxidation reaction as the signal producer. Each step of modification on

the working electrode was monitored by electrochemical impedance spectroscopy (EIS) and differential pulse voltammetry (DPV). Attributing to the catalytic signal amplification, high sensitivity was achieved. The anti-interference and inhibitor screening abilities of the MTase activity biosensor were also demonstrated.

Chapter 6 investigates a fluorescent Dam MTase activity biosensor which employed a newly emerging two dimensional transition metal dichalcogenides, $MoS_2$ nanosheets, as the fluorescence quencher. The $MoS_2$ nanosheets were firstly prepared by mixed solvent exfoliation, and then characterized by atomic force microscopy (AFM) and UV-vis spectrometry. The fluorescence quenching mechanism and the feasibility of MTase activity sensing were carefully studied. Finally, the calibration study, interference study, and the inhibitor screening study were conducted.

In Chapter 7, a personal glucose meter was adapted to detect M.SssI MTase activity. The substrate DNA of M.SssI MTase was firstly conjugated with invertase which catalyzes the hydrolysis of sucrose to glucose and fructose, and the conjugates were characterized by gel imaging. The invertase-DNA conjugates were immobilized onto magnetic beads via streptavidin-biotin interaction. The experimental conditions including methylation time and cleavage time were optimized. Under the optimal conditions, calibration study, interference study and inhibition study were investigated accordingly.

# Chapter 2. An interference-free glucose biosensor based on an anionic redox polymer-mediated enzymatic oxidation of glucose

## 2.1 Introduction

In this work, an amperometric biosensor based on immobilized GOx and an $Os(bpy)_2$ (bpy=2,2'-bipyridine)-based anionic redox polymer (Os-RP) mediator was developed for the determination of glucose. GOx and the water-soluble crosslinkable Os-RP were co-immobilized on a glassy carbon electrode (GCE) in one step by employing glutaraldehyde as a crosslinker. In addition to its excellent electrocatalytic power, the crosslinked membrane acted as a thin permselective polymeric membrane with excellent selectivity for glucose over interferants such as ascorbic and uric acid. The interferant-eliminating property was obtained through the presence of a large number of sulfonic acid groups in the redox polymer. In addition, the high hydrophilic nature of the membrane effectively retarded the diffusion of molecular oxygen. This biosensor showed high sensitivity and excellent selectivity for glucose over interferants such as molecular oxygen, ascorbic acid, and uric acid.

## 2.2 Experimental

### 2.2.1 Materials and apparatus

GOx, (EC 1.1.3.4, from *Aspergillus niger*, 191 units $mg^{-1}$) was purchased from Fluka (CH-9407 Buchs, Switzerland). Glucose, glutaraldehyde (25 %), ascorbic acid, and uric acid were obtained from Sigma–Aldrich (St. Luis, MO,

USA). All other reagents were of analytical grade and used without further purification. Ultrapure deionized water with an electric resistance of 18.3 MΩ was used for all solution preparations. Glucose stock solutions were allowed to mutarotate for 24 h before use. Freshly prepared ascorbic acid and uric acid solutions were used in the interference study. PBS was used as the supporting electrolyte and was prepared weekly using deionized water. $[Os(bpy)_2Cl_2]$ was synthesized from $(NH_4)_2OsCl_6$ by the procedure developed by Lay and coworkers.[140] The water-soluble and crosslinkable Os-RP (Scheme 2.1), poly(4-vinylimidazole-coacrylamide-co-2-acrylanmido-2-methylpropanesulfonic acid) partially complexed with $[Os(bpy)_2Cl]^+$, was synthesized following a previously reported procedure.[141] Spectroscopic and elemental analysis showed that the synthesized redox polymer, on average, consisted of 16 $[Os(bpy)_2Cl]^+$, 18 amide, and 66 sulfonic acid moieties.

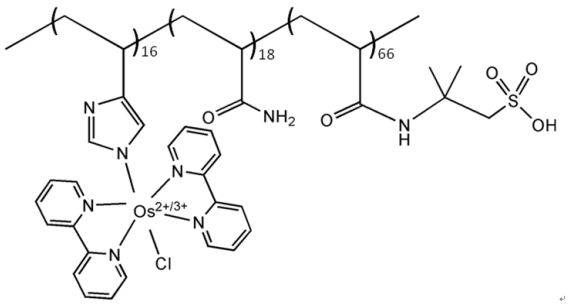


**Scheme 2.1.** Structure of the Os-RP.

Electrochemical experiments were carried out on a CHI760D electrochemical workstation (CH instruments, Austin, Texas). A conventional three-electrode system, consisting of the GCE working electrode, an Ag/AgCl (saturated KCl) reference electrode, and a platinum wire counter electrode, was employed. All potentials reported in this work were referred to the

Ag/AgCl reference electrode. Cyclic voltammetric tests of the biosensor were performed at a potential scan rate of 50 mV $s^{-1}$ in a potential window between -0.20 and 0.60 V. In amperometry, the background current was allowed to stabilize first before readings were taken. Small aliquots of glucose stock solution were added sequentially to reach the desired glucose concentrations in the test solutions.

### 2.2.2 Glucose Biosensor Fabrication

As for the biosensor fabrication, the GCE was first polished on a microcloth with 0.05 μm alumina slurry, followed by sonication in ultrapure water and ethanol for 5 min, successively. After drying the cleaned electrode, 4 μL of a mixed solution consisted of GOx, Os-RP, and glutaraldehyde was applied onto the GCE surface. The GCE was then incubated for at least 12 h under ambient conditions. During incubation Os-RP/and GOx were irreversibly crosslinked, forming the desired glucose sensing membrane on the GCE. The biosensor was kept at 4 °C when not in use. Little activity loss was observed within six months of storage.

## 2.3. Results and discussion

### 2.3.1 Electrochemical Characteristics of the Biosensor

In the absence of glucose, cyclic voltammetric tests of the biosensor in phosphate-buffered saline solution (PBS) (pH 7.4, 0.15 M NaCl, 20 mM phosphate) showed a pair of well-defined current peaks that were assigned to

the reversible electrochemical transformation between $Os^{2+}$ and $Os^{3+}$ embedded in the Os-RP/GOx membrane.[142] The charge under either the oxidation or the reduction current peak indicated the amount of the redox polymer deposited on the GCE surface (Figure 2.1, trace 1). Moreover, the magnitudes of the anodic and cathodic peak current were practically the same and the peak-to-peak potential separation was ~60 mV, close to the theoretical value of 59 mV at 25 °C. This implies that the electron exchange process between the redox polymer and the substrate GCE is rapid and the electron-mediating power of the redox polymer is excellent. The electrode process is diffusion-controlled[143] due to the relatively thick membrane on the electrode surface,[144] which means that in this case the diffusion of the glucose substrate will be the rate determining step. It can also be inferred from the cyclic voltammogram of the Os-RP/GOx membrane that GOx in the membrane does not noticeably affect the electrochemistry of the $Os^{2+}/Os^{3+}$ redox couple.

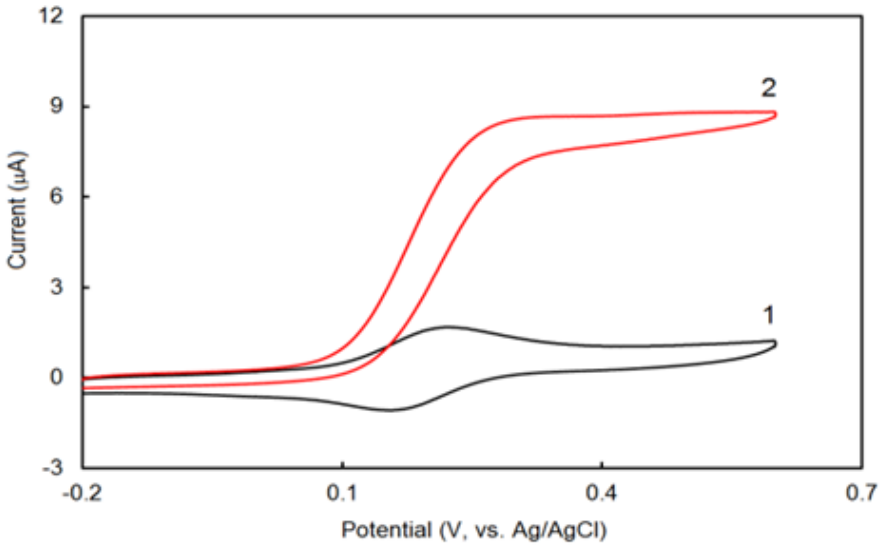


**Figure 2.1.** Cyclic voltammograms of the Os-RP/GOx/GCE biosensor (1) in the absence and (2) presence of 10 mM glucose. Supporting electrolyte: PBS, potential scan rate: 50 mV/s.

On the other hand, as depicted by trace 2 of Figure 2.1, in the presence of glucose the cyclic voltammogram became sinusoidal with a greatly increased oxidation current and a severely diminished reduction current—a typical electrocatalytic voltammogram,[145] resulting from the Os-RP-mediated glucose oxidation by GOx. Supportive evidence was found from the low hysteresis of the voltammogram between the oxidation and reduction branches. The absence of the reduction current peak in the cyclic voltammogram implies that the Os-RP/GOx membrane is homogenously maintained in the reduced state by the excellent electron relaying power of the redox polymer in the membrane through the transfer of electrons from the reduced GOx to the oxidized Os-RP ($Os^{3+}$) sites and to the substrate GCE. This means that the $Os^{2+}/Os^{3+}$ moieties in the Os-RP/GOx membrane act as artificial electron donors in the place of molecular oxygen for GOx and electron shuttles between GOx and the substrate GCE. As illustrated in Figure 2.2, glucose in solution is first enzymatically oxidized to gluconolactone, leaving behind two electrons. Meanwhile, the redox center (FAD) of GOx receives the two electrons returning to its reduced state. The electrooxidized Os-RP ($Os^{3+}$) then reacts with the reduced GOx, accepting the aforementioned electrons from the reduced GOx to become reduced ($Os^{2+}$) and regenerating the oxidized GOx. The reduced Os-RP then gives up its electrons to the substrate GCE, generating a current while $Os^{2+}$ returns back to its oxidized state $Os^{3+}$. Since the redox potential of GOx is -0.36 V, which is much more cathodic than that of the $Os^{2+}/Os^{3+}$ couple in the redox polymer and as there are plenty of $Os^{3+}$ ions in the vicinity of the redox centers of GOx, the electron transfer between $Os^{3+}$ and the reduced GOx is kinetically rapid, consuming all $Os^{3+}$ moieties in

the membrane as soon as they are formed. The oxidation current is now controlled by either the diffusion of glucose or by the kinetics of the enzymatic oxidation of glucose, depending on the concentration of glucose. For the amperometric determination of glucose, in order to maximize the sensitivity of the biosensor, to minimize background current, and to eliminate possible interferences from oxidizable species, the potential should be poised on the anodic side of the current peak and in the vicinity of the peak potential. So in this case, 0.25 V was chosen as the voltammogram peaked off at ~0.22 V. The time needed to reach 90% of the maximum response (response time) in amperometry at 0. 25 V was within 5 s.

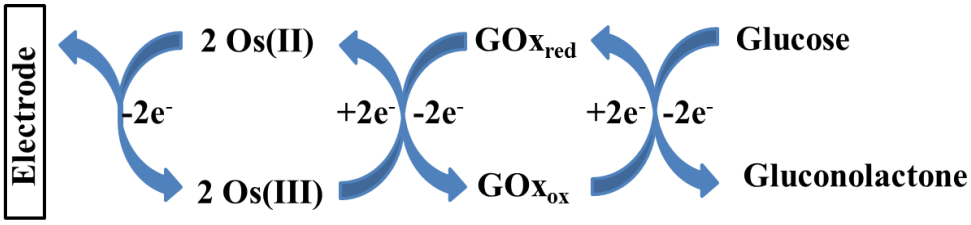


**Figure 2.2.** Working principle of the Os-RP-mediated glucose sensing process.

### 2.3.2 Optimization

The above results confirmed that Os-RP-mediated enzymatic oxidation of glucose is successfully achieved at the proposed biosensor with sufficient sensitivity. In the case of electrocatalytic oxidation of glucose, the oxidation current must be determined by one or a combination of the following processes: 1) mass-transport of glucose, 2) GOx-catalyzed oxidation of glucose at the biosensor–solution interface and within the membrane, and 3) the electron-mediating power of the redox polymer.[146] However, for a successful adaptation of the biosensor in the quantification of glucose, the

oxidation current must be exclusively associated with the concentration of glucose in a straightforward manner, preferably a linear correlation between the oxidation current and the glucose concentration. This solely glucose-controlled process can only be achieved by speeding up the electron-mediating power and the enzymatic oxidation process. High electron-mediating power is easily attainable when working with a high concentration of the redox polymer in the membrane and high enzymatic reaction rate is achievable by increasing the loading of GOx in the membrane.

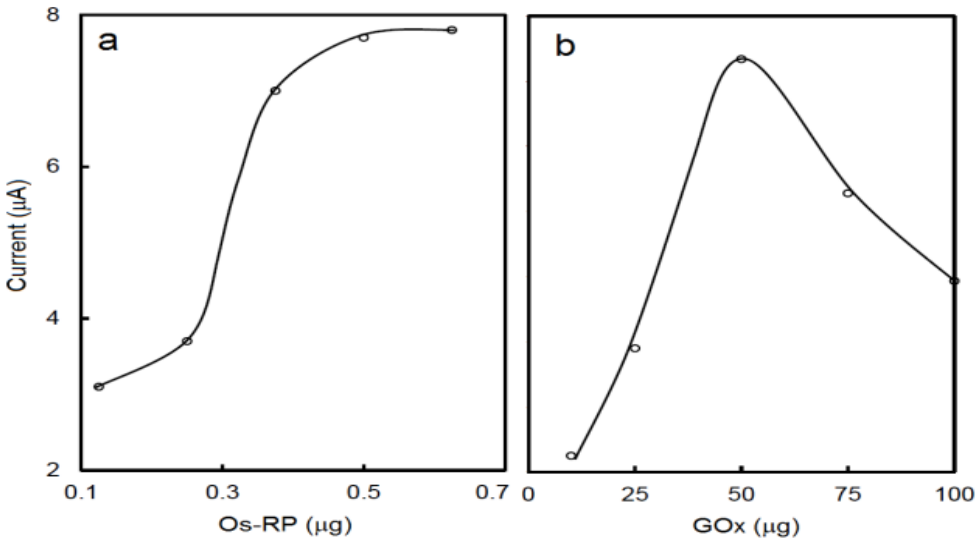


**Figure 2.3.** The effect of (a) Os-RP loading and (b) GOx loading on the amperometric response of 10 mM glucose. Supporting electrolyte: PBS, poised potential: 0.25 V.

The effect of Os-RP loading on the performance of the biosensor was first evaluated and the results were summarized in Figure 2.3a. The loading mass of GOx and GA both were fixed, the loading amount of Os-RP was evaluated from 0.1 to 0.6 μg. As seen in Figure 2.3a, as the redox polymer loading in the membrane was increased, the oxidation current of glucose rose rapidly at first, but then leveled off at ~0.50 μg. It was observed that the oxidation current of

glucose is practically independent of the redox polymer loading beyond 0.50 μg, suggesting that the mediating power of Os-RP reaches its maximum at this quantity. In addition to the detrimental effect on the background current, too high an Os-RP loading may also adversely affect its mediating power. Therefore, 0.50 μg Os-RP was chosen for all subsequent experiments. The oxidation current of glucose is now determined by either the enzymatic oxidation or the diffusion of glucose. Figure 3b describes the dependence of the oxidation current of glucose on the loading of GOx in the Os-RP/GOx membrane. As anticipated, the GOx loading had a profound effect on the oxidation current of glucose.

The loading mass of Os-RP and GA were both fixed, the loading amount of GOx was evaluated from 10 to 100 μg. As illustrated in Figure 2.3b, when the GOx loading was increased from 10 to 50 μg, the oxidation current increased sharply, due to the increase in the enzymatic oxidation rate, because the reaction rate of a catalytic process generally scales up with the catalyst, GOx in this case. The highest current was attained when 50 μg of GOx was loaded on the biosensor. A further increase in GOx loading did not result in any appreciable increase in the oxidation current. On the contrary, being a natural insulator, it was found that the oxidation current decreases when an excessive amount of GOx was loaded. For example, a ~50% drop in the oxidation current was observed when 100 μg of GOx was loaded onto the biosensor, probably due to a drastically reduced electron exchange rate between the Os-RP/GOx membrane and the substrate GCE, since GOx itself does not exchange electrons with the substrate electrode. On the contrary, the presence of the large excess of GOx in the membrane severely impedes (blocks) the

electron exchange pathways between the redox polymer and the substrate GCE. Therefore, the amount of GOx loaded onto the biosensor was fixed at 50 μg to ensure sufficiently high sensitivity and good signal-to-noise ratios.

### 2.3.3 Analytical Performance of the Biosensor

The performance of the proposed biosensor was investigated through a calibration and interference study. The correlation between the amperometric response and glucose concentration was studied in a series of glucose solutions in PBS under optimized experimental conditions. The interference study was carried out in PBS that contained 5 mM glucose, 0.1 mM ascorbic acid, or/and 0.2 mM uric acid, which are all in the normal ranges that exist in human blood.[147]

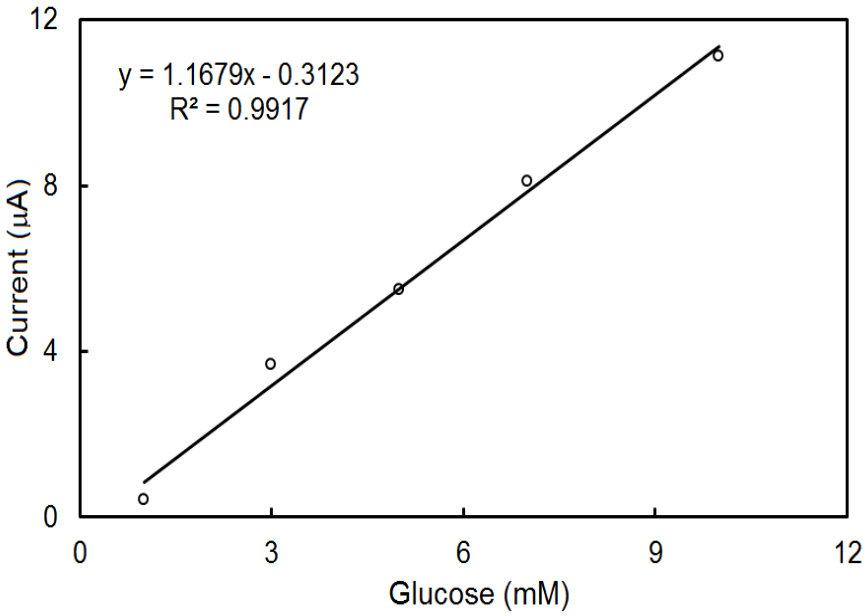


**Figure 2.4.** Calibration curve of the Os-RP/GOx/GCE glucose biosensor. Supporting electrolyte: PBS, poised potential: 0.25 V.

Under the optimized experimental conditions, a linear correlation between the oxidation current in amperometry and the glucose concentration was found between 0 and 10 mM at the Os-RP/GOx/GCE glucose biosensor with a correlation coefficient ($R^2$) of 0.992 and a detection sensitivity of 16.5 μA $mM^{-1}$ $cm^{-2}$ (Figure 2.4). In this concentration range, glucose is the limiting factor in the reaction and GOx is in excess. Above 10 mM the current increased at a much lower rate and it eventually started to level off beyond 15 mM. As all the active sites on the enzyme were fully saturated and operating at a maximum speed at 40 mM, any further increase in glucose concentration beyond 40 mM did not appreciably increase the catalytic oxidation current.

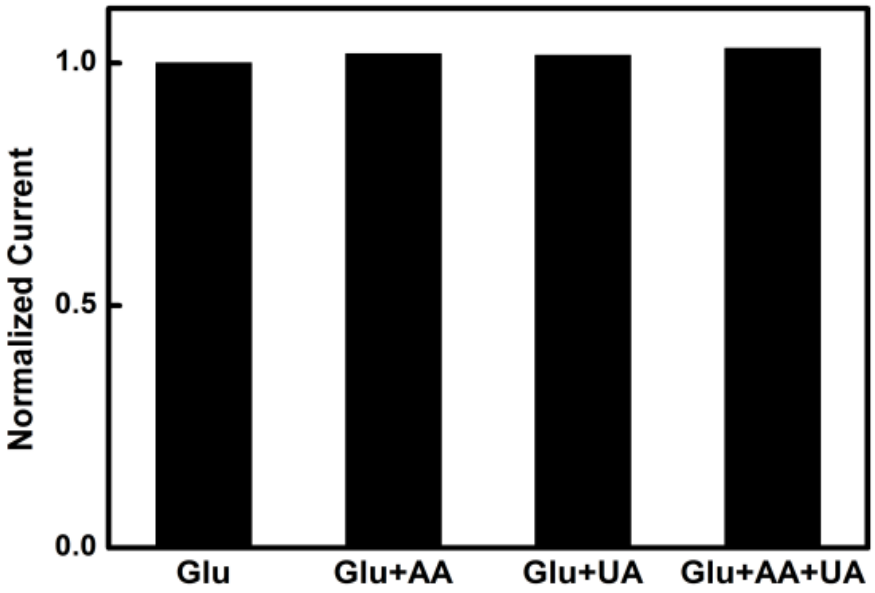


**Figure 2.5.** Normalized amperometric responses of 5 mM glucose, 5 mM glucose + 0.1 mM AA, 5 mM glucose + 0.2 mM UA and 5 mM glucose + 0.1 mM AA + 0.2 mM UA, respectively. Supporting electrolyte: PBS, poised potential: 0.25 V.

Because of their low redox potentials,[148, 149] ascorbic acid and uric acid are the common redox active interferants in blood when detecting blood glucose

using the amperometric method. In the absence of an analyte-regulating mechanism, the electrochemical oxidations of anionic ascorbic acid and uric acid were disproportionately high since the redox polymer used was usually polycationic.[150, 151] This is due to the accumulation of anionic interferants within the redox polymer scaling with the density of cationic sites. The introduction of a high density of sulfonic acid groups into the redox polymer is expected to result in a marked improvement of the performance of the biosensor in terms of selectivity. To confirm this hypothesis, the anti-interference ability of the proposed glucose biosensor was studied in a 5 mM glucose solution in the presence of 0.1 mM AA and 0.2 mM UA. As shown in Figure 2.5, the presence of AA and UA contributed less than 5% to the overall oxidation current. This is mainly due to the presence of a high density of anionic sulfonic acid groups in the redox polymer. Strong electrostatic repulsion between sulfonic acid groups and the AA and UA greatly suppress the access of these anionic species to the biosensor.

As mentioned earlier, depending on the kinetics of the mediated glucose oxidation, dissolved molecular oxygen may affect the sensitivity of the biosensor. In the proposed biosensor, the introduction of the high density of anionic sulfonic acid moieties in the redox polymer made the Os-RP/GOx membrane highly hydrophilic, which efficiently facilitates electron transfer and effectively suppresses the transport of molecular oxygen as molecular oxygen is largely hydrophobic, granting the biosensor good insensitivity to dissolved molecular oxygen. Indeed, a difference smaller than 2% was observed between the amperometric responses of 5.0 mM glucose solution before and after thorough purging with nitrogen. The engagement of the

anionic redox polymer in the construction of the glucose biosensor allows glucose to be selectively determined by the biosensor at its maximal sensitivity. In practice, this level of selectivity satisfactorily meets the requirement for the quantification of glucose in human blood samples. The only drawback of this biosensor was the relatively low mechanic strength.

## 2.4. Conclusion

In this work, an enzymatic amperometric glucose biosensor was fabricated by using an anionic $Os(bpy)_2$-based redox polymer as a mediator. The analytical signal of the biosensor was directly generated from the catalytic oxidation of glucose in the sample. This contributes to the high sensitivity of this biosensor and sets it apart from other glucose sensors that relying on indirect measurements of glucose through dissolved molecular oxygen or hydrogen peroxide. A linear dynamic range between 0 and 10 mM glucose with excellent sensitivity was obtained. More notably, the biosensor showed high anti-interference ability. Practically no interference from the common coexisting species such as dissolved molecular oxygen, ascorbic acid, and uric acid were observed. As compared to other approaches, the much enhanced selectivity and sensitivity are attractive features for further study, particularly in the development of miniature implantable glucose biosensors.

# Chapter 3. An interference-free glucose biosensor based on a novel low potential redox polymer mediator

## 3.1 Introduction

As mentioned in *Section 1.2.3.2*, one of the strategies to eliminate interferences from the mediated oxidation of glucose is to operate the glucose biosensor at a low enough applied potential so as not to provoke interfering reactions from the interferants. Using this strategy, Nam and co-workers showed that when $[Ru(NH_3)_6]^{3+}$ was used as the mediator, it allowed the use of a relatively low applied potential of 0.0 V(vs. Ag/AgCl) and could effectively eliminate interferences from AA, DA, UA, and AMP.[76] Following this argument, if one could design a mediator-based glucose biosensor which operates at even lower applied potential, the contribution to the oxidation current from undesirable interferants can be further reduced or may even be completely eliminated.

In this report, the feasibility of developing an interference-free amperometric glucose biosensor which can mediate enzymatic oxidation of glucose at a considerably low potential was investigated. A novel water-soluble and crosslinkable ruthenium complex-tethered redox polymer (Ru-RP) was first successfully synthesized. Excellent electron mediating power between GOx and substrate electrode at -0.15 V (vs. Ag/AgCl) was observed when the Ru-RP was crosslinked with GOx on a glassy carbon electrode (GCE). In addition to its high sensitivity and fast response time, the biosensor was practically immune to all potential interferants commonly encountered in glucose monitoring. This superior interference-free property was achieved

through the use of an ultralow applied potential which would not provoke interferences from other easily oxidizable species. Moreover, the excellent mediating power of the Ru-RP and the hydrophilic nature of the membrane also effectively retarded the interference from molecular oxygen.

## 3.2 Experimental

### 3.2.1 Reagents and appratus

GOx (EC 1.1.3.4, from *Aspergilus niger*, 191 units $mg^{-1}$) was purchased from Fluka (CH-9407 Buchs, Switzerland). Hexaammineruthenium(III) chloride [$Ru(NH_3)_6Cl_3$] was from Strem Chemicals (Newburyport, MA, USA). All other chemicals of certified analytical grade were obtained from Sigma-Aldrich (St. Louis, MO, USA) and used without further purification. Glucose stock solutions were allowed to mutarotate for 24 h before use. Freshly prepared AA, DA, UA, and AMP solutions were used in the interference study. All electrochemical studies were carried out in pH 7.4 PBS (20 mM phosphate, 0.15 M NaCl). All aqueous solutions were prepared with ultrapure deionized water (18.3 ΩM).

Electrochemical measurements were performed with a CHI650D electrochemical workstation (CH Instruments, Austin, Texas). A conventional three-electrode system comprising a GCE (3 mm in diameter) working electrode, an Ag/AgCl reference electrode, and a platinum wire counter electrode, was employed in all electrochemical experiments. All potentials reported in this work were referred to the Ag/AgCl reference electrode. Electrochemical impedance experiments were conducted with an IM6

electrochemical workstation (Zahner Elektrik, Germany). UV-vis spectra were recorded on an Agilent Cary 60 UV-vis spectrophotometer (Agilent Technologies, Palo Alto, CA, USA). Molecular weight was determined through high performance gel permeation chromatography (GPC) in water and standard poly (ethylene oxide) was used for calibration.

### 3.2.2. Preparation of the redox polymer

The copolymer backbone [poly (vinylpyridine-co-acrylamide), PVPAA] was synthesized according to a published procedure.[152] The Ru-RP was prepared according to the following procedure: 50 mg of PVPAA and 50 mg of $Ru(NH_3)_6Cl_3$ were dissolved in 4 mL of mixture solvent (ethylene glycol:water 1:1, v/v). The mixture was refluxed for 3 h at 80-90°C. Upon cooling, the reaction mixture was centrifuged. To a rapidly stirred acetone, the supernatant was added drop-wise to precipitate the redox polymer. Further purification was carried out by treating the precipitated redox polymer with multiple water-dissolving acetone-precipitating cycles. The purified product was then dried under vacuum at 50°C. Typical yields were between 55 and 90%.

### 3.2.3. Preparation of the biosensor

A GCE was polished on a microcloth with 0.3 and 0.05 μm alumina slurry sequentially and sonicated for 5 min in water and ethanol between each polishing step. Upon drying, 5 μL of a mixed solution containing 3 μL Ru-RP, 1 μL GOx, and 1 μL glutaraldehyde (GA) was applied onto the cleaned

electrode. The electrode was kept under ambient conditions for at least 12 h. During this period of time, an irreversible crosslinking reaction took place and formed the desired glucose sensing membrane on the GCE. The glucose biosensor was stored at 4°C when not in use.

## 3.3 Results and discussion

### 3.3.1. Synthesis and characterization of the Ru-RP

As depicted in Figure 3.1A, vinylpyridine in the copolymer affords the availability of the pyridine ring which allows subsequent N-coordination with the redox active ruthenium complex; while acrylamide offers good chemical and mechanical stability and resistance to microbial degradation and serves as a support matrix.[153] The amide group present in acrylamide also allows chemical crosslinking with GA to enhance the stability of the enzyme in the glucose sensing membrane. Figure 3.1B shows the synthesis route for the Ru-RP. Results from GPC showed a monomodal elution peak for the Ru-RP. This provided the first hint of a successful synthesis and that Ru-RP was a copolymer rather than blends of two homopolymers. The weight-average molecular weight (Mw) of the redox polymer was found to be 53,200 and the polydispersity index (PDI) was 1.56. Ruthenium loading in the Ru-RP, determined from elemental analysis, was found to be ~14%. To further confirm the formation of the Ru-RP, FT-IR and UV-vis experiments were carried out. As shown in Figure 3.2A, the FT-IR spectrum of the Ru-RP clearly showed the complete disappearance of vinyl absorption at 1650 $cm^{-1}$ and this suggests that the vinyl monomers were successfully polymerized and

the resulting redox polymer was of high purity and free of monomers. Further evidence can be found in the 400-500 $cm^{-1}$ region. The weak absorption at 444 $cm^{-1}$ indicates the presence of ruthenium-pyridine bond in the Ru-RP. This absorption peak is in addition to the pyridine-ammine absorption peak at 466 $cm^{-1}$ found in the FT-IR spectra of both the Ru-RP and $Ru(NH_3)_6Cl_3$. UV-vis spectra (Figure 3.2B), again, confirmed the successful synthesis of the Ru-RP. Firstly, the UV-vis spectrum of the Ru-RP indicates that it is not a simple blend of its two starting materials, PVPAA and $Ru(NH_3)_6Cl_3$. Secondly, the UV-vis spectrum of the Ru-RP displays a more intense d → π* metal-to-ligand charge-transfer (MLCT) band associated with the pyridine ring at 540 nm and a less intense intraligand, π → π*, electronic transition at 375 nm and both of which are consistent with the proposed structure of the Ru-RP.

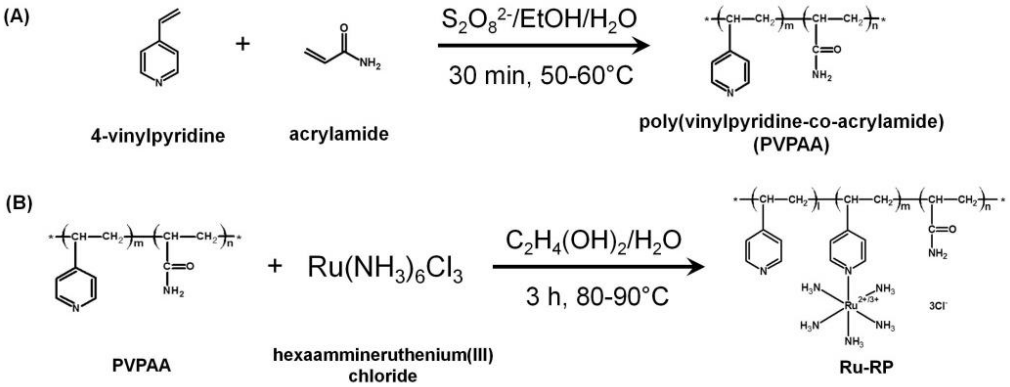


**Figure 3.1.** (A) Reaction scheme of the PVPAA backbone. (B) Synthetic route of the Ru-RP.

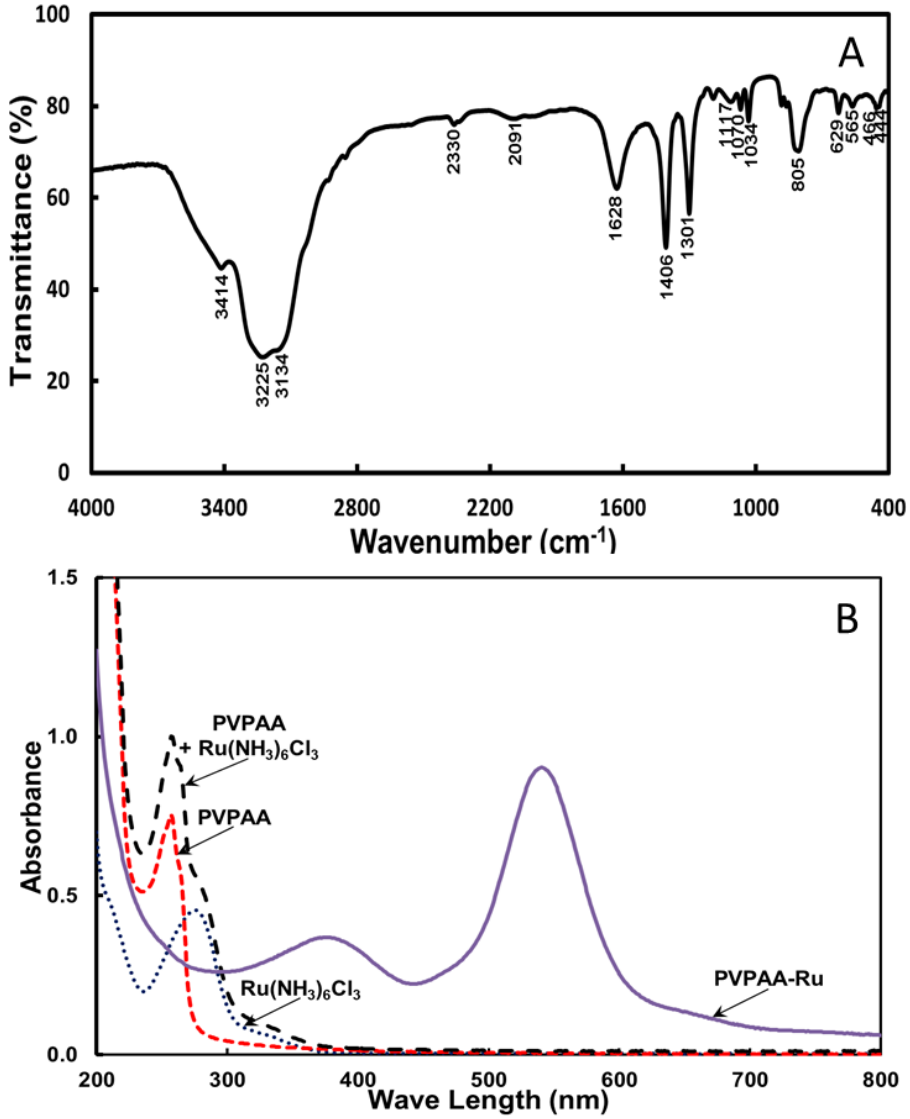


**Figure 3.2.** (A) The FT-IR spectrum of the Ru-RP. (B) UV-vis spectra of the Ru-RP, PVPAA, $Ru(NH_3)_6Cl_3$, and PVPAA + $Ru(NH_3)_6Cl_3$.

### 3.3.2. Electrochemical characteristics of the biosensor

The operating principle of the biosensor is based on the enzymatic oxidation of glucose catalyzed by GOx (Figure 3.3). Due to the presence of GOx, glucose in solution is first enzymatically oxidized to gluconolactone and leaving behind two electrons. These two electrons are accepted by the redox center (FAD) of GOx to return to its reduced state. The electro-oxidized Ru-RP ($Ru^{3+}$) then reacts with the reduced GOx and accepts the aforementioned

electrons to become electroreduced Ru-RP ($Ru^{2+}$) and regenerating the oxidized GOx. Finally, the electrons are transferred from $Ru^{2+}$ to the substrate GCE and an oxidation current is generated when $Ru^{2+}$ returns to its oxidized state $Ru^{3+}$.

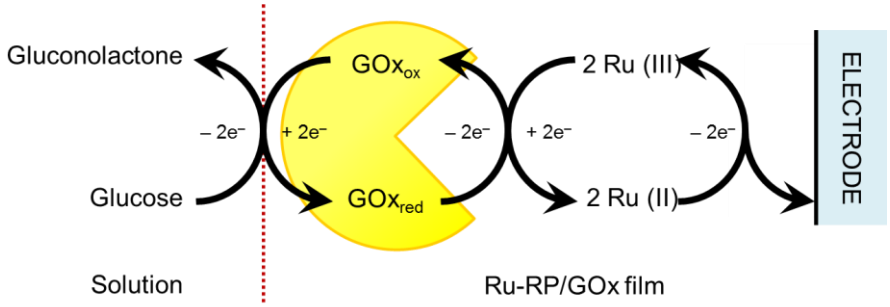


**Figure 3.3.** Schematic illustration of the working principle of the glucose biosensor.

Figure 3.4 trace 2 presents the cyclic voltammogram of the biosensor in PBS in the absence of glucose. A pair of well-defined current peaks which centered at -0.28 V was observed and this could be attributed to the reversible transformation between $Ru^{2+}$ and $Ru^{3+}$ of the Ru-RP. It can be further observed that due to the successful attachment of the copolymer backbone (PVPAA), Ru-RP displayed a noticeably different electrochemical behavior from that of its starting material, $Ru(NH_3)_6Cl_3$, since a pair of reversible voltammetric peaks which centered at -0.14 V were obtained for the latter instead (Figure 3.4 trace 1). In addition, since the magnitudes of the anodic and cathodic peak currents for Ru-RP were similar and their peak-to-peak potential separation was close to the theoretical value of 59 mV at 25°C, this provided further evidence that the electron transfer process between the Ru-RP/GOx membrane and the substrate electrode is rapid and diffusion-controlled.[143] This is most likely due to the relatively thick membrane coated

on the electrode surface.[144] Based on the rapid kinetics and symmetry of the reduction and oxidation peaks, it could also be inferred that GOx does not noticeably affect the electrochemistry of the $Ru^{2+}/Ru^{3+}$ redox couple in the Ru-RP/GOx membrane.

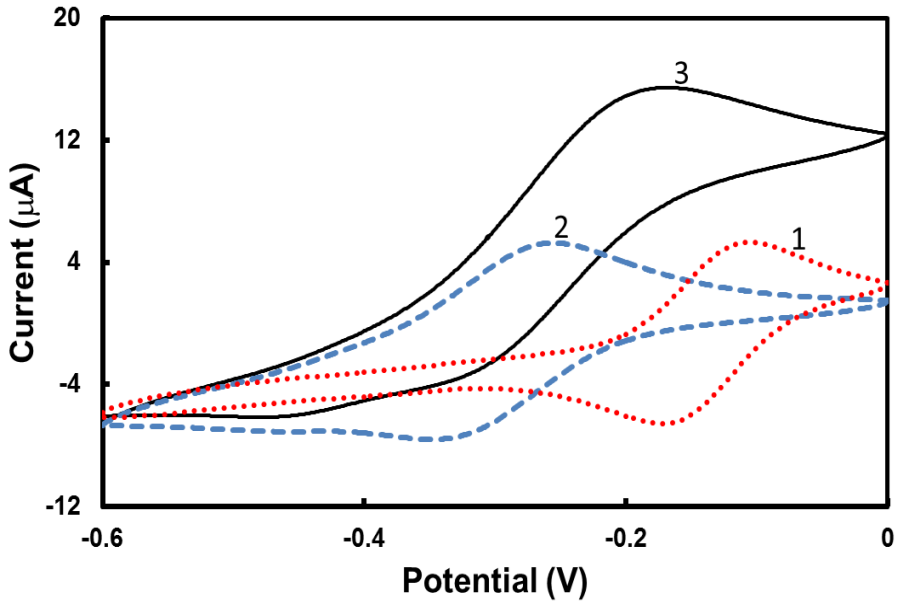


**Figure 3.4.** Cyclic voltammograms of (1) $Ru(NH_3)_6Cl_3$, and a glucose biosensor in the absence (2) and presence (3) of 8 mM glucose. Supporting electrolyte: PBS, potential scan rate: 50 mV/s.

When glucose was added to the PBS, a typical sinusoidal electrocatalytic cyclic voltammogram (Figure 3.4 trace 3) was observed with a greatly increased oxidation current and a severely diminished reduction current. The absence of the reduction current peak in the voltammogram implies that at a scan rate of 50 mV $s^{-1}$, the glucose sensing layer is homogeneously maintained in the reduced state by the rapid electron transfer from the reduced GOx to the oxidized Ru-RP ($Ru^{3+}$) sites and to the substrate GCE. Indeed, the $Ru^{2+}/Ru^{3+}$ moieties in the Ru-RP/GOx membrane could serve as artificial electrons donors and compete effectively with molecular oxygen in the oxidation of

glucose by rapidly shuttling electrons between GOx and the substrate electrode to generate a current signal.

For amperometric determination of glucose, the choice of the applied potential has to be a compromise between sensitivity and selectivity. While increasing the applied potential increases the driving force between the enzyme and the mediator which subsequently increases the current density and sensitivity, it has to be noted that the applied potential has to be decreased in order to maximize selectivity by minimizing the current contribution from the oxidation of endogenous species such as AA, DA, UA, and AMP. Therefore, the applied potential has to be poised on the anodic side of the current peak and in the vicinity of the peak potential in order to strike the right balance between sensitivity and selectivity. Considering all of the above, the applied potential for all amperometric measurements was poised at -0.15 V (vs. Ag/AgCl) as the voltammogram peaking off from approximately -0.20 V onwards. The response time, which is the time required to reach 90% of the maximum response, was found to be within 10 s.

The proposed biosensor was characterized by electrochemical impedance spectroscopy (EIS). A semicircle was observed for bare GCE, as shown in the Nyquist plots in Figure 3.5. The diameter of the semicircle slightly diminished for the GCE that modified with the glucose sensing membrane. Fitting results showed that the charge transfer resistance ($R_{ct}$) of the bare GCE and modified GCE were 792.9 Ω and 719.6 Ω, respectively. Thus, the crosslinked sensing membrane did not retard the electron transfer between the redox centers of the redox polymer and the substrate electrode.

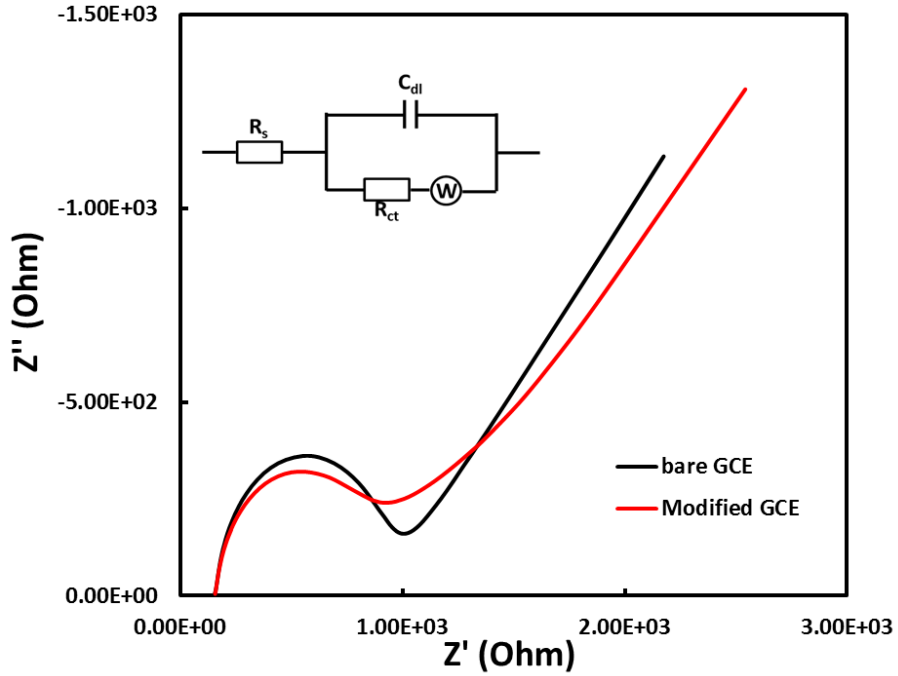


**Figure 3.5.** Nyquist plots of a bare GCE and a modified GCE. Inset: Randles equivalent circuit.

### 3.3.3. Optimization of the biosensor

Since the proposed biosensor system capitalized on the catalytic reaction between the Ru-RP and GOx, for a successful application in glucose monitoring, the oxidation current has to be associated with the concentration of glucose in a straightforward manner. This implies a simple linear relationship between glucose concentration and oxidation current is sought and that the loading amount of the Ru-RP and GOx must be sufficiently large. Since GOx is immobilized on the GCE through chemical crosslinking between GOx and the Ru-PR by GA. Certainly, GA also plays an important role in achieving an optimum immobilized membrane on the electrode surface with maximum catalytic efficiency. Therefore, in order to enhance the performance of the biosensor, the formulation of the glucose sensing membrane was optimized.

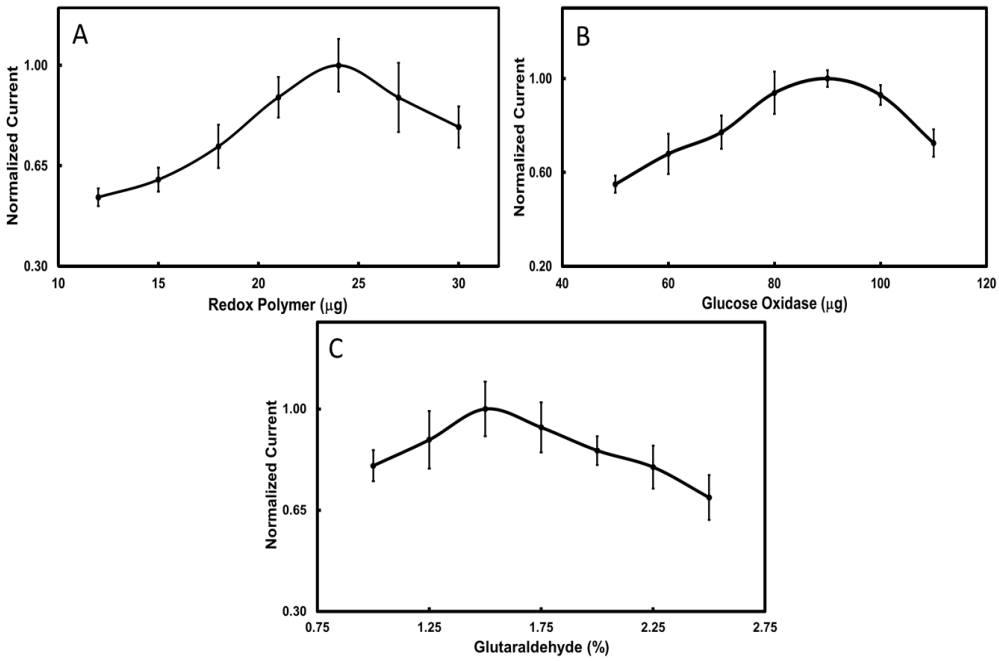


**Figure 3.6.** The effect of (A) the Ru-RP, (B) GOx, and (C) GA loading on the amperometric response of 10 mM glucose. Supporting electrolyte: PBS, poised potential: -0.15 V.

The effect of the Ru-RP loading on the response was first studied in the range of 12-30 μg (Figure 3.6A). Meanwhile, the loading amount of GOx was fixed at 50 μg, and GA 1.25% (w/v). The current response increased with increasing Ru-RP loading from 12 to 24 μg. The response reached a maximum at 24 μg and then decreased when the loading amount of Ru-RP was higher than 24 μg. This suggested that the mediating power of the Ru-RP has reached its maximum at 24 μg and further increase in the Ru-RP loading could adversely affect the membrane permeability for both glucose and gluconolactone. Therefore, 24 μg of the Ru-RP was chosen in the following experiments in order to maximize the sensitivity of the biosensor.

The dependence of the oxidation current on the loading of GOx is shown in Figure 3.6B. In this case, Ru-RP was fixed at its optimal value 24 μg, and GA

1.25% (w/v). The highest response current was observed when 90 μg GOx was loaded in the membrane and further increase of GOx loading even decrease the oxidation current. This could be due to the insulating nature of the enzyme which reduces the electron exchange rate between the sensing membrane and the substrate GCE and impedes the electron exchange pathways between the Ru-RP and the substrate GCE when excess amounts of GOx are loaded onto the GCE.

Finally, the concentration of the GA was investigated and the results are depicted in Figure 3.6C by fixing the loading amount of Ru-RP and GOx to 24 μg and 90 μg, respectively. The oxidation current increased with an increase of GA loading and reached a maximum at 1.5% (w/v) GA. Thereafter, further increase in GA loading beyond 1.5% resulted in a decrease in the oxidation current resulting from the increased diffusion resistance caused by excessive crosslinking. In addition, when excess amounts of GA were loaded onto the electrode, the activity of GOx was also adversely affected due to excessive crosslinking.

### 3.3.4. Analytical performance of the biosensor

The analytical performance of the biosensor was evaluated through calibration and interference studies. It was found that under the optimized experimental conditions, the oxidation cur-rent in amperometry at -0.15 V gave a good linear correlation ($R^2$= 0.9962) with glucose concentration from 0 to 10 mM and with a sensitivity of 24.3 μA $mM^{-1}cm^{-2}$ (Figure 3.7A). In this concentration range, glucose was the limiting factor in the reaction while GOx

existed in a large excess and a simple linear relation-ship between glucose concentration and the oxidation current was achieved. However, the oxidation current increased at a slower rate above 10 mM and eventually leveled off beyond 15 mM. This is probably due to the saturation of active sites of GOx in the membrane since a finite amount of GOx is loaded and any furtherincrease in glucose concentration would not give any appreciable increase in the oxidation current. Nevertheless, given that a typical healthy blood glucose concentration would be between 4.4 and 6.6 mM, this linear dynamic range of the biosensor was more than sufficient to quantify at both the higher and lower ends of the healthy blood glucose concentration levels. The detection limit, estimated as three times of the standard derivation of the background, was found to be 0.29 mM. The apparent Michaelis–Menten constant $K_m$, frequently used to evaluate the biological activity of immobilized enzyme, could be calculated according to the Lineweaver–Burk equation $1/i = (K_m/i_{max})(1/C) + 1/i_{max}$, where i is the current, $i_{max}$ is the maximum current, and C is the glucose concentration.[154, 155] The Lineweaver–Burk plot of 1/i vs.1/C is shown in Figure 3.7B. Based on the Lineweaver–Burk plot, the KMapp was calculated to be 11.1 mM. Since $K_m$ characterizes the enzyme electrode instead of the enzyme itself and that this value is close to that reported for the free enzyme (12.4 mM),[156] the calculated apparent Michaelis–Menten constant $K_m$ illustrates the non-denaturating characteristic of the enzyme immobilization process.

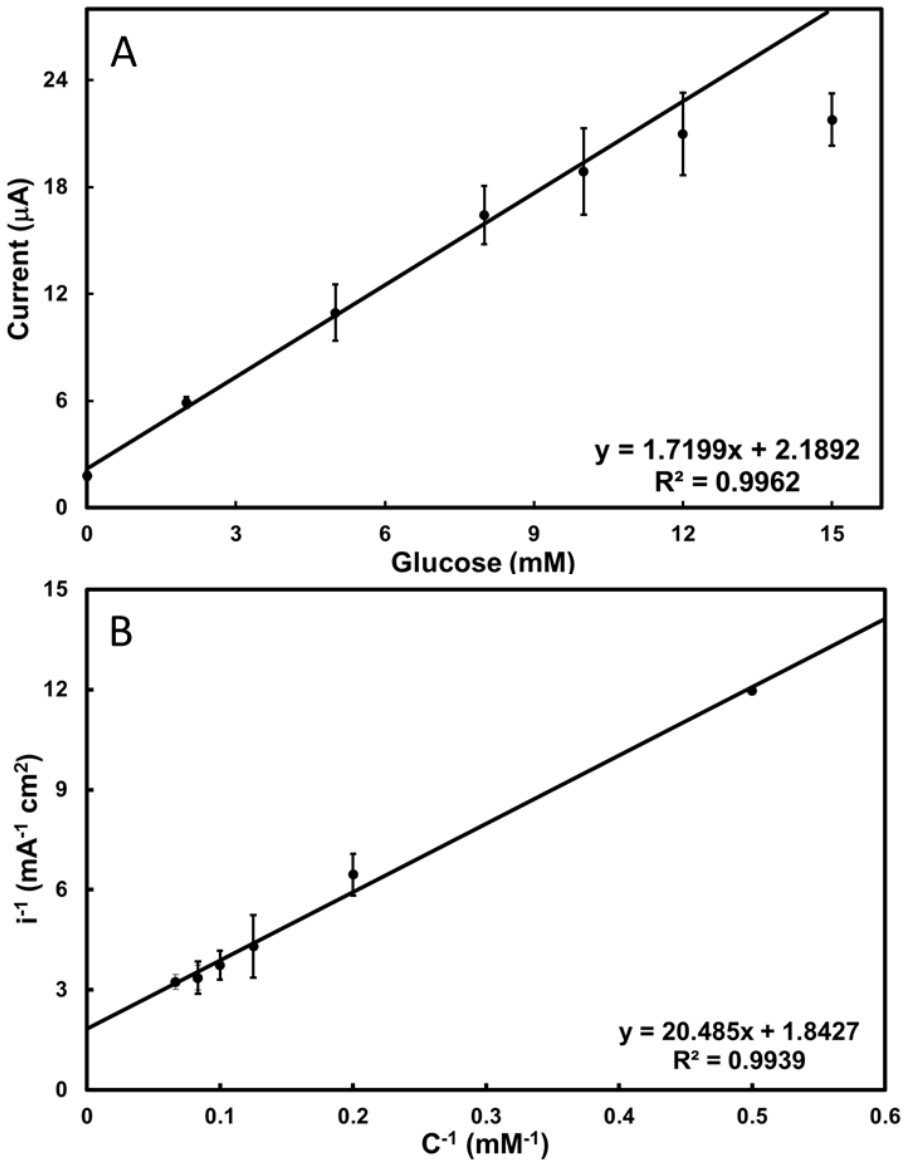


**Figure 3.7.** (A) Calibration curve of the glucose biosensor. Supporting electrolyte: PBS, poised potential: -0.15 V. (B) The Lineweaver–Burk plot of the biosensor at -0.15 V.

It is worth mentioning that this newly developed glucose biosensor exhibits prominent electrocatalytic performance for glucose sensing in terms of the linear range, limit of detection (LOD), and sensitivity compared to those previously reported mediators, as listed in Table 3.1. This outstanding electrocatalytic performance is largely attributed to the crosslinked membrane

which displays an excellent catalytic activity toward the oxidation of glucose by shuttling electrons rapidly between GOx and the substrate GCE.

One of the main challenges in glucose analysis is the elimination of interference response generated by some endogenous species such as AA, DA, and UA. These potential interferences were studied with respect to their normal physiological levels found in human blood. It was found that the presence of 0.1 mM AA, 0.5 μM DA, and 0.5 mM UA contribute only 1.9, 0.9, and 2.0% to the overall oxidation current of 5 mM glucose, respectively; while a mixture of 0.1 mM AA, 0.5 μM DA, and 0.5 mM UA contributed only 4.9% to the total oxidation current of glucose. This extremely low level of interference observed is mainly due to the ultralow operating potential of -0.15 V which almost fully eliminates the oxidation current contribution from undesirable interferants.

**Table 3.1.** Comparison of the analytical performance of the glucose sensor based on novel Ru-RP mediator and other mediators.

| Mediator | Operating potential (V) | Linear range (mM) | LOD (mM) | Sensitivity (μA $mM^{-1}$ $cm^{-2}$) | Reference |
|---|---|---|---|---|---|
| Os-complex | 0.00 | 0-0.7 | 0.0003 | 28.24 | [75] |
| $Os(2,2'bpy)_2$-RP | 0.25 | 0-10.0 | - | 16.5 | [157] |
| 1,1'-di-methylferrocene | 0.205 | 1.0-30 | - | 6.63 | [50] |
| Ferrocene | 0.35 | 0.1-10.0 | 0.13 | 12.42 | [158] |
| $[Ru(NH_3)_6]^{3+}$ | 0.00 | 0-27.7 | - | - | [76] |
| $Ru_3(\mu_3\text{-}O)(AcO)_6(Py)_3(ClO_4)$ | 0.00 | 0.01-0.5 | - | 15.4 | [159] |
| $Ru(trpy)(phen)(OH_2)]^{2+}$ | 0.52 | - | - | - | [37] |
| *trans*-$[Ru(2,2'bpy)_2(OH_2)(OH)]^{2+}$ | 0.50 | 0-24.0 | - | 0.4 | [37] |
| $[Ru(4,4'bpy)(NH_3)_5]^{2+}$ | 0.24 | 0-5.6 | - | 7.2 | [37] |
| Ru-RP | -0.15 | 0-10.0 | 0.29 | 24.3 | This work |

Furthermore, a common drug, AMP, was previously reported to be an interferant in glucose measurements.[160] The psychological level of AMP in blood is between 0.066 and 0.2 mM and it is believed that the diffusion of AMP across a porous membrane to the electrode surface will produce an interfering current[161] due to the oxidation of the free phenolic hydroxyl group present in AMP.[162] Nevertheless, at the upper limit of 0.2 mM, AMP only contributed to 1.8% of the total oxidation current. Such a low level of interferences, again, was mainly due to the ultralow operating potential of -0.15 V.

As mentioned previously, molecular oxygen present in blood can lead to the natural enzymatic oxidation of glucose by taking away electrons from the enzyme and resulting in a lower oxidation current observed in the biosensor. Nonetheless, oxidation of the reduced GOx by molecular oxygen still occurs in the presence of mediator in most cases as oxygen is always freely diffusing in blood and test solution. This could pose a limit on the accuracy of the biosensor, particularly at low glucose levels. Therefore, in order to achieve a highly selective glucose biosensor, there is a need to suppress the oxygen interference. It was found that the presence of acrylamide moieties in the Ru-RP renders the crosslinked membrane highly hydrophilic which improved the glucose/oxygen permeability ratio by effectively retarding the diffusion of molecular oxygen. Less than 0.5% difference was observed between the oxidation current of 5 mM glucose in PBS before and after thorough purging with nitrogen gas. Obviously, this negligible effect from molecular oxygen is likely attributed to the excellent mediating power of the Ru-RP and the largely retarded oxygen diffusion within the sensing membrane.

**Table 3.2.** Determination of glucose concentration in fruit juice samples.

| Juice sample | Measured (g/L) | Relative error (%, n = 3) | *Reference (g/L) | Recovery (%) |
|---|---|---|---|---|
| Apple | 83.4 | 5.2 | 85.8 | 97.2 |
| Blackcurrant | 33.7 | 12.5 | 31.0 | 108.7 |
| Guava | 29.6 | 7.8 | 25.9 | 114.3 |
| Mango | 46.8 | 7.5 | 45.8 | 102.2 |
| Orange | 38.4 | 10.1 | 39.6 | 97.0 |

* Reference glucose concentrations were obtained by using a commercial TRUEbalance™ blood glucose monitoring system produced by Nipro Diagnostics, Inc.

In order to verify the reliability of this newly developed glucose biosensor for routine analysis, the biosensor was employed to determine the glucose concentration in real samples like fruit juices and blood. However, because of the tight safety and ethical regulations governing the use of real blood samples, a commercially available control solution (synthetic blood from Roche Diagnostics) for glucose meters which contains several basic components that mimic human blood was employed in this study instead. The results, as listed in Tables 3.2 and 3.3, indicate that this newly developed glucose biosensor can be utilized for practical sample testing as desirable accuracy, precision, and recovery are obtained.

**Table 3.3.** Determination of glucose concentration in synthetic blood samples.

| Sample | Measured (mM) | Relative error (%, n = 3) | Reference (mM) | Recovery (%) |
|---|---|---|---|---|
| 1 | 3.51 | 7.5 | 3.41 | 102.9 |
| 2 | 5.42 | 5.1 | 5.69 | 95.3 |
| 3 | 7.76 | 8.5 | 7.97 | 97.4 |

## 3.4 Conclusion

In this report, we demonstrated an interference-free glucose biosensor can be constructed by a one-step crosslinking of the ruthenium complex-based

low-potential redox polymer with GOx. As expected, the newly developed glucose biosensor exhibited negligible responses toward all commonly observed interferants in glucose detection. And a good linear correlation between the oxidation current and the glucose concentration up to 10 mM was obtained. These attractive characteristics will open new opportunities in the development of miniature biosensors for continuous blood glucose monitoring.

# Chapter 4. Detection of glucose with a lamellar-ridge architecture gold modified electrode

## 4.1 Introduction

Nanocrystallized gold is one of the most widely studied materials due to their unique catalytic properties, efficient electron transfer performance, and good biocompatibility.[163-166] For example, gold-based nonenzymatic glucose sensors are of great interest, due to their intimate connection with the worldwide public health problem diabetes mellitus and other applications.[167-170] Unlike macrocrystallized metal electrodes with unsatisfying sensitivity,[171] gold nanograins exhibit great electrochemical activities derived from their high density of edge-plane-like defective sites and large specific surface areas.[172] However, these nanocrystallized gold particles are usually randomly scattered or aggregated, which makes it difficult to ensure the utmost catalytic active surfaces to interact with reactants. Obviously, it is also impossible to precisely describe the mass transport behavior that plays an irreplaceable role in electrochemical reactions.[173-175] So manipulating these nanograin building blocks into three-dimensional architecture and optimizing the mass transport process is highly required in order to enhance and even modulate the sensing performance.[176, 177]

Various efforts, such as electrostatic interactions and asymmetric functionalization of nanoparticle surfaces,[178-180] have been devoted to assemble individual particles into controllable architectures with limited success. In contrast, biological systems from nature form sophisticated

configurations from macro-, micro- to nano-sizes which provide a large structural pool for architecture design.[181] Recent biotemplated and biomimetic strategies include using DNA,[180] bacteria,[182] virus cages,[183] or ordered protein assemblies[184] have been utilized to synthesize and assemble metal nanograin architectures; however, those biological templates are easily curved or agglomerated themselves.[185] Thus, searching for a biological template which is both rigidly constructed and elaborate in micro/nano-scale for nanograin assembly is of great significance. By precise morphology control, we can investigate to what extent the architecture impacts on electrochemical performance and explore what arrangement is effective for sensing applications.

Having been evolving for over 250 million years, the beauty and variety of butterfly wings can hardly be matched by any other species in nature. Nearly 20,000 types of butterflies are identified solely by the patterns or colors of their wings, which comprise scales with different complex microarchitectures.[181, 186-188] This provides a great template warehouse for nanograin assembly and for the architecture design of efficient electrochemical sensors. In this work, we chose the blue scales from *Morph* butterfly wings, whose brilliant color derives from their lamellar-ridge architecture, as a template to synthesize lamellar-ridge architectured gold (*lamellar ridge*-Au) using an electroless deposition method.[189] Its unarchitectured counterpart flat gold (*flat*-Au) was also synthesized as a control using the flat wing membrane as template under the conditions. By simply modifying as-prepared *lamellar ridge*-Au on a glassy carbon electrode with Nafion, a sensitive nonenzymatic glucose sensor with good selectivity

and stability was developed. The lamellar-ridge architecture arrangement showed great promise for electrochemical sensing with enhanced sensitivity and lower detection limit compared to its unarchitectured counterpart. Finite element modeling and simulation were also carried out to analyze the mass transport behavior in the lamellar-ridge architecture and to illustrate the architecture assisting effect in mass transport.

## 4.2 Experimental

### 4.2.1 Reagents and apparatus

Tetrachloroaurate hydrate was purchased from Sigma-Aldrich (St. Luis, MO, USA). Tartaric acid, sodium borohydride, and other chemicals for gold preparation were all obtained from Sinopharm Group Co., Ltd. Nafion 117 solution, glucose, uric acid, and ascorbic acid were obtained from Sigma-Aldrich. All other chemicals of certified analytical grade were obtained from Sigma-Aldrich and used as received. All aqueous solutions were prepared with ultrapure deionized water (18.3 MΩ).

The morphology of *lamellar ridge*-Au was examined under low vacuum field emission scanning electron microscope (LV FESEM, NOVA NanoSEM 230) operated at 5 kV. The composition was verified by X-ray diffraction (XRD) using an X-ray diffractometer (D8 ADVANCE) with Cu Kα radiation. The surface condition was examined by X-ray photoelectron spectroscopy (XPS, AXIS UltraDLD) using Al Kα radiation as the X-ray source. Thermal gravimetric analysis (TGA) was carried out on a thermo gravimetric analyzer (Pyris 1, PerkinElmer) from room temperature to 800 °C with a heating rate of 10 °C/min to obtain the net content of gold in the as-synthesized samples.

All electrochemical experiments were performed with a CHI760D electrochemical workstation (CH Instruments, Austin, TX, USA) at room temperature (25°C). A conventional three-electrode system, comprising a GCE working electrode modified with gold samples, an Ag/AgCl reference electrode, and a platinum wire counter electrode, was employed. All potentials reported in this work were referred to the Ag/AgCl reference electrode.

### 4.2.2 Preparation of gold samples

Blue scales of *Morph* butterflies were used as templates for the preparation of *lamellar ridge*-Au. The synthetic process is depicted in Figure 4.1. The butterfly wing samples were first immersed in 10 vol% nitric acid for 1 h followed by washing with deionized water. Then, the samples were aminated by socking in ethanolic solution of ethanediamine (25 vol%) for 6 h followed by washing with ethanol. After dried in air, the aminated samples were then immersed in aqueous solution of $HAuCl_4$ (0.2 wt%) for 3 h to allow gold adsorption. After washing with deionized water, the samples were then immersed into 0.1 M aqueous solution of $NaBH_4$ for 120 s to reduce the bound gold into gold nanoparticles. The surface functionalized templates were achieved after washing with deionized water and dried in air. Further gold deposition was achieved by immersing the gold nanoparticle functionalized templates into electroless plating solution for 15 min in 25 °C. After the deposition, the gold-coated scales were removed from the membrane and collected for further detemplating process to obtain *lamellar ridge*-Au. The gold-coated membrane was also collected for *flat*-Au. The as-prepared gold-coated scales and gold-coated membrane were treated in phosphoric acid at

room temperature for 72 h to remove the bio-templates. These samples were then further washed with absolute ethanol and collected by centrifugation and dried at 60°C for 12 h.

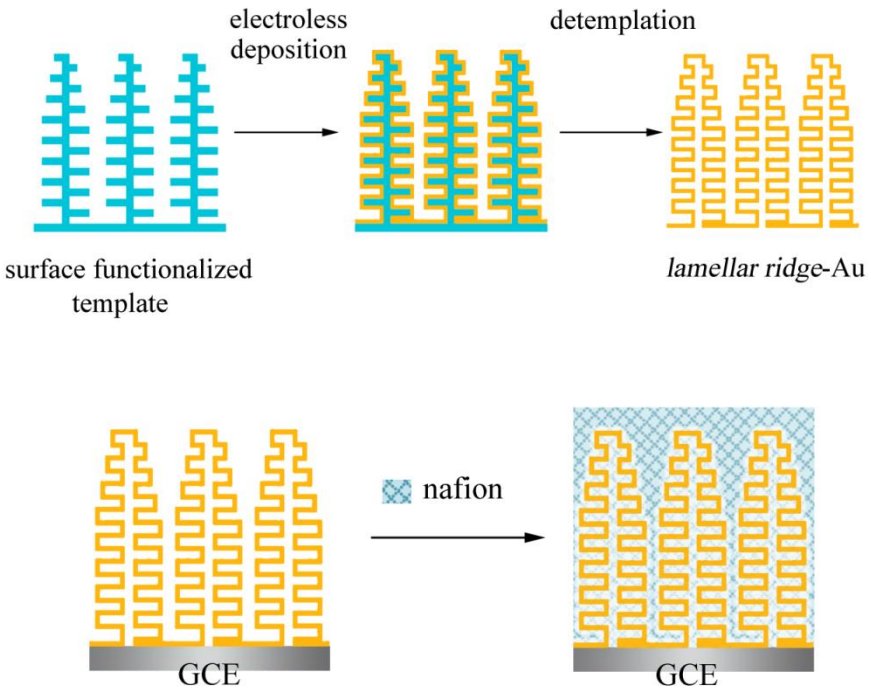


**Figure 4.1.** Schematic diagram for the fabrication of lamellar ridge-Au and the preparation of the corresponding biosensor.

### 4.2.3 Glucose sensor fabrication

A GCE (3-mm diameter) was sequentially polished on a microcloth with 0.3- and 0.05-μm alumina slurry and sonicated in water and ethanol between each polishing step. The as-synthesized gold samples were dispersed in deionized water by sonication (1 mg/ml), and then a 5-μl drop of the suspension was cast on the freshly cleaned electrode. After drying under ambient conditions, 4 μl of 0.5 wt% Nafion solution in ethanol/water (1:2, volume ratio) was further dropped on the electrode surface forming a thin coating on gold samples after solvent evaporation.

### 4.2.4 Cyclic voltammetric and amperometric experiment

Cyclic voltammetry was conducted in 0.5 M $H_2SO_4$ at a scan rate of 50 mV/s to determine the electrochemical active surface area (*EASA*) of the modified electrodes. The electrocatalytic behavior of the modified electrode was investigated by cyclic voltammetry in 0.1 M NaOH containing 5 mM glucose at 50 mV/s. Amperometric detection of glucose was conducted at a constant potential of 0.21 V (vs. Ag/AgCl).

### 4.2.5 Finite element simulation

Finite element modeling and simulation were conducted with Comsol Multiphysics 4.2 software from CnTech using a diffusion domain approach.[190] Glucose concentration profiles were portrayed to investigate the mass transport behavior in the electrode architecture.

## 4.3 Results and discussion

### 4.3.1 Architecture and composition characterization

As shown in Figure 4.2, the delicate lamellar-ridge architecture of *Morph* butterfly-scale was successfully duplicated by the electroless deposition. After removing the template, the final architecture of as-synthesized gold was hollow lamellar ridges with a thickness of ~27 nm. The ridge height of *lamellar ridge*-Au was ~1.7 μm and the distance between ridges was ~650 nm. Each ridge was substructured by 7–8 lamellae staggeringly-patterned on either side of the ridge stem with a lamellar distance of ~120 nm.

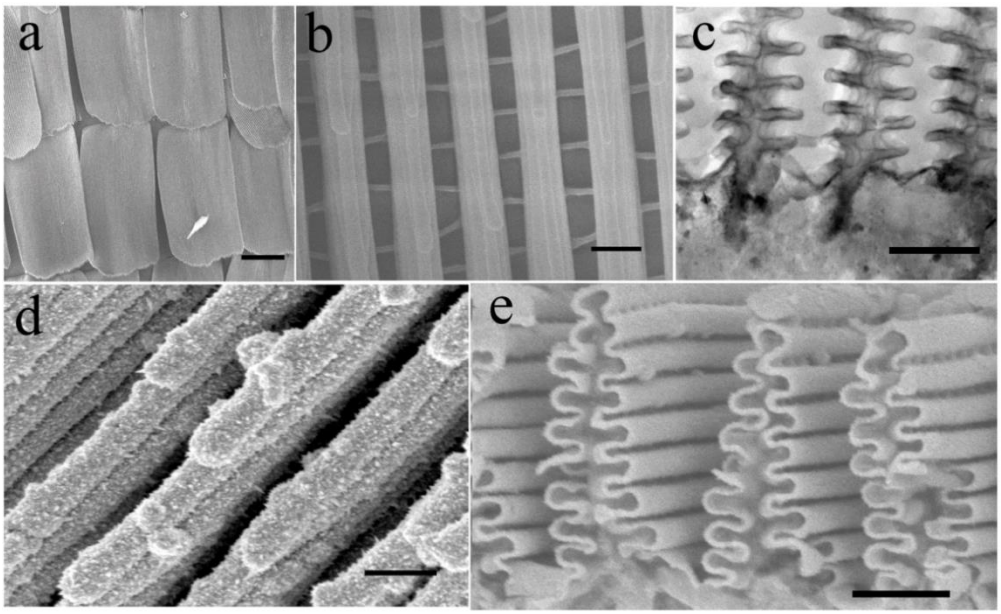


**Figure 4.2.** Microarchitectures of original Morph butterfly scale template and as-synthesized lamellar ridge-Au. (a, b) FESEM image of the scale template, (c) TEM image showing the cross-sectional view of lamellar-ridge architecture of the original scale template, and (d, e) FESEM images showing the front and cross-sectional views of lamellar ridge-Au. Scale bar: 50 μm for (a), 500 nm for (b–e).

According to XRD patterns in Figure 4.3a, both *lamellar ridge*-Au and *flat*-Au exhibited a typical face-centered cubic lattice structure. The grain size, calculated by the Williamson-Hall method, was 7.3 nm and 7.5 nm for *lamellar ridge*-Au and *flat*-Au, respectively. XPS experiments were then conducted to characterize their surfaces. The spectra indicated that both *lamellar ridge*-Au and *flat*-Au exhibit similar surface conditions. As shown in Figure 4.3b, the doublet at 83.5 eV and 87.2 eV correspond to Au $4f_{5/2}$ and $4f_{7/2}$, respectively.[191] The 3.7 eV splitting of each doublet, corresponding to the spacing between $4f_{5/2}$ and $4f_{7/2}$ levels, confirmed the presence of gold in zero valent oxidation state.[192, 193] From the TGA results after detemplation, the net content of gold was 88% and 87% for lamellar ridge-Au and flat-Au, respectively, suggested that both samples contain a small quantity of residual templates (Figure 4.4).

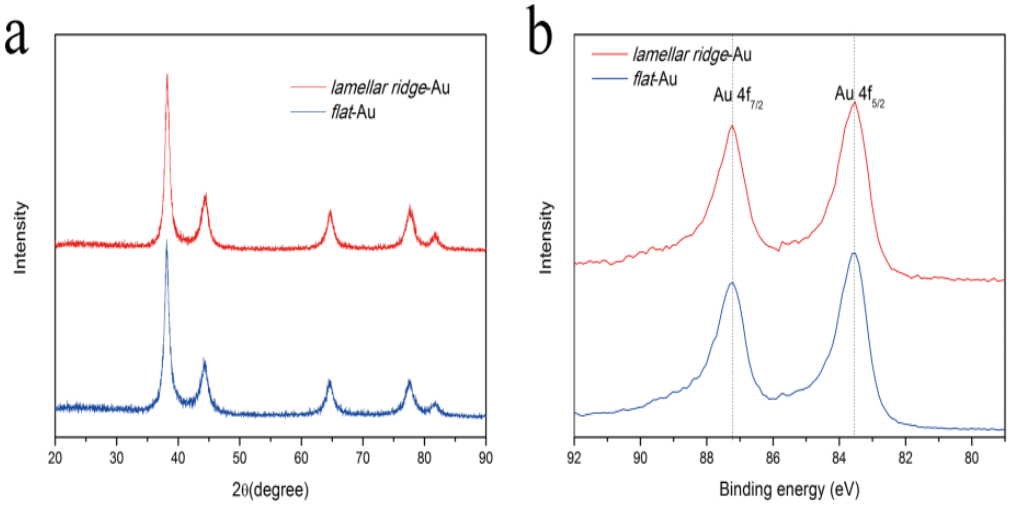


**Figure 4.3.** Composition characterization for lamellar ridge-Au and flat-Au. (a) XRD patterns and (b) XPS spectra.

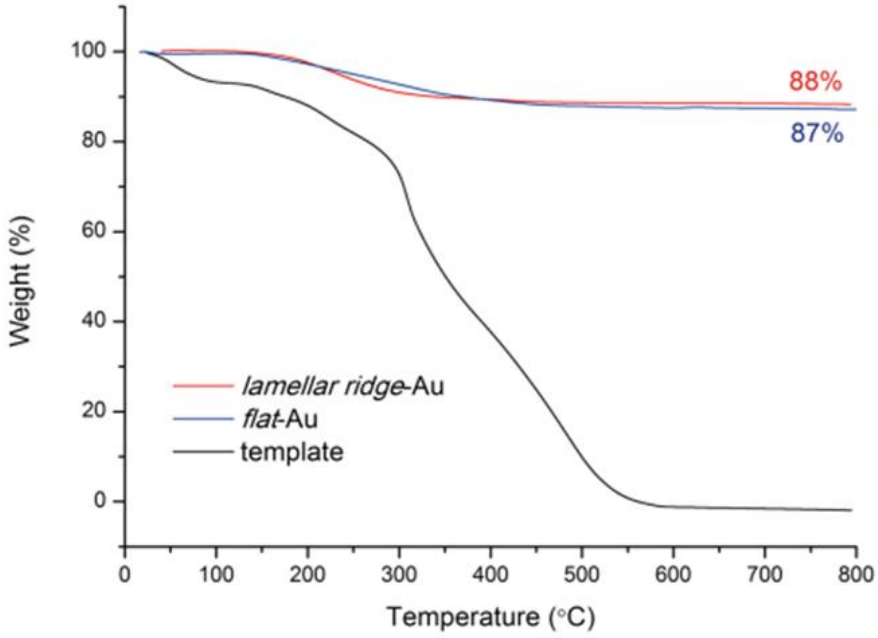


**Figure 4.4.** Thermal gravimetric analysis of lamellar ridge-Au, flat-Au, and butterfly wing template.

### 4.3.2 Electrochemical examination

The *EASA* of the as-prepared gold modified electrodes was determined from the charge of the reduction of an oxide monolayer in the cathodic sweep of the

cyclic voltammograms in 0.5 M $H_2SO_4$ (Figure 4.5a), based on a reported charge density of 420 μC/cm$^2$.[168, 194] The *EASA* for *lamella ridge*-Au modified electrode was estiminated to be 23.8 $m^2/g_{Au}$, which was 4.8 times higher than its unarchitectured counterpart (5.0 $m^2/g_{Au}$). The electrocatalytic behavior for glucose was investigated by cyclic voltammetry in 0.1 M NaOH with 5 mM glucose at a scan rate of 50 mV/s (Figure 4.5b). In the positive scan, a current bump around -0.35V was observed, which is due to glucose electrosorption forming the gluconolactone intermediate.[167, 195] As the potential was swept more positively, AuOH formed on gold surfaces by the partial discharge of $OH^-$, and consequently catalyzed the oxidation of glucose.[196] The corresponding anodic peak was at 0.21 V for *lamellar ridge*-Au, which was 30 mV more negative than that of *flat*-Au (0.24 V). The peak current density was 0.87 mA/cm$^2$ for *lamellar ridge*-Au, which was 5.4 times that of *flat*-Au (0.16 mA/cm$^2$), indicating great elevation for glucose oxidation. The current density dropped at higher potentials because of the formation of gold oxides which lead to the decrease of AuOH sites and suppressed oxidation current.[167, 196] In the negative scan, the sharp increase of anodic current was due to the reduction of gold oxides and the regeneration of AuOH.

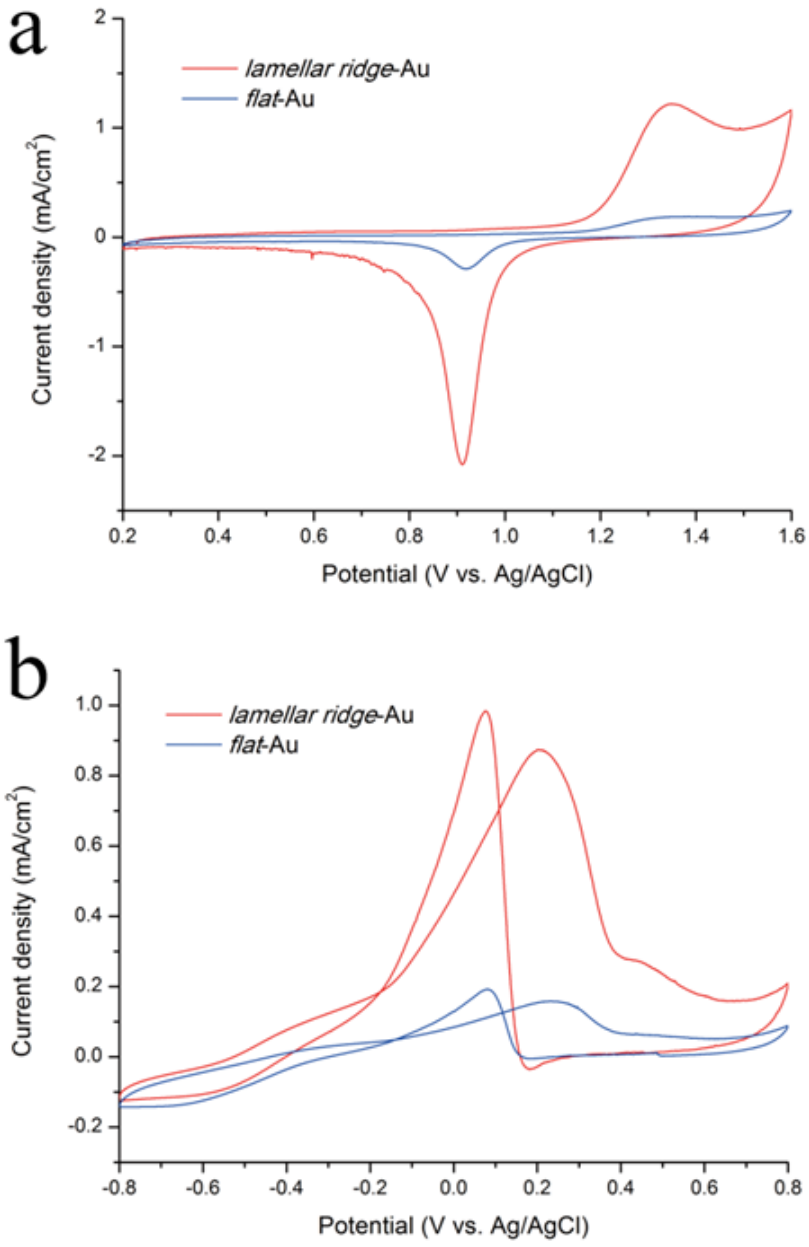


**Figure 4.5.** Cyclic voltammograms at 50 mV/s of *lamellar ridge*-Au and *flat*-Au biosensors in (a) 0.5 M $H_2SO_4$ and (b) 0.1 M NaOH containing 5 mM glucose.

### 4.3.3 Amperometric detection of glucose

Figure 4.6a shows the amperometric plot at the *lamellar ridge*-Au and *flat*-Au modified electrodes with successive addition of different quantity of glucose in 0.1 M NaOH solution at an applied potential of 0.21 V. It is

apparent that the response time was within 5 s to reach 95% of the steady-state current. The current response exhibited a good linear correlation with glucose concentration for both electrodes. As shown in Figure 4.6b, the linear range for the *lamellar ridge*-Au modified electrode was from 2 μM to 23 mM ($R^2$=0.996) with a sensitivity of 29.0 μA/(mM $cm^2$). The detection limit, estimated as three times of standard derivation of background levels, was found to be 0.87 μM. As a comparison, the linear range for the unarchitectured counterpart (*flat*-Au) was from 20 μM to 23 mM ($R^2$=0.998) with a sensitivity of 5.0 μA/(mM $cm^2$) and a detection limit of 3.26 μM. Considering the same composition, grain size, and surface conditions for both *lamellar ridge*-Au and *flat*-Au, it is apparent that the 5.8 times increase of sensitivity and 3.7 times decrease of detection limit should solely originate from the lamellar-ridge architecture arrangement. It is also worth noting that architecture effect was more impressive at the lower concentrations of linear range, where mass transport efficiency is pivotal for the performance of the modified electrode,[197] whereas the saturation of active sites play an important role at higher concentrations of the linear range.

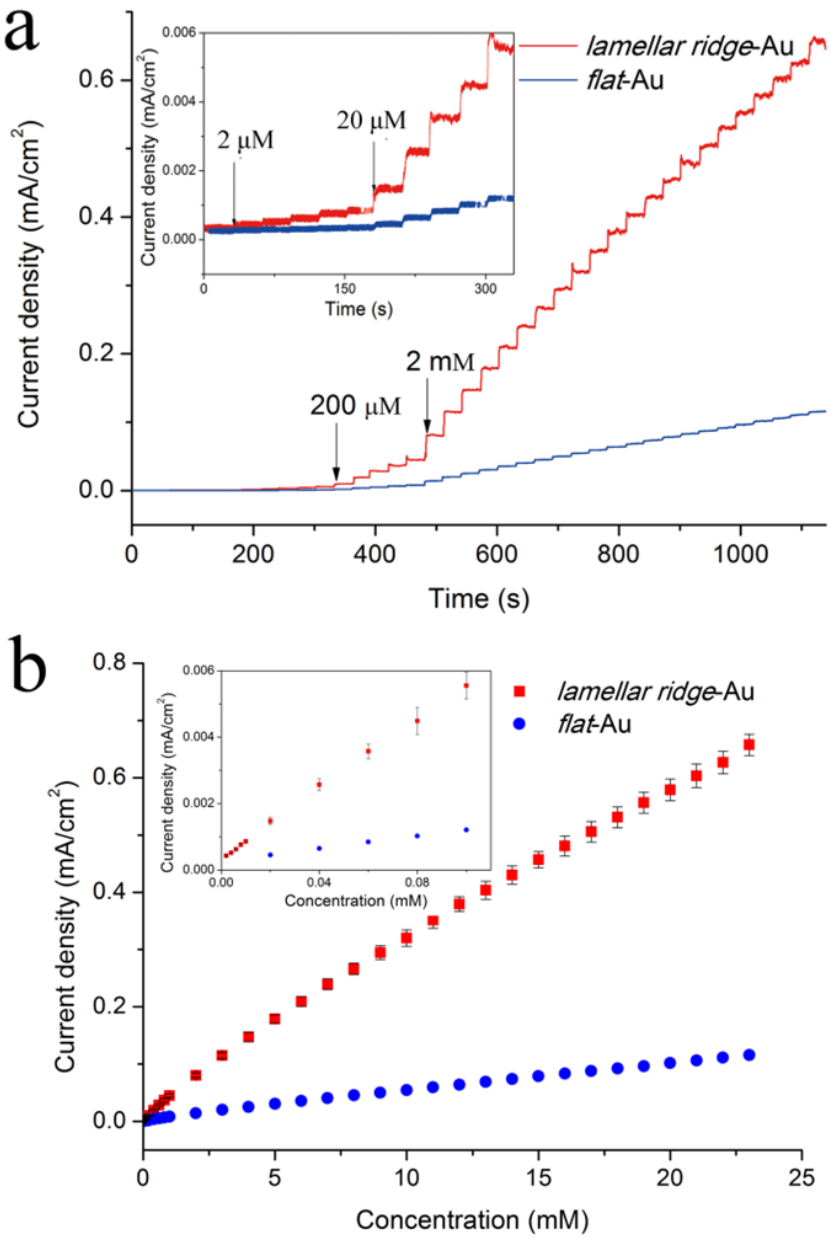


**Figure 4.6.** (a) Amperometric responses and (b) the corresponding calibration curves for lamellar ridge-Au and flat-Au biosensors to the successive addition of glucose from 2 μM to 23 mM. Poised potential: 0.21 V.

Moreover, the *lamellar ridge*-Au modified electrode also showed good selectivity for glucose detection. As shown in Figure 4.7, the addition of 0.1 mM UA and 0.1 mM AA at normal physiological level contributed only 2.3% to the overall current of 5 mM glucose. The reason is two-fold. First, the low applied potential of 0.21 V minimizes the responses of UA and AA;[196] second,

the negatively charged Nafion coating effectively blocks the access of UA and AA to the electrode surface.[198-200]

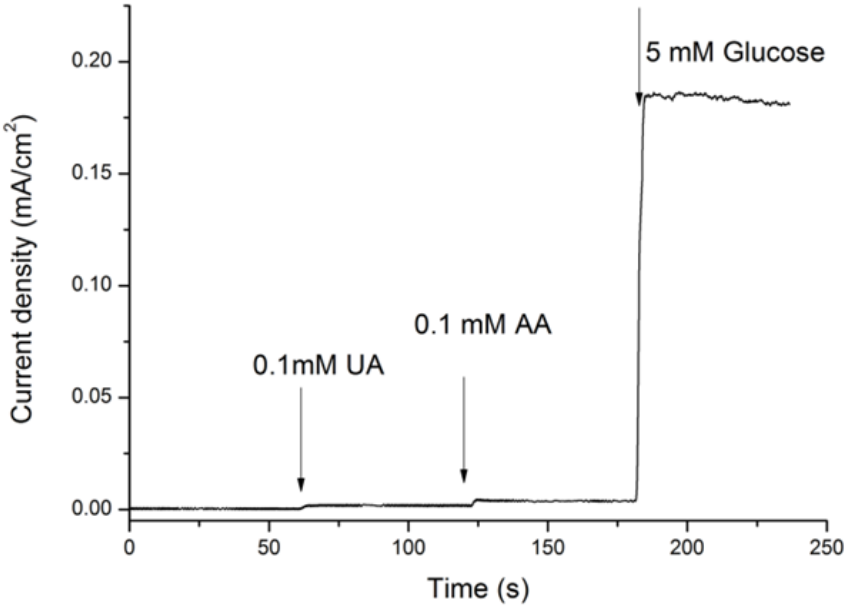


**Figure 4.7.** Amperometric response to the successive addition of 0.02 mM uric acid and 0.1 mM ascorbic acid interfering compounds, as well as 2 mM glucose, for lamellar ridge-Au biosensor.

In order to verify the reliability for routine analysis, a commercial synthetic blood from Roche Diagnostics for glucose meters was employed in this study. The synthetic blood was diluted 20 times by 0.1 M NaOH before testing. As listed in Table 4.1, desirable accuracy, precision, and recovery were obtained.

**Table 4.1.** Determination of glucose concentration in mimic blood samples.

| Sample | Measured (mM) | Relative error (%, n = 4) | Reference (mM) | Recovery (%) |
|---|---|---|---|---|
| 1 | 16.83 | 7.0 | 17.01 | 98.6 |
| 2 | 10.43 | 4.4 | 10.24 | 101.9 |
| 3 | 8.22 | 2.1 | 7.96 | 103.3 |

### 4.3.4 Mass transport analysis

As discussed above, the 5.8 times increase of sensitivity was more significant than the 4.8 times increase of *EASA* for the *lamellar ridge*-Au modified electrode compared to *its flat*-Au counterpart, which indicates that the enhanced sensitivity should not be solely attributed to the increased *EASA*. As mentioned above, the architecture effect was more impressive at lower concentrations, thus suggesting notable influence from mass transport assisting effect.[197] Here, a lamellar-ridge architectured model was built for finite element simulation using a diffusion domain approach with a one-ridge period as a domain unit.[190] Glucose concentration profiles were portrayed to investigate the mass transport behavior in the electrode architecture. As shown in Figure 4.8, compared to the simple one-direction planar diffusion of the unarchitectured model, the lamellar-ridge arrangement showed a more efficient diffusion behavior, characterized by a zigzag route which is a brilliant unimpeded approach to access the catalytic surface efficiently.[175] Moreover, the trapping and depleting of electrolyte between adjacent lamellae also greatly promoted diffusion efficiency via thin layer effect, which is of great importance in promoting electrochemical reaction.[201, 202] In fact, thin layer diffusion is most frequently discussed in carbon nanotube (CNT) modified electrodes. However, electron transfer promotion by CNT is also essential in those systems. On the contrary, by constructing the elaborate lamellar-ridge architecture and flat two-dimensional structure, this work gives a clear answer to the architecture (diffusion) contribution. Furthermore, the negative shift in anodic peak for the *lamellar ridge*-Au modified electrode in Figure 4.5b also verified the diffusion effect. Unlike simple planar diffusion for the

unarchitectured sample,[203] small volume of glucose trapped between the adjacent lamellae became significantly depleted on the voltammetric timescale leading to more efficient current rising and dropping.[204]

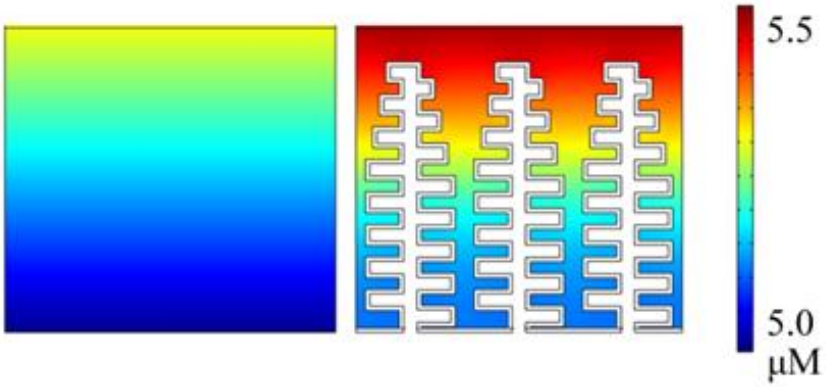


**Figure 4.8.** Reactant concentration profiles at t = 100 s in the simulation process for lamellar ridge-Au and flat-Au models.

This methodology can be extended to other butterfly-scale architectures or even to other natural configurations for more comprehensive investigation of different architecture effect, which may provide an efficient approach for designing and selecting effective architectures for electrochemical sensors. For example, gold samples with inverse-V ridge architecture and ridge/nano-hole architecture have been synthesized in our laboratory. This strategy may also be extended to other catalytic materials such as platinum, carbon, ceramic oxides, and so forth to obtain more efficient electrochemical reactions.

## 4.4 Conclusion

In summary, we synthesized gold samples with lamellar-ridge architecture templated by blue scales from *Morph* butterfly wings using an electroless deposition method. Benefiting from the elaborate structural arrangement, the

*lamellar ridge*- Au modified electrode exhibited prominent performance for glucose sensing in terms of linear range, sensitivity, and detection limit. Compared to its unarchitectured counterpart, the electrochemical active surface area and the sensitivity for the detection of glucose were dramatically increased by 4.8 and 5.8 times, respectively, The lamellar-ridge architecture also lowered the detection limit by 3.7 times to 0.87 μM. Besides increased electrochemical active surface area, this significant promoting behavior is also attributed to the unique zigzag mass transport property and efficient thin layer diffusion effect in the lamellar-ridge architecture. This work demonstrated the architecture effect on electrochemical detection of glucose, and presented an exemplary strategy of using the vast configuration pool from nature to blueprint the structural design of efficient electrochemical sensors.

# Chapter 5. A highly sensitive electrochemical methyltransferase activity biosensor

## 5.1 Introduction

In this work, a simple and highly sensitive electrochemical biosensor for DNA MTase activity measurement was described. DNA cytosine MTase and methylation sensitive restriction endonuclease HpaII (recognizes the duplex symmetrical sequence 5'-C/CGG-3') were selected in the biosensor. In addition, a synthetic threading intercalator, N,N'-bis(3-propylimidazole)-1,4,5,8-naphthalene diimide (PIND) functionalized with electrocatalytic redox $Os(bpy)_2Cl^+$ moieties (PIND-Os), was employed for signal amplification. PIND-Os strongly and selectively binds to double-stranded DNA and catalyzes the oxidation of ascorbic acid at a relatively low potential of 0.22 V (vs. Ag/AgCl), thus resulting in the high sensitivity of the MTase activity biosensor.

## 5.2 Experimental

### 5.2.1 Reagents and apparatus

M.SssI CpG methyltransferase (M.SssI MTase) supplied with 10 x NEBuffer 2, restriction endonuclease HpaII supplied with 10 x CutSmart buffer, HaeIII methyltransferase (HaeIII MTase), AluI methyltransferase (AluI MTase) and S-adenosyl-L-methionine were purchased from New England Biolabs (Ipswich, MA). 5-azacytidine (5-Aza), 5-aza-2'-deoxycytidine (5-Aza-dC), and 6-mercapto-1-hexanol (MCH) were from Sigma-Aldrich (St.

Louis, MO, USA). Tris(hydroxymethyl)aminomethane (Tris), tris(2-carboxyethyl)phosphine hydrochloride (TCEP) were obtained from Alfa Aesar (Lancashire, England). PIND-Os (Scheme 5.1) was synthesized according to a published procedure.[205] Reverse-phase high performance liquid chromatography-mass spectrometric test showed that the desired compound has been successfully synthesized and its purity was ~97%, as indicated by a single elution peak and a molecular weight of 1560. Also, various spectroscopic tests have confirmed its purity and intercalating properties. All other chemicals of certified analytical grade were used without further purification. All solutions were prepared with ultrapure water (18.3 MΩ). Oligonucleotides used in this work were custom-made by 1st Base Pte Ltd. (Singapore). The sequences of the oligonucleotides were as following: oligonucleotide 1 (oligo 1): 5'-HS-$(CH_2)_6$-AAT CTC AGT GAT TCA TCC GGA TAC AAG TAC TCT ATT GAC T-3' and its partially complementary oligonucleotide 2 (oligo 2): 5'-AGT CAA TAG AGT ACT TGT ATC CGG ATG AAT CA-3'. The two oligonucleotides were dissolved in TE buffer (10 mM Tris, 1 mM EDTA, pH 8.0) to the desired concentrations and stored at -20 ºC.

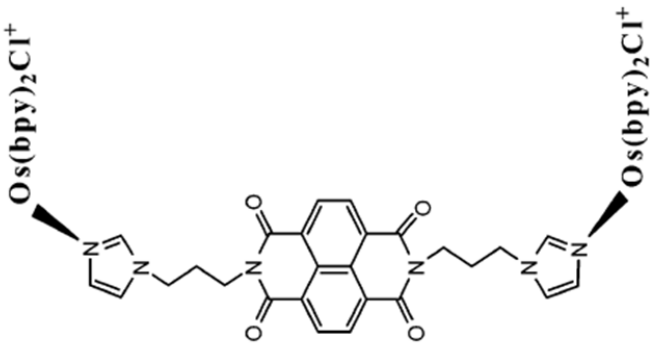


**Scheme 5.1.** Structure of the threading intercalator PIND-Os.

Electrochemical experiments including differential pulse voltammetry (DPV) and cyclic voltammetry (CV) were performed with a CHI 650D electrochemical workstation (CH Instruments, Austin, TX, USA). A conventional three-electrode system comprising of a gold working electrode, an Ag/AgCl reference electrode, and a platinum wire counter electrode, was employed in all electrochemical experiments. All potentials reported in this work were referred to the Ag/AgCl reference electrode. Electrochemical impedance spectroscopic experiments were conducted with an IM6 electrochemical workstation (Zahner Elektrik, Germany).

### 5.2.2 M.SssI MTase catalyzed DNA methylation event confirmation by gel electrophoresis

An oligonucleotide (oligo 3: 5'-AGT CAA TAG AGT ACT TGT ATC CGG ATG AAT CAC TGA GAT T-3') which is fully complementary with the thiolated oligo 1 was firstly hybridized with oligo 1 to form the ds-DNA. Then, a reaction mixture consisted of 4.0 μM ds-DNA, 160 μM SAM, 8 U CpG MTase (M.SssI) in 20 μL 1 x NEBuffer 2 was incubated at 37 ºC for 3 h to form the methylated DNA. After that 5 μL of methylated DNA sample was mixed with 20 μL 1 x CutSmart buffer that containing 5 U HpaII endonuclease, and then incubated at 37 ºC for another 3 h. The ds-DNA that only treated with HpaII was prepared by the incubation of a reaction mixture that consisting of 1.0 μM ds-DNA and 5 U HpaII endonuclease in 1 x CutSmart buffer. Subsequently, the samples were applied to a polyacrylamide gel (15%) to evaluate the efficiency of enzyme in 1 x TBE buffer at a constant voltage (150 V) for 2 h. The gel was silver-stained.

### 5.2.3 Double-stranded DNA and electrode preparation

Double-stranded DNA was prepared as follows: The mixture of the two oligonucleotides (1.0 μM each) and 1.0 mM TCEP was prepared in a hybridization buffer (10 mM Tris, 1.0 mM EDTA, 1.0 M NaCl, pH 7.4). The solution was then heated to 90 ºC and slowly cooled down to room temperature. The prepared ds-DNA stock solution (1.0 μM) was kept at 4 ºC when not in use.

The gold electrode was pretreated according to a reported procedure.[206] Briefly, the gold electrode was carefully polished on a microcloth with 0.3 and 0.05 μm alumina slurry sequentially, and followed by a period of 5 min sonication in ultrapure water. Then, electrochemical cleaning was performed in 0.2 M $H_2SO_4$ by applying an anodic potential of 2.0 V for 5 s, and thereafter a cathodic potential of -0.35 V for 10 s. Next, repetitive CV scans were conducted within a potential window between -0.3 and 1.55 V at a scan rate of 4 V/s (20 cycles) and 0.1 V/s (4 cycles) in 0.2 M $H_2SO_4$, respectively. Finally, the electrode was rinsed with copious amount ultrapure water and dried in a $N_2$ stream.

The immobilization of the ds-DNA to the gold electrode was performed by applying 2.5 μL of 1.0 μM ds-DNA on a freshly cleaned gold electrode surface and incubated for 4 h at 37 ºC. The electrode was then washed with wash buffer (10 mM Tris, pH 7.4) and ultrapure water sequentially to remove the non-specifically adsorbed ds-DNA. Subsequently, the electrode was treated with 1.0 mM MCH for 1 h to block the defective sites on the electrode and to obtain a well-aligned ds-DNA monolayer. The modification process was monitored by both DPV and EIS after each step. DPV was performed in

0.10 M $Na_2SO_4$ containing 5.0 mM $Fe(CN)_6^{3-/4-}$ (1:1 ratio) and within a potential window range of -0.2 to 0.6 V. EIS experiments were conducted in the same solution in the frequency range of 10 mHz to 100 kHz at the standard redox potential of the $Fe(CN)_6^{3-/4-}$ redox couples.

### 5.2.4 MTase activity detection

The ds-DNA coated electrode was first incubated with 2.5 μL 1 x NEBuffer 2 containing a specific concentration of M.SssI MTase, and 160 μM SAM at 37 ºC for 2 h to achieve the methylation at the CpG dinucleotide sites of the immobilized ds-DNA. After washing with NEBuffer 2 and drying, the electrode was then incubated with 2.5 μL 1 x CutSmart buffer containing 50 U/mL HpaII restriction endonuclease at 37 ºC for 2 h to allow the cleavage reaction to take place. After another round of washing with CutSmart buffer and drying, the electrode was incubated in 100 μg/mL PIND-Os aqueous solution for 10 min. Finally, after a thorough rinsing with PBS the AA electrooxidation current on the electrode was measured by cyclic voltammetry in PBS (20 mM phosphate, 0.15 M NaCl, pH 7.4) containing 5 mM AA.

### 5.2.5 Selectivity and inhibition investigation of the M.SssI MTase biosensor

To investigate the selectivity of the proposed M.SssI MTase biosensor, two other cytosine MTases, namely HaeIII MTase and AluI MTase, were selected as the potential interfering enzymes. The selectivity experiments were conducted with 100 U/mL MTase in the same way as the M.SssI activity

detection procedure, except for that M.SssI MTase was replaced by HaeIII/AluI MTase in the methylation step.

To further study the inhibitor screening ability of the proposed biosensor, the inhibition effect of 5-Aza and 5-Aza-dC on M.SssI MTase activity was carried out by incubating the ds-DNA coated electrode in 1 x NEBuffer 2 consisting of 120 U/mL M.SssI and 160 μM SAM with various concentrations of the inhibitors. After the HpaII digestion and PIND-Os intercalation steps as described above, the electrocatalytic oxidation current of AA was recorded on the inhibitor treated electrode. The relative activity of M.SssI MTase was estimated using the following equation:

$$\text{Relative activity (\%)} = \frac{I_2 - I_0}{I_1 - I_0} \times 100\ \%$$

where $I_0$ is the catalytic current of 0 U/mL M.SssI MTase, $I_1$ is the catalytic current of 120 U/mL M.SssI MTase and $I_2$ is the catalytic current after the inhibitor treatment.

## 5.3 Results and discussion

### 5.3.1 MTase activity biosensor principle

As schematically depicted in Figure 5.1, thiol-modified ds-DNA containing the specific M.SssI MTase and HpaII recognition sequence (5'-CCGG-3') is firstly immobilized on a gold electrode. After the methylation and digestion steps that catalyzed by M.SssI MTase and HpaII respectively, PIND-Os is inserted into the remaining ds-DNA. Finally, the electrode is brought into a phosphate buffer solution that contains ascorbic acid, and the electrocatalytic oxidation current of AA is recorded. According to the

procedure, HpaII endonuclease catalyzed cleavage of the immobilized ds-DNA will be blocked once the CpG dinucleotide site in the 5'-CCGG-3' sequence is methylated, the amount of the remaining ds-DNA after the HpaII cleavage is in principle proportional to the activity of M.SssI MTase. Thus, the catalytic oxidation current of AA directly reflects the methylation event and M.SssI MTase activity. It is worth to note that the oligonucleotides used in this work are designed in a way to minimize the background signal as much as possible. Oligo 2 is partially complementary to oligo 1, a relatively short segment of ds-DNA (9 base pairs) remains at the electrode after HpaII cleavage. Considering the low melting temperature (~24 ºC) of this short ds-DNA strand, it is expected to readily dehybridize under the restriction endonuclease incubation conditions, thus achieving a relatively low background signal. On the other hand, as little as a single layer of PIND-Os on the electrode surface is needed to generate maximal signal in the electrocatalytic oxidation of AA. As for the length of the ds-DNA, it should be long enough to hold up at least one monolayer equivalent of PIND-Os, but not too long to impede the ds-DNA immobilization efficiency. It was found that ds-DNA strands with 30-40 base pairs are sufficient.

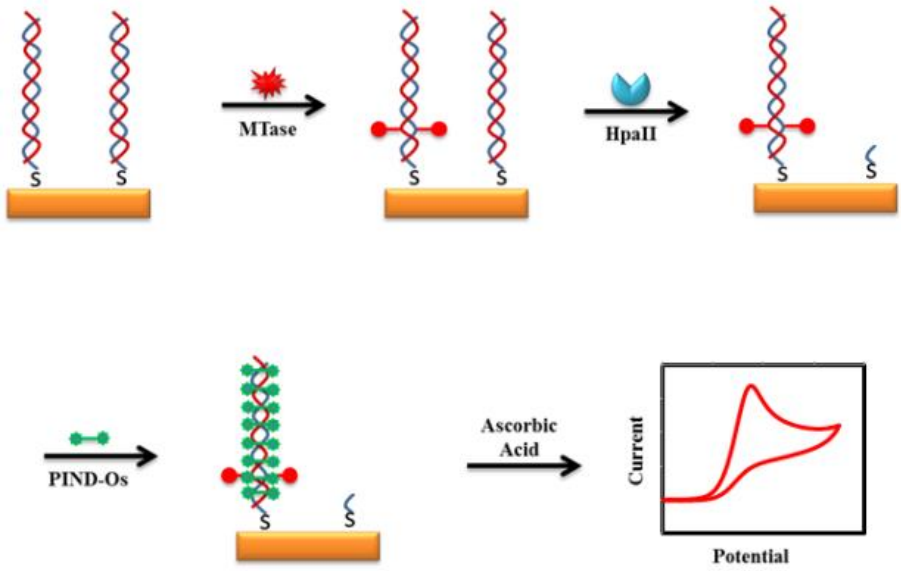


**Figure 5.1.** Schematic illustration of the M.SssI MTase activity biosensor.

Notably, the DNA methylation event that catalyzed by M.SssI MTase was successfully confirmed by gel electrophoresis (Figure 5.2). Meanwhile, the two enzymes employed in this work were also confirmed to be active. Thus, the obtained evidence by gel electrophoresis makes the proposed electrochemical method promising.

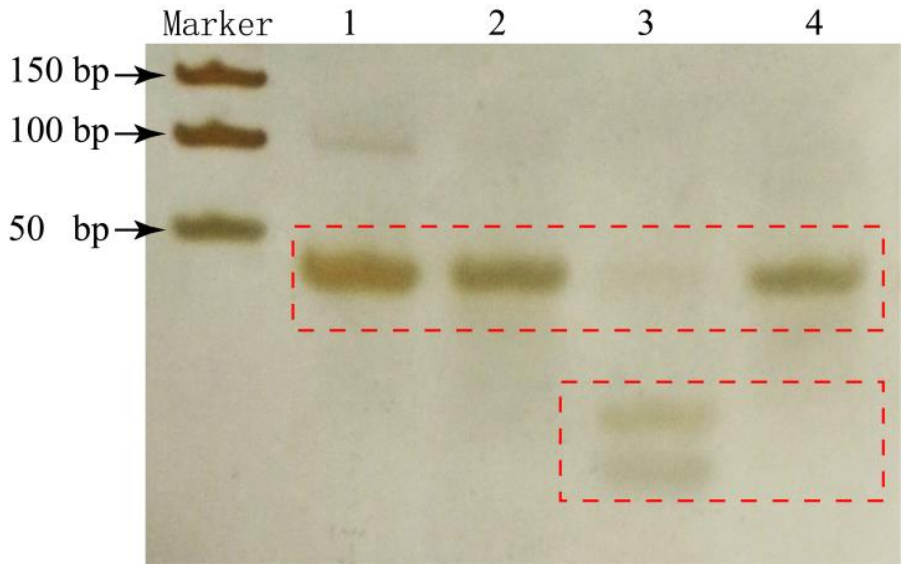


**Figure 5.2.** Gel image of (1) ds-DNA, (2) ds-DNA treated with M.SssI MTase, (3) ds-DNA treated with HpaII, and (4) ds-DNA treated with M.SssI MTase/HpaII.

### 5.3.2 Electrochemical characterization of modified electrode and feasibility study

To confirm that the proposed strategy (as illustrated in Figure 5.1) can be successfully employed for the M.SssI MTase activity biosensor, DPV measurements were performed with the electrode at different stages of the modification procedure. As shown in Figure 5.3A, the bare gold electrode (trace 1) exhibited a high DPV signal due to free electron transfer of the $Fe(CN)_6^{3-/4-}$ redox probes at the bare gold electrode. However, when the ds-DNA was self-assembled on the gold electrode through Au-S covalent bonds and followed by the MCH blocking, the ds-DNA/MCH modified gold electrode (trace 2) showed a sharp decrease in the DPV current of the $Fe(CN)_6^{3-/4-}$ redox probes. The decrease in the DPV current is caused by two factors–one being the electron transfer impeding power of the ds-DNA and MCH mixed monolayer and the other being the electrostatic repulsion between the negatively charged phosphate backbone of the ds-DNA and the anionic $Fe(CN)_6^{3-/4-}$ ions. Thereafter, when the electrode was incubated with 10 U/mL M.SssI MTase and 50 U/mL HpaII subsequently, as illustrated in trace 3, the DPV current of thus treated electrode increased slightly. This is due evidently to the cleavage of the unmethylated ds-DNA by the restriction endonuclease HpaII. A control experiment was also conducted with a blank buffer, i.e. the methylation process was performed in 1 x NEBuffer 2 that only contained 160 μM SAM. As compared to the M.SssI MTase treated electrode, more ds-DNA was removed from the electrode surface after HpaII digestion since no methylation is expected in the absence of M.SssI MTase. An even higher DPV current was recovered accordingly (trace 4).

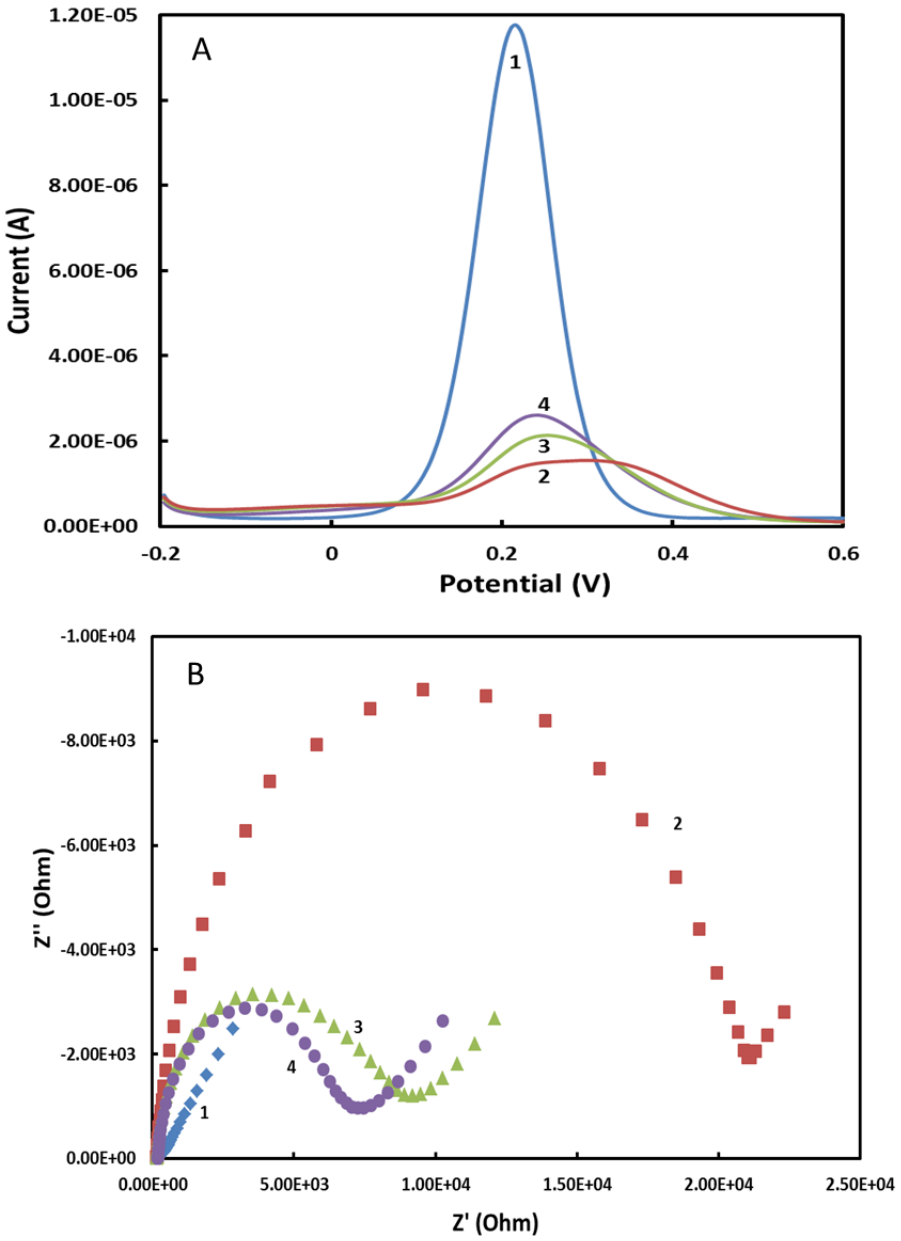


**Figure 5.3.** (A) DPV and (B) EIS of (1) a bare gold electrode, (2) ds-DNA/MCH, (3) ds-DNA/MCH electrode treated by M.SssI MTase/HpaII, and (4) ds-DNA/MCH electrode treated by HpaII in 0.10 M $Na_2SO_4$ containing 5.0 mM $Fe(CN)_6^{3-/4-}$ (1:1 ratio).

As an effective technique to characterize the electrode/electrolyte interface properties and monitor the electron exchange process at the interface,[207] EIS was chosen to further investigate the ds-DNA coated electrode at different stage of the biosensor. EIS measurements were performed at the gold

electrode during the modification procedure and after the incubations. The obtained EIS results coincided well with the DPV results, except for the fact that the charge transfer resistance ($R_{ct}$) is straightforwardly reflected by the impedance spectra. As seen in Figure. 5.3B, the bare Au electrode (curve 1) shows an almost straight line, implying that there is practically little electron transfer resistance. The EIS spectrum of the ds-DNA-MCH mixed monolayer coated electrode displayed a semicircle in the high frequency region, and the diameter of the semicircle represents the $R_{ct}$. Moreover, it was found that the $R_{ct}$ of the ds-DNA/MCH-modified electrode (curve 2) is larger than that of the M.SssI MTase/HpaII treated electrode (curve 3) and the $R_{ct}$ of the M.SssI MTase/HpaII treated electrode is larger than that the HpaII treated electrode (curve 4). The systematic decrease in $R_{ct}$ agreed well with the DPV results. Therefore, based on the above results, it was confirmed that the procedure for the preparation of the ds-DNA-MCH coated gold electrode is appropriate and the ds-DNA at the electrode surface is fully functional with respect to M.SssI MTase and HpaII.

Furthermore, cyclic voltammogram (CV) characterization of the modified electrodes was conducted by using the electrodes that treated with the same procedures as the electrodes employed in DPV and EIS characterization experiments. The CV results agree with that of DPV and EIS, as can be seen in Figure 5.4.

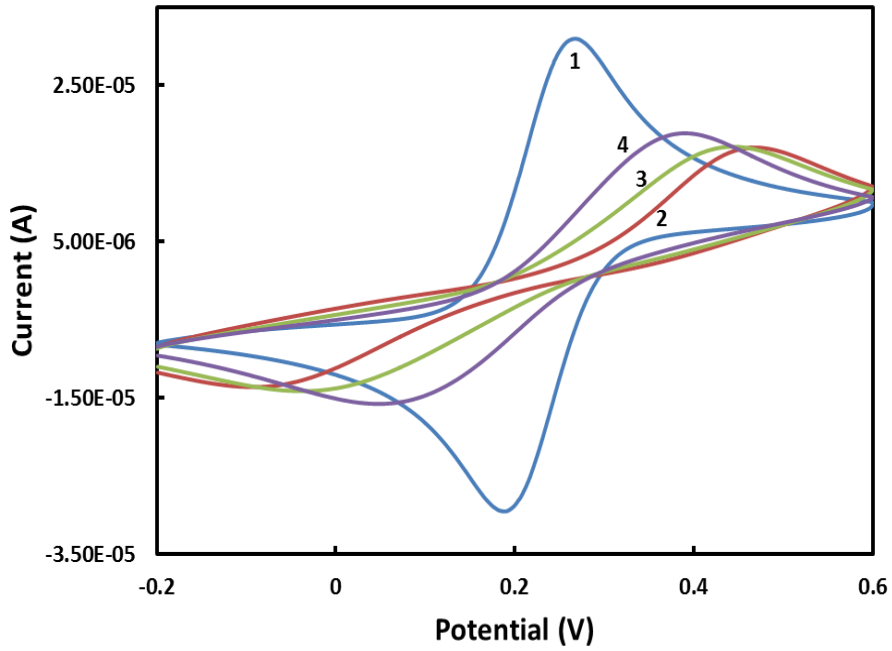


**Figure 5.4.** Voltammetric characterization of (1) a bare gold electrode, (2) ds-DNA/MCH, (3) ds-DNA/MCH electrode treated by M.SssI MTase/HpaII, and (4) ds-DNA/MCH electrode treated by HpaII in 0.10 M $Na_2SO_4$ containing 5.0 mM $Fe(CN)_6^{3-/4-}$ (1:1 ratio). Potential scan rate: 100 mV/s.

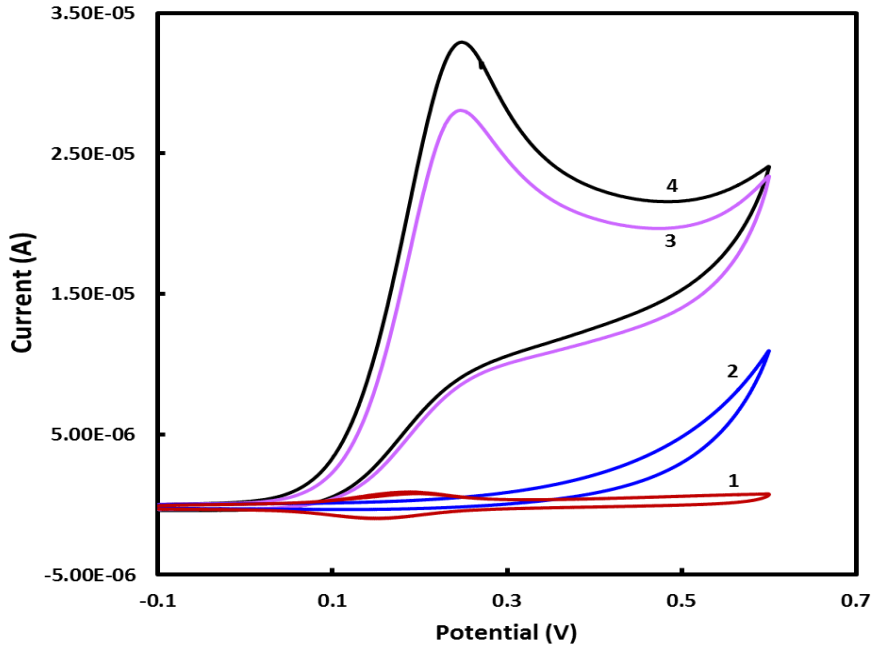


**Figure 5.5.** Voltammograms of (1) a PIND-Os treated ds-DNA/MCH electrode in blank PBS; (2) a ds-DNA/MCH electrode, (3) a HpaII treated ds-DNA/MCH/electrode, and (4) a M.SssI MTase/HpaII treated ds-DNA/MCH/ electrode in PBS containing 5 mM AA. 2 h methylation, 2 h incubation in 50 U/mL of HpaII, and 10 min incubation in 100 μg/mL PIND-Os. Potential scan rate: 100 mV/s.

In order to verify the intercalating property of PIND-Os, the ds-DNA/MCH coated electrode was incubated in 100 μg/mL PIND-Os for 10 min, and then the electrode was characterized by CV in blank PBS after a thorough washing. As shown in trace 1 in Figure 5.5, a pair of reversible voltammetric peaks centered at 0.18 V that are assigned to the redox reactions of PIND-Os were observed,[205] thus suggesting the successful attachment of PIND-Os to the ds-DNA via threading intercalation. The charge under either the oxidation or the reduction current peak is directly associated with the amount of the intercalated PIND-Os and hence the amount of the ds-DNA on the electrode surface. Furthermore, as expected, the voltammogram of the ds-DNA coated electrode without PIND-Os treatment showed little current for the oxidation of AA at potentials <0.40 V due to the slow heterogeneous electron-transfer rate of AA caused by a high oxidation overpotential at gold electrode (trace 2). It is well-documented that direct electrooxidation of AA is totally irreversible and suffers from very high overpotentials. Reported values for its oxidation range from 0.3 to 0.6 V.[148, 149] The presence of the ds-DNA/MCH mixed monolayer on the electrode further impedes the electron transfer. Also, the voltammetric behavior of the electrode in PBS containing 5 mM AA after the PIND-Os incubation was investigated. As seen in trace 3 and trace 4 of Figure 5.5, after the PIND-Os intercalation step, the anodic peak potential ($E_p$) for the oxidation of AA is significantly shifted to ~0.22 V at both the ds-DNA/MCH electrodes treated by HpaII/PIND-Os and M.SssI MTase/HpaII/PIND-Os, a direct consequence of the improvement in the reversibility of the electron transfer from AA to the gold electrode. In addition, the anodic peak current ($I_p$) is also improved as much as ~3 folds, which is attributed to the excellent

electrocatalytic effect of PIND-Os. Remarkably, the $I_p$ for the electrode treated with 100 U/mL M.SssI MTase is ~5 μA higher than that without the M.SssI MTase treatment. As a result, the M.SssI MTase activity can be quantified in principle through monitoring the electrocatalytic oxidation current of AA.

### 5.3.3 M.SssI MTase activity determination

To evaluate the analytical performance of the proposed M.SssI MTase activity biosensor, the ds-DNA/MCH modified electrodes were treated with various concentrations of M.SssI MTase (0-120 U/mL) in the methylation step and followed by the incubation with 50 U/mL HpaII and 100 μg/mL PIND-Os successively. Under selected experimental conditions, the correlation between the electrocatalytic oxidation current of AA and the activity of M.SssI MTase was investigated. It was found that the catalytic oxidation current of AA increases with the increase of the activity of M.SssI MTase. This is because the higher the M.SssI MTase activity, the higher the methylation level, the more ds-DNA remaining on the electrode surface, and thus, the higher the concentration of PIND-Os bound to the ds-DNA, which in turn, generates a higher catalytic oxidation current of AA. As illustrated in Figure 5.6, the electrocatalytic oxidation current of AA exhibited a linear correlation to the activity of M.SssI MTase ranged from 0 to 120 U/mL with a current sensitivity of 0.046 μA mL $U^{-1}$and an $R^2$ of 0.991. Owing mainly to the excellent electrocatalytic property of PIND-Os toward AA oxidation, the sensitivity of this method is much higher than previously reported graphene oxide nanomaterial-based[111] and enzymatic HRP-based[115] signal amplification systems.

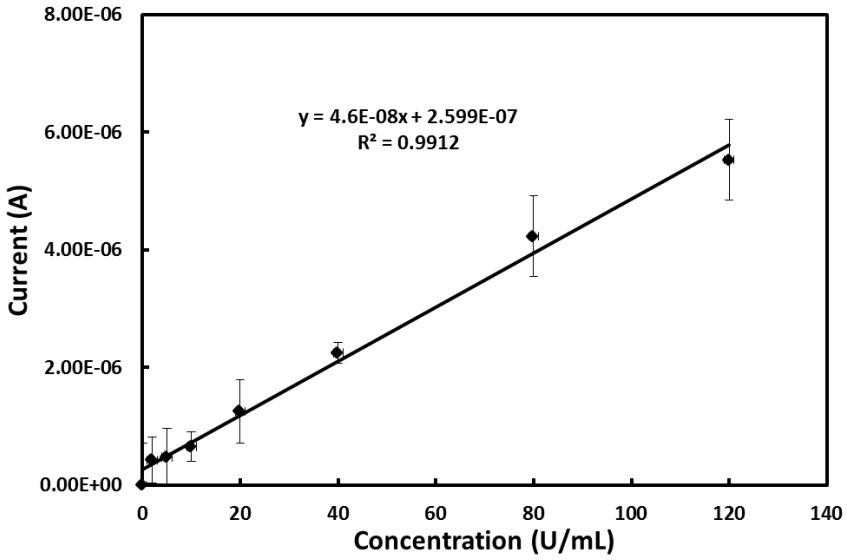


**Figure 5.6.** The calibration curve of the M.SssI MTase activity biosensor.

### 5.3.4 Selectivity of the M.SssI MTase activity biosensor

HaeIII MTase modifies the internal cytosine residues in the sequence of symmetric tetranucleotide 5'-GGCC-3', and AluI MTase methylates the cytosine residues in the double-stranded symmetric 5'-AGCT-3' sequence. As shown in Figure 5.7, the catalytic current of M.SssI MTase was about 39 and 17 times higher than that of HaeIII and AluI, respectively. This is evidently due to the fact that the CpG dinucleotide site in the HpaII endonuclease recognition sequence (5'-CCGG-3') cannot be methylated by the HaeIII and AluI cytosine MTase. Consequently, the ds-DNA strands were cleaved off from the electrode surface in the HpaII incubation step. Therefore, the proposed biosensor exhibited good selectivity toward M.SSSI over HaeIII MTase and AluI MTase.

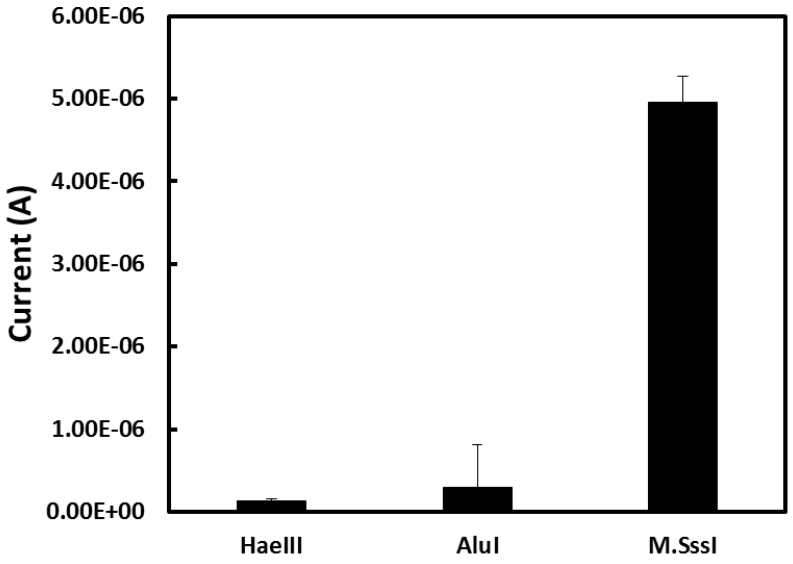


**Figure 5.7.** Responses of ds-DNA/MCH electrodes when treated with 100 U/mL HaeIII MTase, AluI MTase and M.SssI, respectively.

### 5.3.5 Influence of inhibitors on M.SssI MTase activity

Many studies have revealed that DNA MTase inhibitors can reversibly alter the methylation level in DNA methylation-associated tumor and cancer, and hence the development of MTase inhibitors has provided an effective tool for epigenetic cancer therapy.[208] To investigate the inhibitor screening ability of the proposed biosensor, 5-Aza and 5-Aza-dC were selected as the model inhibitors. Both of the compounds are nucleoside analogues and proven to be able to be incorporated into DNA to trap and inactivate DNA MTase.[209] The inhibition effects of 5-Aza and 5-Aza-dC on M.SssI MTase are illustrated in Figure 5.8A and B, respectively. As shown in Figure 5.8, in both cases, the relative activity of M.SssI MTase decreased monotonically with the increasing concentrations of the inhibitors in a dose-dependent manner. It is worth to note that, 5-Aza-dC exhibited a higher inhibition efficiency than that of 5-Aza. This is in accordance with the fact that 5-Aza-dC does not need to be modified to a

deoxy form and can be more directly incorporated into DNA.[209] The half maximal inhibitory concentration ($IC_{50}$) represents the concentration of a drug that is required for 50% decrease in enzyme activity in vitro. The $IC_{50}$ values for 5-Aza and 5-Aza-dC were obtained from the plots of the relative activity of M.SssI MTase versus the concentrations of inhibitors, and they were found to be ~4.2 and 3.2 μM, respectively. These results demonstrated that the proposed M.SssI MTase activity biosensor can be successfully applied in MTase inhibitor screening and is a potentially useful tool for anticancer drug discovery.

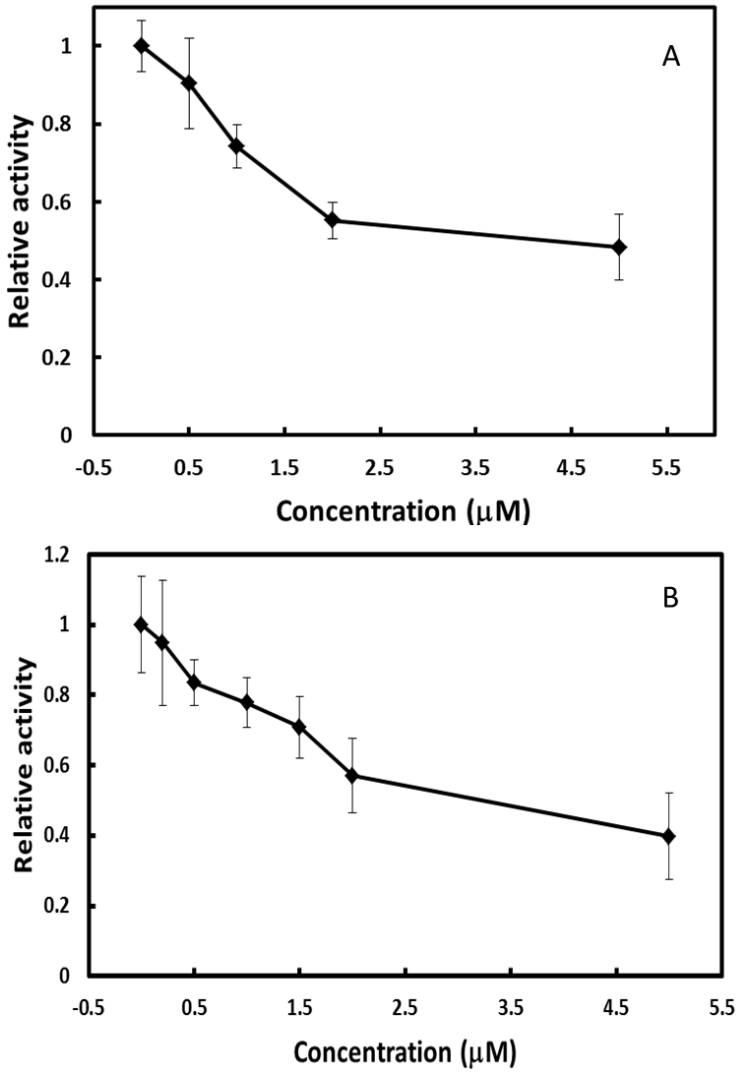


**Figure 5.8.** The inhibition effect of (A) 5-Aza and (B) 5-Aza-dC on M.SssI MTase activity.

## 5.4 Conclusion

In summary, a simple and highly sensitive electrochemical method has been developed for M.SssI MTase activity biosensor. High sensitivity was achieved by employing an excellent electrocatalytic PIND-Os threading intercalator toward the oxidation of AA as the signal amplifier. Inhibitor screening capability of the proposed biosensor has also been demonstrated. Since DNA methylation and DNA MTase play important roles in many biological processes and have become important biomarkers in tumor and cancer. Hence, the developed M.SssI MTase activity biosensor is an attractive candidate for the development of a simple and highly sensitive M.SssI MTase activity monitoring platform for uses in clinical research.

# Chapter 6. $MoS_2$ nanosheets as an effective fluorescence quencher for DNA methyltransferase activity detection

## 6.1 Introduction

Benefited from the rapid development of nanoscience, lots of nanomaterials have been employed in the DNA MTase biosensors to act as either signal producer or signal amplifier. For example, Ouyang and coworkers have reported a low-background Dam MTase activity sensing platform using carboxylated carbon nanoparticle as fluorescent quencher coupled with a DNA intercalator dye.[138] Liu et al. have also established a sensitive Dam MTase activity biosensor based on the methylation/cleavage reaction induced aggregation of duplex DNA substrate modified gold nanoparticles.[122] In addition, based on the signal transduction and amplification of single wall carbon nanotubes, a label-free electrochemical approach for the detection of MTase activity has been confirmed by Wang and collaborators.[210]

As a conceptually new class of nanomaterials, two-dimensional (2D) inorganic graphene analogues (IGAs) have been considered to be an emerging area in nanoscience.[211, 212] Due to the unique electronic properties that driven from their ultrathin structure, IGAs such as layered transition metal dichalcogenides (TMDCs, e.g., $MoS_2$ and $WS_2$) and boron nitride, have drawn intensive attentions in the past few years. These materials have shown various potential applications in catalysis, energy storage, and sensing.[213-215] Up to now, the biosensing applications of IGAs are relatively rare and yet to be fully discovered. In 2013, Zhang's group reported the usage of single-layer $MoS_2$

for homogenously detection of DNA and adenosine for the first time.[216] Much more recently, based on the fact that 2D TMDCs preferentially absorb single-stranded oligonucleotide toward double-stranded one, similar approaches were developed for DNA and MicroRNA sensing by using $WS_2$ nanosheets.[217, 218] Moreover, some other biological sensing systems involving layered $MoS_2$ nanomaterial have been investigated for the detection of glucose, cancer biomarkers, and hydrogen peroxide.[219-221]

Motivated by the above mentioned biological sensing works based on the newly emerging 2D layered IGAs, we explored the application of $MoS_2$ nanosheets in the MTase activity biosensor. In this work, a signal-on fluorescent Dam MTase activity biosensor employing $MoS_2$ nanosheets as fluorescence quencher was successfully demonstrated. Its simplicity, rapidity, low cost in conjunction with high sensitivity and selectivity makes it attractive as a candidate for MTase activity analysis.

## 6.2 Experimental

### 6.2.1 Materials and apparatus

Molybdenum (IV) sulphide and 5-fluorouracil were purchased from Sigma-Aldrich (St. Louis, MO, USA). Tris(hydroxymethyl)aminoethane (Tris) was obtained from Alfa Aesar (Lancashire, England). Dam MTase, AluI MTase, M.SssI MTase, DpnI endonuclease, S-adenosyl-L-methionine were purchased from New England Biolabs (Ipswich, MA). The Dam methylation and DpnI cleavage reactions were performed in a reaction buffer (R buffer: 20 mM Tris-HAc, 50 mM KAc, 10 mM $Mg(Ac)_2$, 100 μg/mL BSA, pH 7.9).

Oligonucleotides used in this work were custom-made by 1st Base Pte Ltd. (Singapore). The sequences of the oligonucleotides were as following: oligonucleotide 1 (oligo 1): 5'-CCT GGA GTT GAT CAT ATC TGG ACC TAT AGT TCA CTT-3' and the FAM dye labeled partially complementary oligonucleotide 2 (oligo 2): 5'-FAM-TAT GAT CAA CTC CAG G-3'. The two oligonucleotides were dissolved in TE buffer (10 mM Tris, 1 mM EDTA, pH 8.0) to the desired concentrations and stored at -20 ºC. All other chemicals of certified analytical grade were used without further purification. All aqueous solutions were prepared with ultrapure water (18.3 MΩ).

Atomic force microscope (AFM) image of layered $MoS_2$ was acquired with a tapping mode on Veeco Digital instruments Dimension 3000 SPM. The fluorescence lifetime decay of FAM-labeled substrate DNA in the absence and in the presence of MoS2 nanosheets was measured by using a time-correlated single photon counting (TCSPC) technique. The frequency-doubled output (420 nm) of an Avesta TiF-100M femtosecond Ti:sapphire oscillator was used as the excitation source. Fluorescence at 520 nm was collected by an optical fiber that is directed to an avalanche photodiode. The signals were processed by a TCSPC module (PicoQuant, PicoHarp 300) with temporal resolution of ~150 ps. UV-vis absorption spectrum was recorded on an Agilent Cary 60 UV-vis spectrophotometer. Fluorescence was recorded on an Agilent Cary Eclipse fluorescence spectrophotometer.

### 6.2.2 Preparation of $MoS_2$ nanosheets

The $MoS_2$ nanosheets were prepared according to a reported mixed-solvent exfoliation procedure with some modifications.[222] Briefly, 150 mg $MoS_2$

powder was added to a 100 mL flask, 50 mL ethanol/water (45%, v/v) was added as dispersion solvent. The mixture was sonicated for 8 h, and then the dispersion was centrifuged at 5000 rpm for 30 min to remove aggregates. The supernatant was collected and the concentration of the $MoS_2$ nanosheets dispersion was measured by UV-vis spectrophotometer.

### 6.2.3 Feasibility study

Double-stranded DNA substrate was prepared by mixing equal moles of oligo 1 and oligo 2 in a hybridization buffer (10 mM Tris-HCl, 100 mM NaCl, pH 7.4), the mixture was heated to 90 ºC for 5 min, then slowly cooled down to room temperature, and stored at 4 ºC if not in use. To investigate the activity of Dam and DpnI in the same R buffer and avoid the change of buffers for different enzymatic reactions, different ds-DNA samples were prepared by treating 4 μM ds-DNA with 16 unit Dam, 20 unit DpnI, and 16 unit Dam + 20 unit DpnI in R buffer containing 160 μM SAM respectively. Both the methylation and cleavage reaction were performed at 37 ºC for 2 h. Then, the DNA samples were characterized by 15% polyacrylamide gel electrophoresis.

On the other hand, to evaluate the fluorescence quenching and recovery mediated by $MoS_2$ nanosheets, 50 μL 100 nM ds-DNA and 50 μL 100 nM Dam/DpnI pre-treated ds-DNA in R buffer were mixed with 50 μL as-prepared $MoS_2$ nanosheets respectively. The mixtures were allowed to stand for 15 min, and then centrifuged at 6000 rpm for 1 min to minimize the background signal. Finally, the supernatant was collected by pipette for fluorescence measurement with an excitation wavelength of 495 nm.

### 6.2.4 Dam methyltransferase activity detection

The enzymatic reactions were conducted in a 200 μL total reaction volume. The typical reaction mixture consisted of 100 nM ds-DNA, 160 μM SAM, and various concentrations of Dam MTase in R buffer. The mixture was first incubated at 37 ºC for 2 h, then 0.5 μL of 20000 U/mL DpnI was added and further incubated for another 2 h. After reaction, 50 μL of the mixture was mixed with 50 μL as-prepared $MoS_2$ nanosheets for 10 min at room temperature, followed by centrifugation at 6000 rpm for 1 min. The fluorescence intensity of the supernatant was recorded finally.

### 6.2.5 Selectivity and inhibition study

The selectivity of the proposed Dam activity biosensor was evaluated by using two other kinds of MTases. The procedure was the same as the above described Dam activity detection procedure, except that Dam was replaced by AluI and M.SssI respectively. The concentration of MTase was 20 U/mL for each. Similarly, the inhibition study was carried out in the same procedure with 20 U/mL Dam MTase, and different concentrations of 5-fluorouracil were added together with Dam in the methylation process. Control experiments were also performed without addition of Dam MTase in both the selectivity and inhibition studies. The relative activity of Dam MTase activity inhibited was calculated as follows:

$$Relative\ activity\ (\%) = \frac{F_2 - F_0}{F_1 - F_0} \times 100\ \%$$

where $F_0$ is the fluorescence intensity of 0 U/mL Dam MTase, $F_1$ is the fluorescence intensity of 20 U/mL Dam MTase and $F_2$ is the fluorescence intensity after the inhibitor treatment.

## 6.3 Results and discussion

### 6.3.1 Characterization of $MoS_2$ nanosheets

The $MoS_2$ nanosheets was prepared by a simple sonication assisted ethanol/water mixed solvent exfoliation method from the bulk $MoS_2$ powder. The obtained dark-green suspension (Figure 6.1 inset) was highly stable, and showed no precipitation after being stored for several weeks under ambient conditions. Figure 6.1 shows the UV-vis spectrum of the suspension which agrees well with the reported results.[212, 222] The two absorption peaks at around 610 nm and 670 nm, which can be attributed to the characteristic A1 and B1 direct excitonic transitions of $MoS_2$ with the energy split from valence band spin-orbital coupling, indicate the existence of layered $MoS_2$ dispersed in the mixed solvent. Assuming that the dispersion obeys Lambert-Beer law, the concentration of the dispersion was calculated to be 3.5 μg/mL by using the extinction coefficient (3400 mL $mg^{-1}$ $m^{-1}$ at 670 nm) reported in literature.[222]

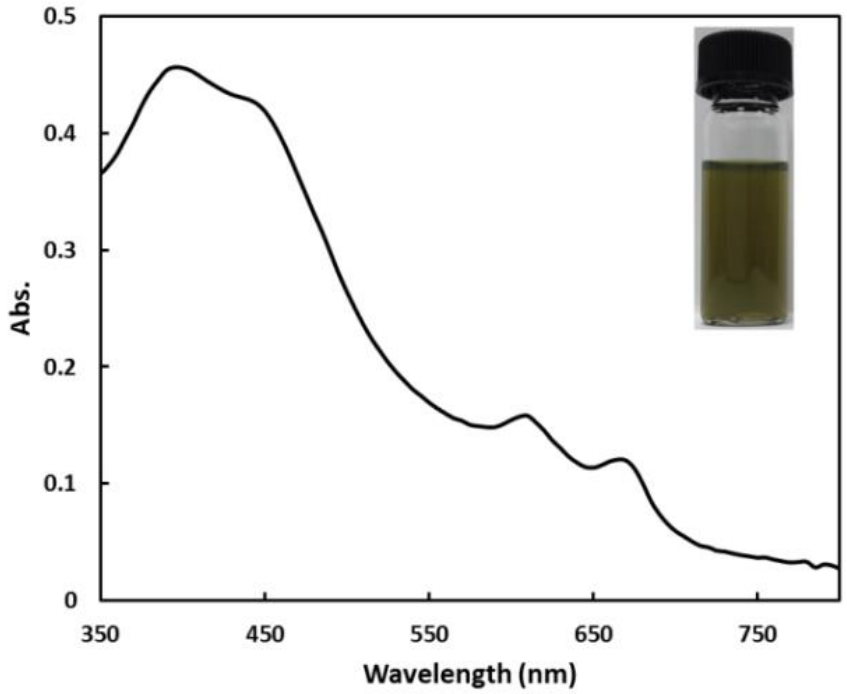


**Figure 6.1.** UV-vis spectrum of as-prepared $MoS_2$ nanosheets. Inset: photograph of the $MoS_2$ nanosheet suspension.

The morphology and thickness of the $MoS_2$ nanosheets were characterized by AFM. As shown in Figure 6.2, the as-prepared $MoS_2$ had an average dimension of few tens of nanometers and a height of around 2 nanometers, indicating that they are not single layered (thickness 0.65 nm) but stacked few layers.

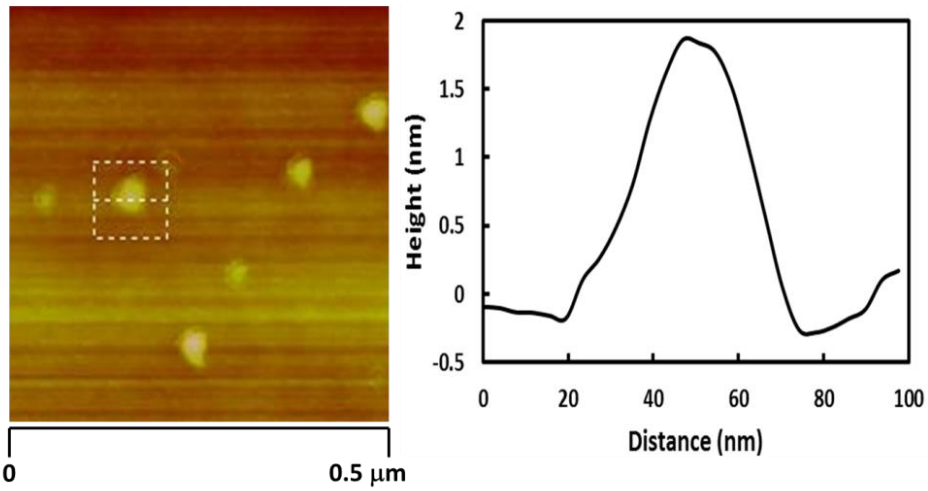


**Figure 6.2.** AFM characterization of the $MoS_2$ nanosheets.

### 6.3.2 Principle and feasibility of the Dam MTase activity biosensor

Early studies have reported that aromatic (e.g. pyridine, purine, etc.) and conjugated compounds can be physically absorbed on the basal plane of $MoS_2$ using either theoretical calculation or experimental studies.[223, 224] Moreover, recent studies have revealed that layered 2D TMDCs, like $MoS_2$ and $WS_2$, could adsorb oligonucleotides via van der Waals and could effectively quench the fluorescence of fluorophores labeled at the end of absorbed single-stranded DNA via energy transfer.[216-218] To adopt $MoS_2$ nanosheets as a fluorescence quencher for homogenously detection of Dam MTase activity, Dam MTase/DpnI, which specifically methylates/cleaves the adenosine residues in the double-strand 5'-GATC-3' DNA sequence, was chosen as the MTase/endonuclease model. The substrate DNA consisted of a single-stranded region for $MoS_2$ absorption and a double-stranded region containing the Dam/DpnI recognition site, a FAM fluorescent dye was conjugated at the inner end of the duplex region. As illustrated in Figure 6.3, substrate DNAs were successively treated with Dam and DpnI, methylated DNAs were specifically cleaved by the methylation sensitive endonuclease DpnI. After cleavage, the remaining fluorophore conjugated 5-bases segment was highly expected to be released as result of the extremely low melting temperature of the 5-base pair duplex region. Upon the addition of $MoS_2$ nanosheets, fluorescence of non-methylated DNA was quenched due to the close contact of fluorophore and $MoS_2$ nanosheets. However, the fluorescence of the short segment was retained because of its weak van der Waals interaction with $MoS_2$.

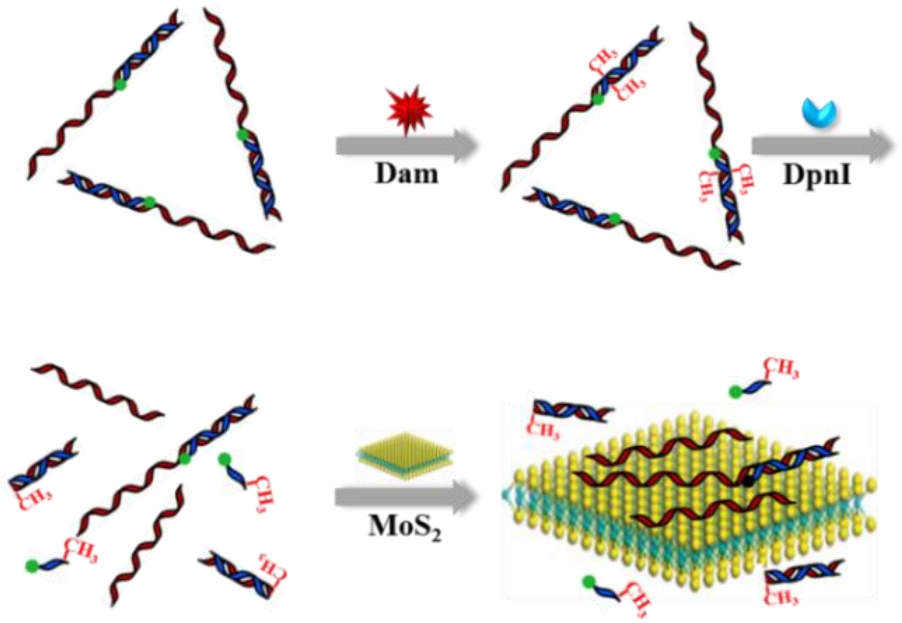


**Figure 6.3.** Schematic illustration of proposed fluorescent Dam MTase activity biosensor.

To avoid changing buffer for different enzymatic reactions, the activity of Dam and DpnI was firstly evaluated in R buffer. DNA substrates were successively treated with Dam and DpnI, and solely treated with Dam or DpnI for contrast as well. The gel image in Figure 6.4a shows that there are two split bands in the Dam + DpnI treated sample (lane 4), the upper band at the same position with controls (lane 1, lane 2, and lane 3) was the non-methylated substrate DNA, and the lower band was the cleaved DNA fragments (25 bases ss-DNA and 24 bases ds-DNA). The result indicated the successful methylation and cleavage reaction and thus the guaranteed activity of the two enzymes in R buffer. The melting temperature of the 5-base pair remaining duplex region is calculated to be less than 10 ºC in R buffer, therefore the fluorophore labeled 5-bases fragment readily dehybridizes and desorbs from the $MoS_2$ nanosheets after the DpnI cleavage. It was found that the fluorophore-labeled fragment of having up to 10 bases readily desorbs

from $MoS_2$ nanosheets after cleavage. Figure 6.4b shows the fluorescence quenching-restoration behavior mediated by $MoS_2$ nanosheets. As can be seen, the fluorescence of FAM-labeled substrate was almost fully quenched in the presence of $MoS_2$ (trace 1, 2), whereas the fluorescence was turned on when the substrate DNA was treated with Dam and DpnI, which resulted from the partially released fluorophores.

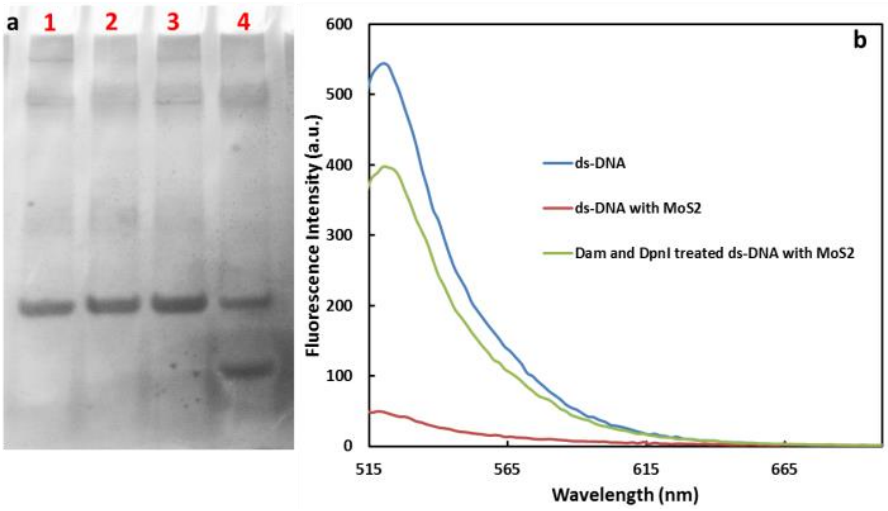


**Figure 6.4.** (a) Gel image of 4 μM substrate DNA. Lane 1: ds-DNA, lane 2: Dam treated ds-DNA, lane 3: DpnI treated ds-DNA, and lane 4: Dam + DpnI treated ds-DNA. (b) Fluorescence emission spectra of substrate ds-DNA, substrate ds-DNA with the $MoS_2$ nanosheets, and Dam/DpnI treated substrate ds-DNA with the $MoS_2$ nanosheets. Excitation wavelength: 495 nm.

In addition, to further understand the quenching mechanism, the fluorescence lifetime of FAM labeled substrate DNA in the absence and in the presence of $MoS_2$ was measured (Figure 6.5). In the presence of $MoS_2$ nanosheets, the fluorophore displayed faster decay than the free FAM-labeled substrate DNA, indicating the quenching mechanism is dynamic, thus clearly confirming the feasibility of employing $MoS_2$ nanosheets as an effective fluorescence quencher for Dam activity biosensor.

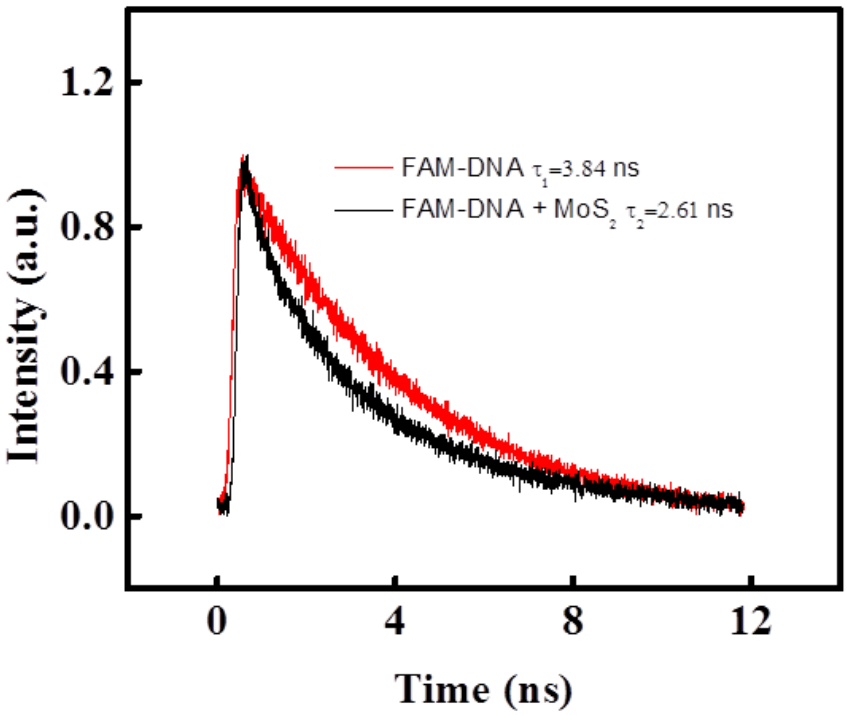


**Figure 6.5.** Fluorescence lifetime decay of FAM-labeled DNA in the absence and in the presence of the $MoS_2$ nanosheets. FAM-labeled ds-DNA: 100 nM, $MoS_2$ nanosheets: 0.5 μg/mL.

### 6.3.3 Dam methyltransferase activity detection

To obtain sufficient quenching efficiency with minimal $MoS_2$ quencher, the amount of $MoS_2$ was optimized (Figure 6.6). It was found that the optimal concentration of $MoS_2$ in the final reaction system is 1.75 μg/mL. It is worth to note that in under the experiment conditions, $MoS_2$ nanosheets showed superior quenching efficiency when compared with graphene oxide (GO) as can be seen in Figure 6.7, which is likely attributed to its excellent energy harvesting property.

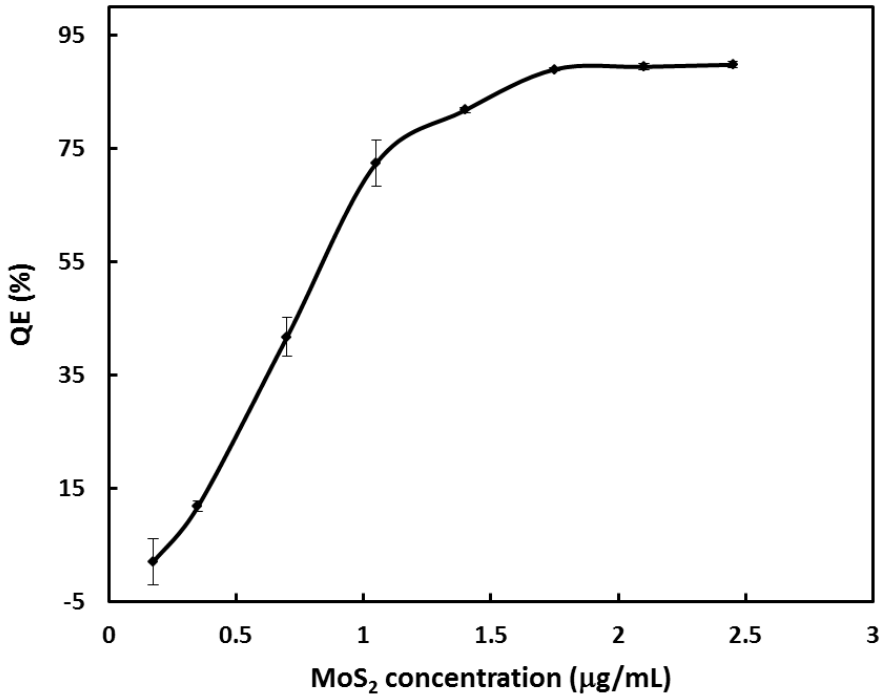


**Figure 6.6.** Quenching efficiency of FAM-labeled substrate DNA with the addition of different concentrations of the $MoS_2$ nanosheets.

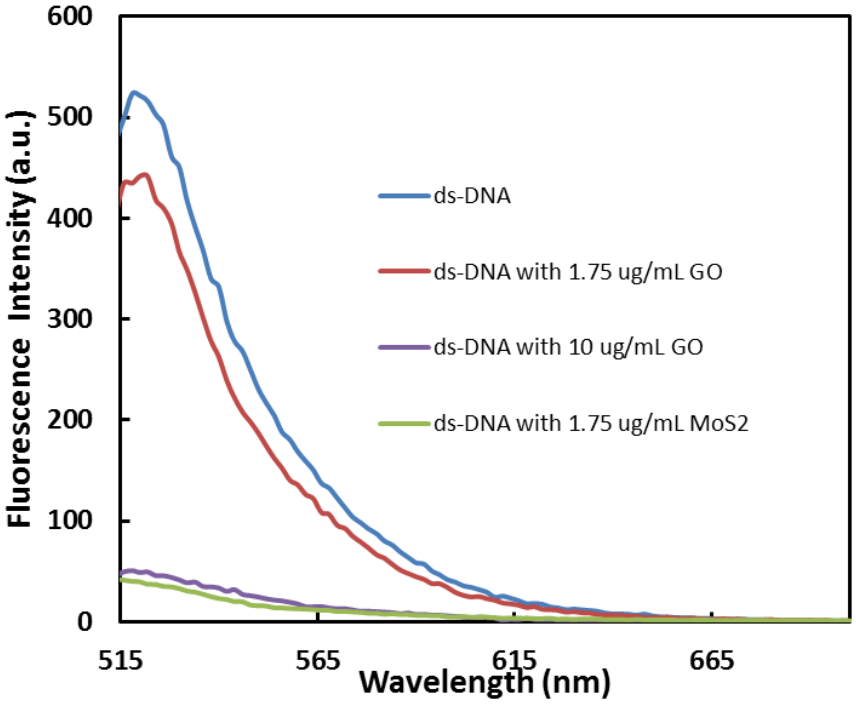


**Figure 6.7.** Fluorescence quenching by the $MoS_2$ nanosheets and GO.

Next, the time needed to reach the equilibrium upon the addition of $MoS_2$ was investigated as well. As shown in Figure 6.8, the quenching process is

very fast. The fluorescence intensity decreased sharply in the first 20 s, and almost reached the equilibrium within 10 min. Thereafter, the DNA sample and $MoS_2$ mixture was allowed to stand for 10 min before fluorescence recording. It is worth to mention that centrifugation could effectively reduce the background signal. This could be attributed to the possibility that the single-stranded region of some FAM-labeled substrate DNA was partially absorbed on $MoS_2$, the FAM fluorophore was hang over outside of the $MoS_2$ nanosheets, the fluorescence of FAM in such case could not be quenched effectively due to the long distance between the fluorophore (energy donor) and $MoS_2$ (energy acceptor). However, the partially absorbed substrate DNA could be separated from the solution together with $MoS_2$ under the centrifugation force, which contributed to the low background signal.

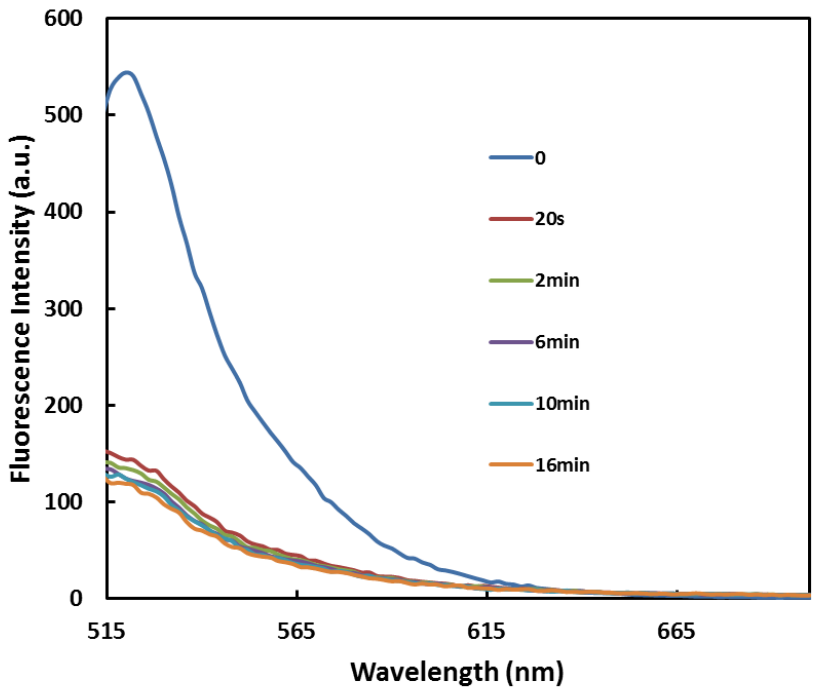


**Figure 6.8.** Fluorescence intensity variation upon the addition of the $MoS_2$ nanosheets.

Under the optimal experiment conditions, the performance of the developed biosensor for quantitative detection of Dam MTase activity was further examined. Figure 6.9a displays the fluorescence emission spectra of the sensing system treated with different concentrations of Dam MTase, the fluorescence intensity increased rapidly as the Dam MTase concentrations varied from 0 to 20 U/mL, and gradually levelled off beyond 20 U/mL. The corresponding calibration curve was plotted in Figure 5.9b. The linear relationship between the fluorescence intensity at 518 nm and the Dam MTase concentration was observed from 0.2 to 20 U/mL with satisfactory sensitivity and a correlation coefficient ($R^2$) of 0.99. The detection limit was estimated to be 0.14 U/mL based on three times the standard deviation of the background fluorescence signal over the slope of calibration curve. The performance of the proposed biosensor is comparable or even better than that of reported Dam MTase activity biosensors.[124, 129]

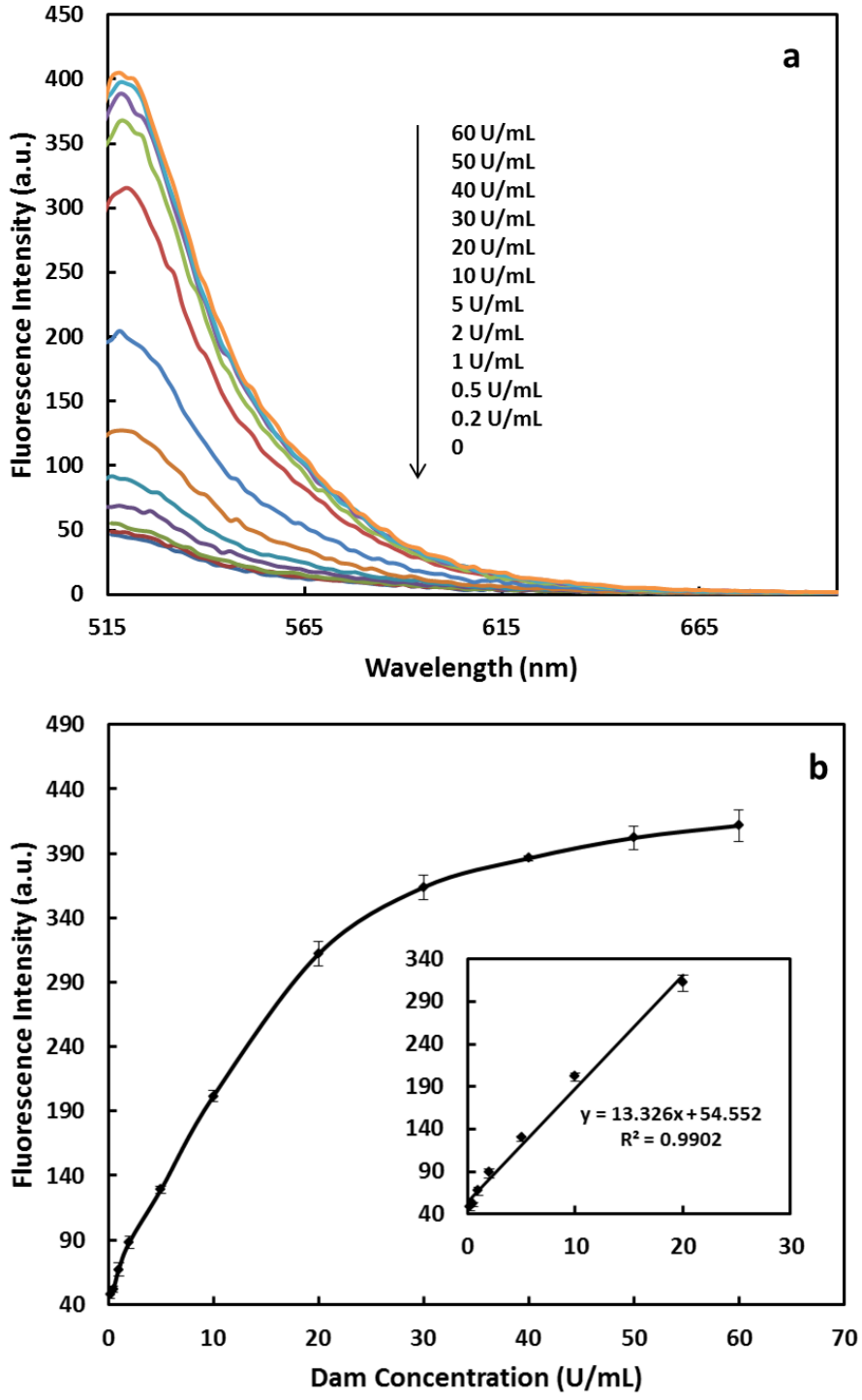


**Figure 6.9.** (a) Fluorescence spectra of FAM-labeled substrate DNA that treated with different concentrations of Dam MTase: 0 (control), 0.2, 0.5, 1, 2, 5, 10, 20, 30, 40, 50, and 60 U/mL. Excitation wavelength: 495 nm. (b) The corresponding plot of fluorescence intensity versus the concentration of Dam MTase from 0 to 60 U/mL. Inset: linear correlation from 0.2 to 20 U/mL.

### 6.3.4 Selectivity and inhibition study

The selectivity of the proposed Dam MTase activity biosensor was further investigated using AluI MTase and M.SssI MTase as the interference enzymes. Both AluI MTase and M.SssI MTase belong to the DNA cytosine methyltransferase family. AluI MTase specifically methylates the cytosine residue ($C^5$) of the sequence 5'-AGCT-3' within the duplex DNA, and M.SssI modifies the cytosine residue ($C^5$) within the double-stranded dinucleotide recognition sequence 5'-CG-3'. As depicted in Figure 6.10, both the fluorescence response of AluI MTase and M.SssI MTase were practically the same as the control. In contrast, significantly higher fluorescence intensity was obtained with Dam MTase, thus readily allowing highly selective detection of Dam MTase activity. Therefore, the proposed biosensor exhibits extraordinary selectivity and can easily discriminate Dam MTase from other interference enzymes owing to the highly specific sequence recognition of Dam MTase towards the substrate DNA.

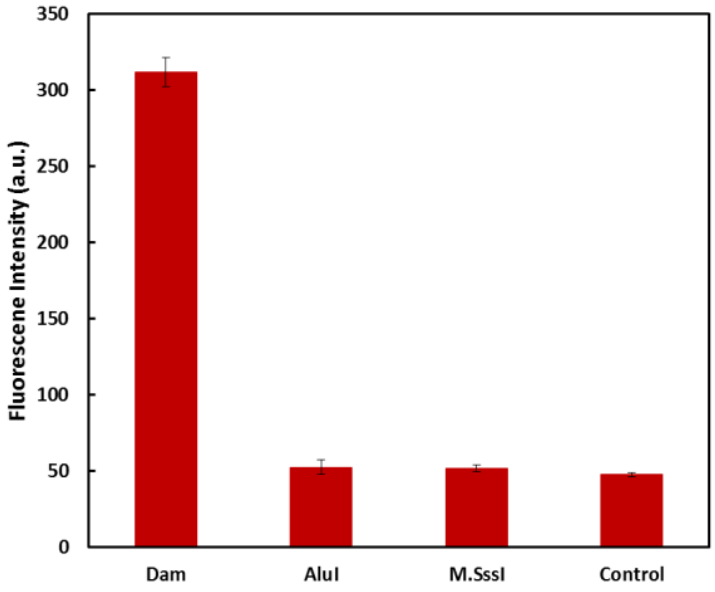


**Figure 6.10.** Selectivity of proposed Dam MTase activity biosensor toward interference enzymes of AluI MTase and M.SssI MTase. MTase concentration: 20 U/mL.

Since Dam MTase is essential for bacterial virulence, Dam inhibitors are likely to have broad antimicrobial action, and the investigation of Dam inhibition is of great importance for antimicrobial drug development.[225] 5-fluorouracil, a well-known inhibitor of MTase which has been popularly used for cancer therapy for about 40 years,[226, 227] was selected as the model Dam MTase inhibitor in this study. Figure 6.11 shows that the relative activity of Dam MTase monotonically decreased with the increasing concentrations of 5-fluorouracil in a dose-dependent manner. The $IC_{50}$ (half maximal inhibitory concentration) value of 5-fluorouracil was calculated to be 17.7 μM. Hence, the proposed method is demonstrated to be a potential useful tool for antimicrobial drug discovery.

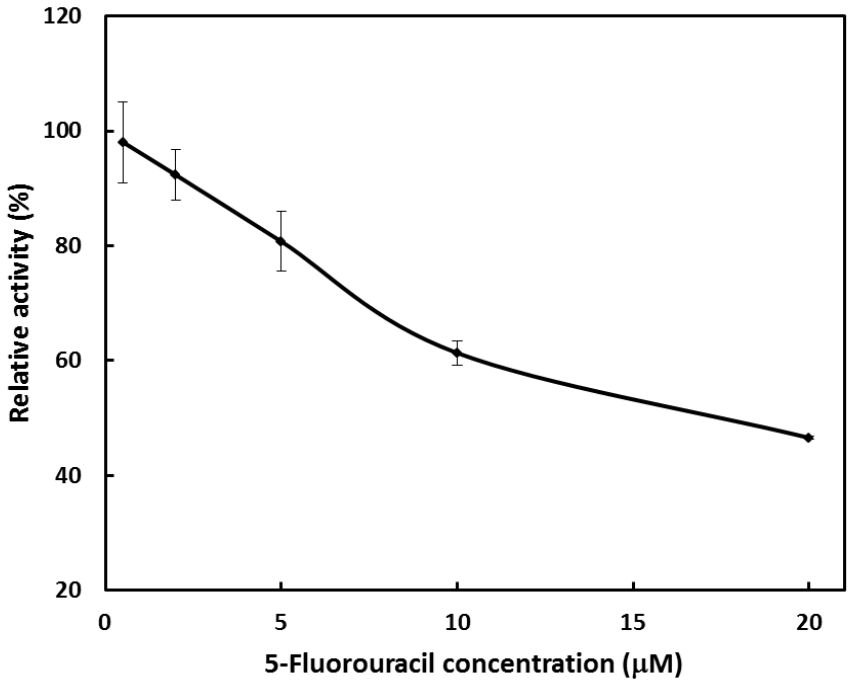


**Figure 6.11.** Relative activity of Dam MTase inhibited by different concentrations of 5-fluorouracil.

## 6.4 Conclusion

In summary, a simple homogeneous fluorescent biosensor for the detection of Dam MTase activity by employing the $MoS_2$ nanosheets as the energy acceptor in fluorescence quenching has been developed. Good sensitivity and selectivity were observed. The fluorescence "turn on" strategy greatly improved the suitability of the biosensor in MTase activity assessments. The simplicity, high sensitivity, and the usage of newly emerging $MoS_2$ nanosheets are some of the interesting features for the development of a simple, robust, low cost, and highly sensitive MTase activity biosensor for uses in decentralized settings. In addition, the successful application of the $MoS_2$ nanosheets in MTase activity quantification not only made the biological applications of the new emerging 2D IGAs a step further, but also provided a potentially useful platform for sensitive Dam MTase activity monitoring and for MTase inhibitor screening in biomedical research and clinical diagnosis.

# Chapter 7. DAN methyltransferase activity detection using a personal glucose meter

## 7.1 Introduction

As reviewed previously, the reported DNA MTase activity monitoring methods depend on either radioisotope labeled substrates, demanding expensive equipment, or/and trained operators, which limit the MTase activity analysis to centralized facilities. Therefore, there is an unmet need for developing simple methods to detect MTase activity at point-of-care.

Due to its miniaturization, low cost, ease of operation, and reliable quantitative results, personal glucose meter (PGM) is one of the most successful portable devices for point-of-care testing.[29] The recent integration of the PGM into mobile phones can further facilitate its even wider use by the public.[228] However, the PGM can only detect glucose depending on the excellent specificity of the GOx or GDH incorporated into the commercially available the PGM. The pioneering efforts on expanding the PGM applications for non-glucose targets were reported by Lu's group.[229-232] In their studies, an invertase,[233] which catalyzes the hydrolysis of sucrose to glucose and fructose, was conjugated with various functional DNAs such as DNAzymes, aptamers and aptazymes. Thus, the use of DNA-invertase conjugates linked glucose detection to the monitoring of other targets, and the concentration of produced glucose was used to quantify the non-glucose targets of interest. Later, following the DNA-invertase conjugation strategy, other researchers reported the PGM-based sensing platforms for DNA,[234-236] platelet-derived growth factor-BB,[237] and telomerase activity[238]. Besides, several sandwich-type

immunoassays that used invertase produced glucose as a signal producer were reported for various targets such as cancer biomarkers,[239, 240] pathogenic bacteria,[241] and transcription factors.[242] In addition, the detection of copper (II) ions and histidine were realized by combining the PGM with click chemistry.[243, 244] It is worth to note that, in addition to invertase, glucoamylase[245] and galactosidase[246] were also utilized to adapt the PGM for non-glucose target analysis. Furthermore, glucose was directly encapsulated into mesoporous materials, the target induced cargo release of glucose which indicates the presence of targets was then detected by the PGM.[247-249]

To the best of our knowledge, no DNA MTase activity biosensors using the PGM as signal readout has been reported up to date. In this work, we proposed to expand the use of the PGM for MTase activity detection by coupling with the methylation sensitive restriction endonuclease. M.SssI and HpaII were chosen as MTase and endonuclease model to demonstrate the working principle of the proposed biosensor. Streptavidin coated magnetic beads were employed to immobilize invertase conjugated MTase substrate DNA and facilitate ease separation. After the methylation/cleavage reaction, the remaining invertase-DNA conjugates on the magnetic beads catalyzed the hydrolysis of sucrose. The final readout from the PGM could quantify the activity of MTase. This simple, robust, and sensitive M.SssI MTase activity biosensor may be a potential candidate for point-of-care diagnosis.

## 7.2 Experimental

### 7.2.1 Reagents and apparatus

M.SssI CpG MTase (M.SssI MTase) supplied with 10× NEBuffer 2, restriction endonuclease HpaII supplied with 10× CutSmart buffer, HaeIII MTase, AluI MTase, Dam MTase, and SAM were purchased from New England Biolabs (Ipswich, MA). Streptavidin-coated magnetic beads (2.8 μm diameter) were purchased from Invitrogen (Oslo, Norway). Grade VII invertase from baker's yeast (S. cerevisiae) and 4-(N-Maleimidomethyl) cyclohexane-1-carboxylic acid 3-sulfo-N-hydroxysuccinimide ester sodium salt (sulfo-SMCC) were from Sigma-Aldrich (St. Louis, MO, USA). Tris (2-carboxyethyl) phosphine hydrochloride (TCEP) and sucrose were obtained from Alfa Aesar (Lancashire, England). All other chemicals of certified analytical grade were used without further purification. All solutions were prepared with ultrapure water (18.3 MΩ·cm). Oligonucleotides used in this work were custom-made by 1$^{st}$ Base Pte Ltd. (Singapore). The sequences of the oligonucleotides were as follows: oligonucleotide 1 (oligo 1), 5'-/5ThioMC6-D/AAA AAA AAA ATC TTG ACA TAA ATA CCG GAA TCT AAC ATT AGT TC-3' and oligonucleotide 2 (oligo 2), 5'-/5Biosg/AAA AAA AAA GAA CTA ATG TTA GAT TCC GGT ATT TAT GTC AAG AT-3'. The two oligonucleotides were dissolved in ultrapure water to 1.0 mM and stored at −20 °C.

The glucose meter (TRUEresult®) and test strips were from Nipro Diagnostics, Inc. The detection range of the glucose meter is 1.1-33.3 mM. Amicon 3k and Amicon 100 K centrifuge filters were from ThermoScientific.

Gel electrophoresis was performed on a Bio-Rad Mini-Protean electrophoresis system.

### 7.2.2 Preparation and characterization of DNA-invertase conjugates

The use of sulfo-SMCC as the linker for the conjugation of thiol-modified DNA (oligo 1) with invertase was carried out according to a published procedure with some minor modifications.[187] To 40 μL of 1.0 mM oligo 1 in ultrapure water, 3 μL of 1.0 M pH 5.5 PBS buffer and 3 μL of 30 mM TCEP in ultrapure water were added, and the mixture was kept at room temperature for an hour to break the disulfide bonds. The reduced oligo 1 was then washed three times with buffer A (0.1 M NaCl, 0.1 M sodium phosphate buffer, pH 7.3) using Amicon 3K. The mixture containing 400 μL of 20 mg/mL invertase in Buffer A and 1 mg of sulfo-SMCC, was placed on the shaker for 1 hour after vortexing for 5 minutes. Excess insoluble sulfo-SMCC was removed by centrifugation and the solution was mixed with the reduced oligo 1 and kept at room temperature for 72 hours. To remove unreacted thiol-DNA, this solution was washed three times by Amicon 100 K with Buffer A.

**Table 7.1.** SDS-PAGE gel preparation.

| Components | Resolving gel | Stacking gel |
|---|---|---|
| 30% acrylamide/bisacrylamide | 1.35 mL | 350 μL |
| 1.5 M Tris-HCl, pH 8.8 | 1.25 mL | - |
| 0.5 M Tris-HCl, pH 6.8 | - | 625 μL |
| 10% SDS | 50 μL | 25 μL |
| 10% ammonium persulfate | 30 μL | 13 μL |
| TEMED | 6.5 μL | 5 μL |
| Deionized water | 2.313 mL | 1.477 mL |

The oligo 1-invertase conjugates were characterized by 8% SDS-polyacrylamide gel electrophoresis (SDS-PAGE). The components of the resolving gel and the stacking gel are summarized in Table 7.1. The samples were loaded after the completion of gels casting, and the gel electrophoresis was performed at a constant voltage of 200 V for 30 minutes. Finally the gel was stained by comassie brilliant blue staining solution.

### 7.2.3 Hybridization of oligo 2 and oligo 1-invertase conjugates

To 40 μL of 1.0 mM oligo 2, 1060 μL of Buffer A and 200 μL of oligo 1-invertase conjugates were added and mixed. The mixture was placed in a 38 °C water bath for 2.5 hours. Thereafter, the solution was purified by 100K filter with Buffer A. The resulting solution (ds-DNA-invertase) was made up to 200 μL with buffer A and stored at 4 °C for further use.

### 7.2.4 Immobilization of ds-DNA-invertase onto magnetic beads

100 μL of 10 mg/mL streptavidin coated MB were firstly washed twice with the 1×B&W buffer (1 M NaCl, 0.5 M EDTA, 5 mM Tris HCl, pH 7.4) recommended by the protocol from Invitrogen, then the magnetic beads were re-suspended in 200 μL buffer B. To immobilize the as-prepared ds-DNA-invertase onto the magnetic beads, 20 μL of the as-prepared ds-DNA-invertase were mixed together with the 200 μL magnetic bead suspension. The mixture was placed on a shaker for 20 minutes, allowing the ds-DNA-invertase to immobilize onto the magnetic beads through avidin-biotin interaction. After the immobilization, the magnetic bead-ds-DNA-invertase conjugates were

separated by magnet and washed with buffer B (0.1 M NaCl, 0.1 M sodium phosphate buffer, pH 7.3, 0.5% Tween-20).

### 7.2.5 Optimization

To optimize the digestion time of HpaII endonuclease, the magnetic bead-dsDNA-invertase conjugates obtained after the immobilization were re-suspended in 200 μL 1×CutSmart buffer containing 200 U/mL HpaII, after placing in the 38 °C water bath for 5, 15, 30, 60, 90, and 120 minutes, respectively, the magnetic beads were separated and washed with buffer B. The obtained magnetic beads were transferred into 10 μL of 1.0 M sucrose in buffer B, and placed on the shaker for 50 minutes. Finally, the produced glucose was detected by the PGM.

To optimize the methylation time of M.SssI MTase, the magnetic bead-dsDNA-invertase conjugates obtained after the immobilization were re-suspended in 200 μL 1×NEBuffer 2 containing 40 U/mL M.SssI MTase and 160 μM SAM. After placing on the shaker for 0.5, 1, 2, 3, and 5 hours, respectively, the magnetic beads were separated and washed with buffer B. And the obtained magnetic beads were treated with 200 U/mL HpaII for 1 hour, and then transferred to 10 μL 1.0 M sucrose.

### 7.2.6 Detection of M.SssI MTase activity using the PGM

The M.SssI activity detection procedure was conducted similarly with the methylation time optimization procedure, except for that the methylation time

was fixed at the optimal and different concentrations of M.SssI were introduced.

### 7.2.7 Selectivity study

The selectivity of the proposed M.SssI activity biosensor was investigated by using HaeIII, AluI, and Dam MTases as the interference enzymes. The procedure was similar to the M.SssI activity detection procedure, except for that interferant MTases replaced M.SssI in the selectivity study. All the MTases were fixed at 40 U/mL.

## 7.3 Results and discussion

### 7.3.1 Principle and feasibility of the portable M.SssI MTase activity biosensor

As illustrated in Figure 7.1, to adapt the PGM for M.SssI MTase activity sensing, invertase was conjugated with substrate DNA as the report probes. The DNA-invertase conjugates are immobilized onto streptavidin coated magnetic beads via the biotin-DNA capture probe. The duplex DNA segemnt is designed to contain the 5'-CCGG-3' sequence, which is methylated by M.SssI MTase. After the methylation, the subsequent treatment with HpaII endonuclease is blocked by the methylation sites, while the unmethylated duplex DNA along with invertase is cleaved off from the magnetic beads. Finally, the glucose produced from the remaining invertase catalyzed hydrolysis of sucrose is detected by the PGM. Thus, the PGM readout is directly associated with the methylation level produced by the MTase.

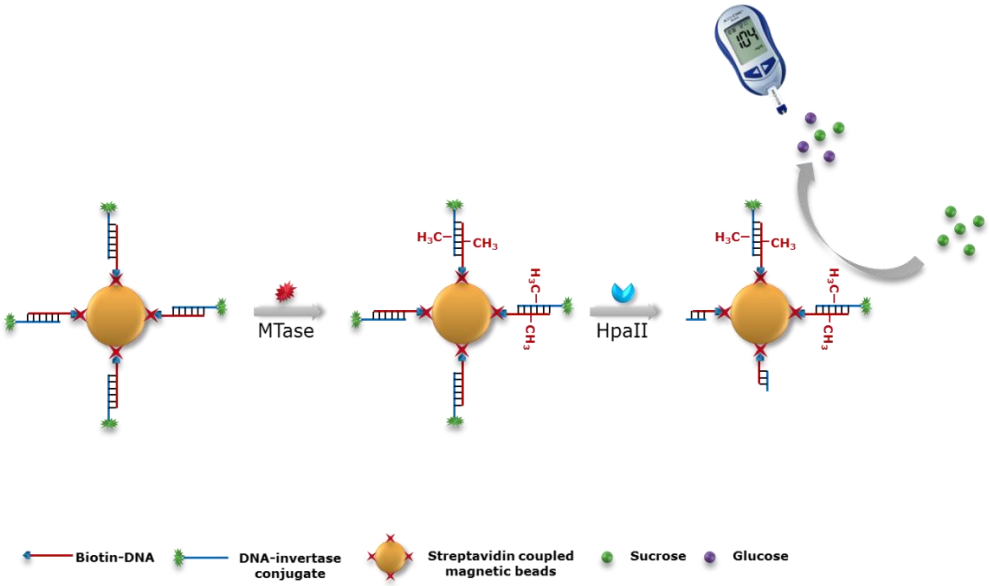


**Figure 7.1.** A schematic illustration of the principle for the detection of M.SssI MTase activity using the personal glucose meter.

The oligo 1-invertase conjugates was characterized by 8% SDS-PAGE, the protein staining gel image was shown in Figure 7.2. The migration of oligo 1-invertase conjugates in lane 3 is less than that in lane 1. This is due to the conjugation of the thiol-DNA with invertase, increasing its molecular size. Hence, the DNA-invertase conjugate band will move slower than the free invertase band in lane 1. Minimal difference was observed, in terms of band positions, between lanes 1 and 2. This was due to the fact that the oligo 1 not being conjugated with invertase in this mixture of invertase and oligo 1. These results confirmed that invertase has successfully been conjugated to oligo 1.

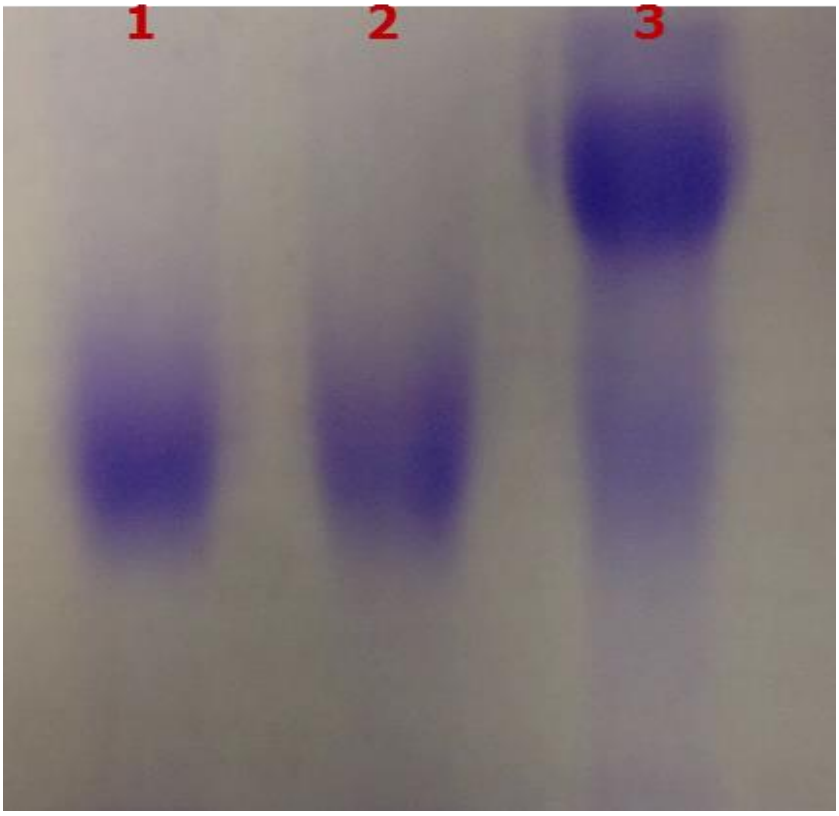


**Figure 7.2.** 8% SDS-PAGE characterization of oligo 1-invertase conjugate by protein staining. Lane 1: invertase, 2: oligo 1 mixed with invertase, 3: oligo 1-invertase conjugate.

The feasibility studies were carried out and the results are shown in Figure 7.3. In control 1, there was no methylation or digestion been carried out, the PGM signal showed "Hi", beyond the detection limit of the PGM. This suggested that the ds-DNA-invertase conjugates have been successfully captured onto the streptavidin coated magnetic beads and a large signal can be produced. For control 2, methylation was not carried out, but HpaII restriction digest was performed. The low signal indicated that 200 U/mL of Hpa II is enough to cleave off all invertase from unmethylated sites. On the other hand, Sample 1, upon methylation, showed a much larger reading than control 2, but less than that of control 1. This indicated that the methylation step does make effect, but not all ds-DNA have been methylated and thus have a lower signal

than that of control 1. This also showed that a larger or smaller M.SssI MTase concentration than 40 U/mL can be used in this study and the signal will still be within the detection limits. This study confirmed that the biosnesor proposed is feasible for the detection of M.SssI MTase activity.

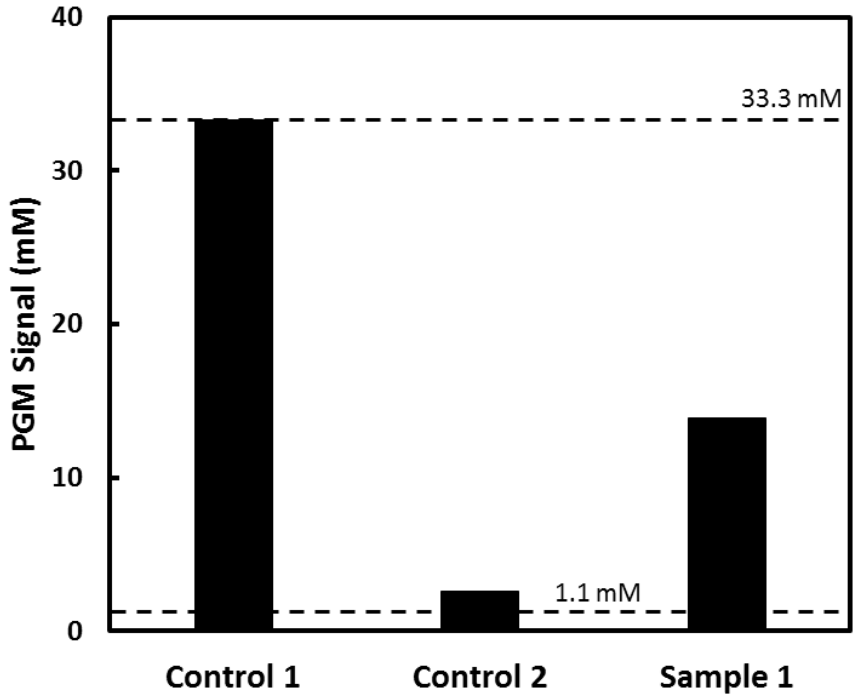


**Figure 7.3.** The PGM responses for control 1 (methylation: -, digestion: -), control 2 (methylation: -, digestion: +), and sample 1 (methylation: +, digestion: +).

### 7.3.2 Optimization

As the endonuclease digestion efficiency and the MTase methylation efficiency are closely associated with the final PGM readout, the digestion time and methylation time were optimized to achieve better results. Figure 7.4 shows the time dependence of the PGM signal when the magnetic bead-ds-DNA-invertase conjugates were treated with 200 U/mL HpaII. There was a sharp drop in the PGM signal between 5 and 30 minutes, before reaching a plateau after 60 minutes. This indicates that 60 minutes is the optimum duration for HpaII restriction digestion.

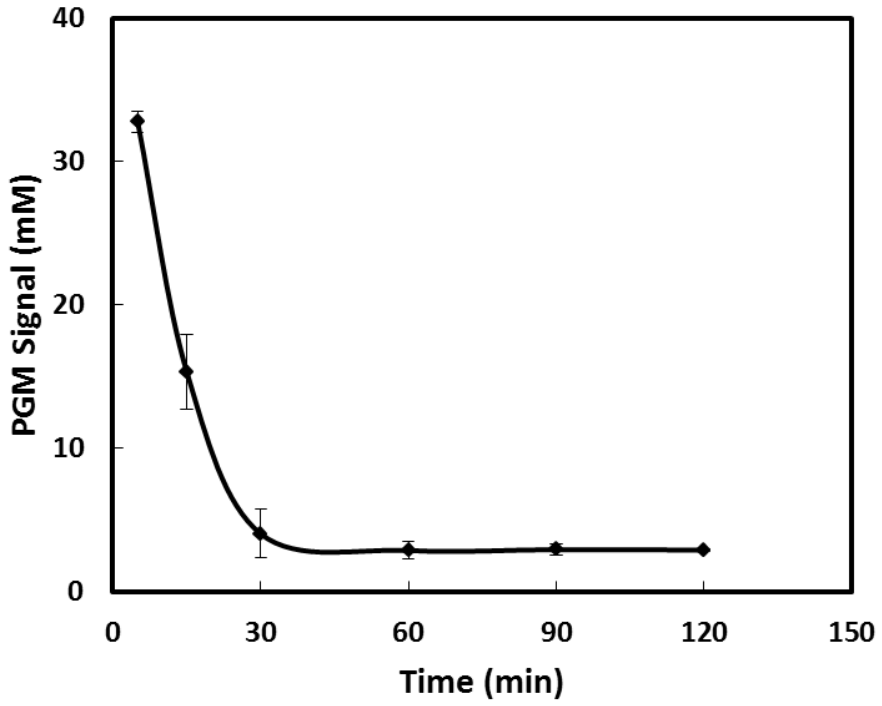


**Figure 7.4.** The effect of digestion time on the PGM signal.

Next, the HpaII digestion time was fixed at 1 hour, the methylation time was optimized. Figure 7.5 depicts the dependence of the PGM signal on the methylation time. The PGM signal increased with increasing methylation time, and reached a plateau after 3 hours. Hence, 3 hours was chosen as the optimal methylation time. Therefore, a period of 1 hour HpaII digestion and 3 hours of M.SssI MTase methylation time have been chosen as the optimal reaction conditions for the following studies.

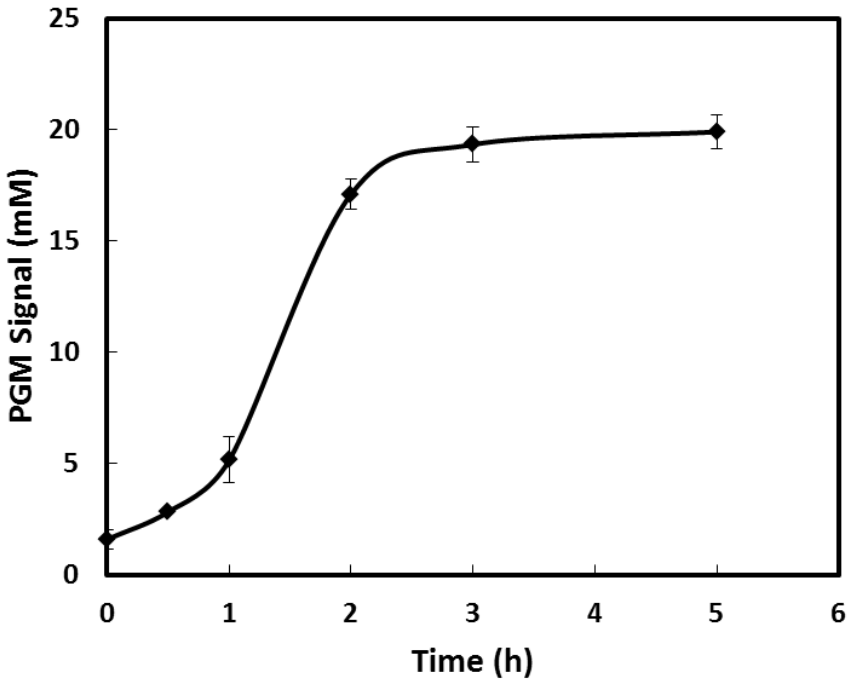


**Figure 7.5.** The effect of methylation time on the PGM signal.

### 7.3.3 Calibration study

Under the optimal experimental conditions, the relationship between the activity of M.SssI MTase and PGM signal was investigated. From Figure 7.6, it was observed that the PGM signal increases with increasing concentration of M.SssI MTase linearly. This is because, a higher M.SssI MTase concentration leads to a higher methylation activity and that this allows more strands of the DNA duplexes to be methylated, effectively blocking more recognition sites of HpaII restriction enzyme. This leads to more invertase moieties remain on the magnetic beads to produce a greater signal. The regression equation within the linear range of 0.5 – 80 U/mL is $y = 0.3863\ x + 1.9961$ ($R^2 = 0.9904$) where y is the PGM signal (mM) and x is the concentration of M.SssI MTase (U/mL). A detection limit of 0.37 U/mL, using the 3 times standard deviation of the blank approach, is obtained.

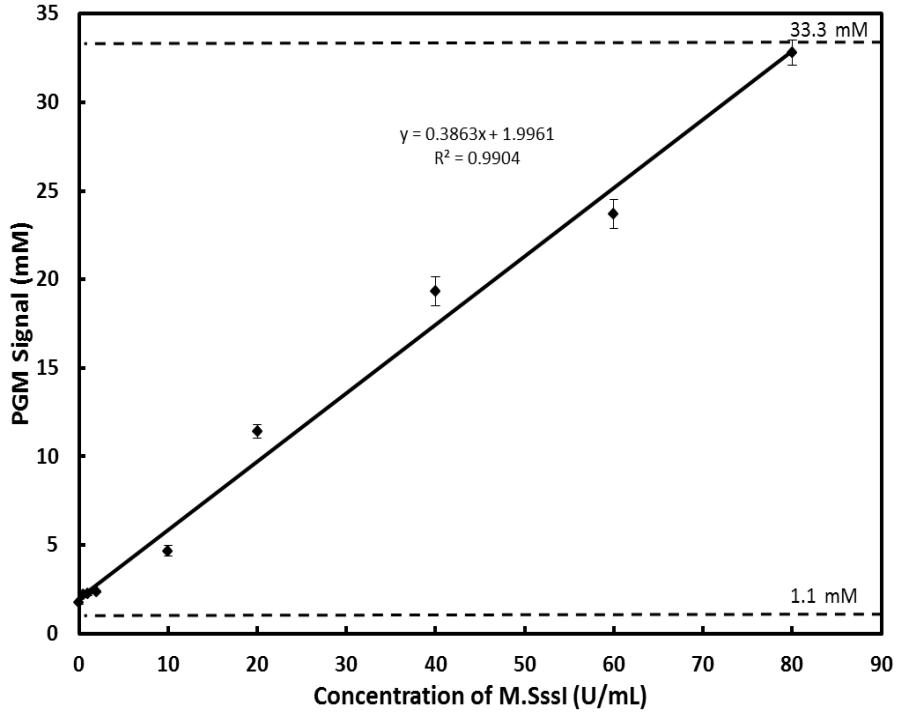


**Figure 7.6.** Calibration plot between the PGM signal and M.SssI MTase activity.

### 7.3.4 Selectivity study of the proposed M.SssI MTase activity biosensor

Other DNA MTases which act as interferants were added to test the selectivity of this iosensor. The MTases used were AluI, HaeIII, and Dam DNA MTases, at 40 U/mL each, the same concentration as M.SssI MTase. As seen in Figure 7.7, M.SssI MTase showed a much higher PGM signal than those of all other DNA MTases, while those DNA MTases showed similar readings which are close to the control sample (no DNA MTases added). This good selectivity is due to the unique recognition sequences of DNA MTases. Each of the interfering DNA MTases has a different recognition sequence from that of M.SssI MTase (5'-CG-3'). The recognition sequences of each of the interfering DNA MTases are 5'-GATC-3' (Dam), 5'-AGCT-3' (AluI), and 5'-GGCC-3' (HaeIII). Hence, since those DNA MTases have specific recognition sites which are not overlapping with M.SssI MTase, they do not

methylate at 5'-CCGG-3' sequence. As there is no methylation at this sequence, HpaII can recognize and digest more methylated substrate DNA-invertase conjugates and hence producing the low PGM signal.

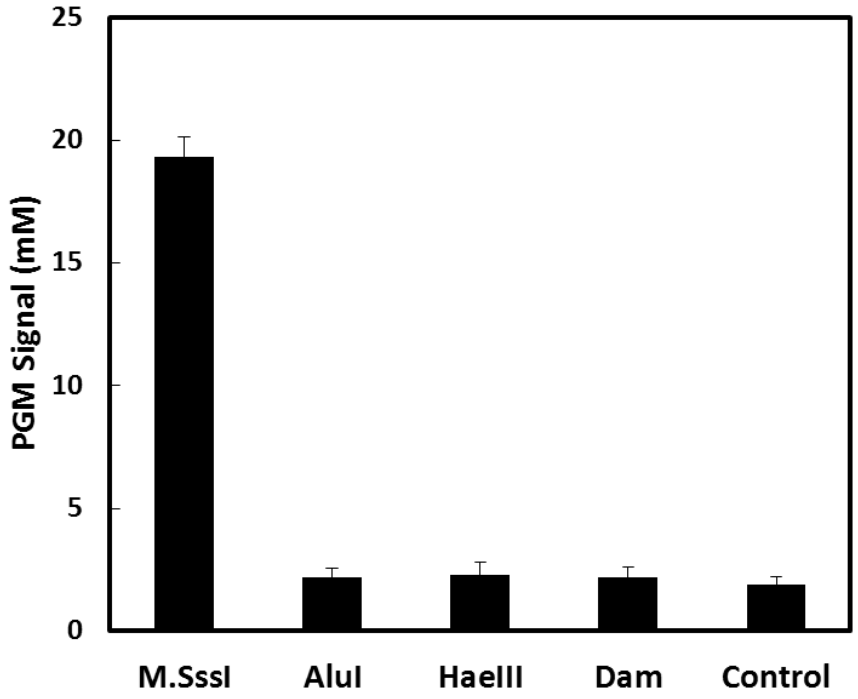


**Figure 7.7.** Selectivity of the proposed M.SssI MTase activity biosensor toward other MTases.

## 7.4 Conclusion

In conclusion, a portable and robust DNA MTase activity biosensor was successfully constructed by using a personal glucose meter as the signal readout. This biosensor showed good analytical performance of a wide linear range, a low detection limit, and excellent selectivity. Attributing to the pocket-size, low cost, ease of operation, and readily accessibility of the glucose meter, the proposed DNA MTase biosensor may act as flexible device for point-of-care applications.

# Chapter 8. Conclusion and future outlook

## 8.1 Conclusion

In summary, this thesis mainly focused on the design and construction of sensing platforms for glucose and DNA MTase activity detection. In terms of these two different kinds of targets, this thesis could be concluded in the following two sections, respectively.

### 8.1.1 Glucose biosensors

In Chapter 2, by incorporating $–SO_3H$ groups in the polymer backbones of Os-RP, the constructed Os-RP/GOx/GCE biosensor was demonstrated to possess marked improvement of the anti-interference ability. Results showed that the presence of 0.1 mM ascorbic acid and 0.2 mM uric acid contributed less than 5% to the overall analytical signal. The remarkable anti-interference ability was largely due to the strong electrostatic repulsion between the high density of sulfonic acid groups presented in Os-RP and ascorbic acid/uric acid under physiological conditions, which greatly suppress the access of these anionic species to the biosensor.

In Chapter 3, another approach of lowering the operating potential of the mediator was adopted to overcome the interference problem in amperometric glucose sensing. In this project, $[Ru(NH_3)_6]^{3+}$, which has already been reported to have a relatively low operating potential (0 mV, vs. Ag/AgCl) when used as the mediator in glucose sensing, was further tethered to PVPAA. The successful tethering of $[Ru(NH_3)_6]^{3+}$ to PVPAA via ligand exchange was

confirmed by FT-IR and UV-vis spectrometry. As expected, the redox potential of $[Ru(NH_3)_6]^{3+}$ was shifted from -0.14 V to -0.28 V after the formation of the Ru-RP. Next, using the Ru-RP as the mediator, an amperometic glucose biosensor was successfully constructed through the co-immobilization of the Ru-RP and glucose oxidase (GOx) on a glassy carbon electrode via a simple one-step chemical crosslinking process with glutaraldehyde. The glucose biosensor displayed excellent catalytic activity toward the oxidation of glucose with a current sensitivity of 24.3 μA $mM^{-1}$ $cm^{-2}$ and a linear correlation between the oxidation current and glucose concentration up to 10 mM. More importantly, owing to the low operating potential of −0.15 V (vs. Ag/AgCl), potential interferences from ascorbic acid, dopamine, uric acid, and acetaminophen were effectively alleviated.

Overall, these two types of smartly designed mediators, the Os-RP and Ru-RP, realize the interference-freely detection of glucose, which may give more options for mediators used for reliable glucose biosensing.

In Chapter 4, *lamellar ridge*-Au with nanograin size and submicrometer structural arrangement using blue scales of *Morph* butterfly as templates was prepared by an electroless deposition method. Unarchitectured gold (*flat*-Au) was also synthesized as a control using the flat wing membranes as templates under the same conditions. The morphology and components of the gold materials were characterized by SEM, XRD, XPS, and TGA. Both the architectured and unarchitectured gold samples were coated on glassy carbon electrodes with Nafion for amperometric detection of glucose in an alkaline medium, with the aim of exclusively demonstrating the architecture effect on electrochemical sensing behavior. Prominent performance in the detection of

glucose was achieved with the *lamellar ridge*-Au modified electrode with a wide linear range from 2 μM to 23 mM. The sensitivity was 5.8 times higher than that of the *flat*-Au modified electrode. Also, the detection limit was lowered by 3.7 times to 0.87 μM compared to its unarchitectured counterpart. The architecture assisting effect was attributed to the combined effect of increased surface area and efficient mass transport, which was demonstrated by finite element simulation. This work presents an exemplary strategy for optimizing nanograin assembled configurations and may provide a useful strategy for future structural design of efficient electrochemical biosensors by drawing inspiration from butterfly-scale architectures.

### 8.1.2 DNA MTase activity biosensors

In Chapter 5, a previously reported electrocatalytic oxidation of AA by a threading intercalator [N,N'-bis(3-propylimidazole)-1,4,5,8-naphthalene diimide (PIND) functionalized with electrocatalytic redox $Os(bpy)_2Cl^+$ moieties (PIND-Os)] was employed as the signal generator and amplifier for DNA MTase activity detection. PIND-Os specifically inserts itself between base pairs of ds-DNA and catalyzes the electrooxidation of AA at ~0.22 V owing to the improvement in the reversibility of the electron transfer from AA to the substrate electrode. This MTase biosensor was constructed by immobilizing the substrate ds-DNA of M.SssI onto a gold electrode and the defective sites of the ds-DNA layer were blocked by MCH. Treatments with MTase/endonuclease resulted in the methylation related retaining of ds-DNA onto the electrode surface. It was found that each step of modification successfully proceeded through the EIS and DPV characterizations. The

remaining amount of ds-DNA, which reflected the methylation level, determined the amount of PIND-Os and the final AA electrocatalytic current. As a result of the catalytic reaction, a high current sensitivity of 0.046 μA mL $U^{-1}$ was achieved for M.SssI activity detection. In addition, it was demonstrated that this M.SssI activity biosensor exhibited absolute selectivity due to the specific sequence recognition. Finally, the inhibitor screening ability of this biosensor was demonstrated by using 5-Aza and 5-Aza-dC as the inhibitor models.

In Chapter 6, depending on the similar DNA MTase coupled methylation sensitive endonuclease strategy described in Chapter 5, a simple and robust fluorometric Dam MTase activity biosensor was constructed. Firstly, $MoS_2$ nanosheets were successfully prepared through a mixed solvent assisted exfoliation method, and characterized by AFM and UV-vis spectrometry to confirm its morphology and the concentration of their suspension. Thereafter, the fluorescence quenching of FAM-labeled Dam MTase DNA substrate by the $MoS_2$ nanosheets was studied in detail (e.g. quenching mechanism, experimental conditions). The $MoS_2$ nanosheeets were confirmed to be an effective quencher for fluorometric Dam MTase activity detection. Finally, the analytical performance of this biosensor was evaluated. It was found that the linear range was from 0.2-20 U/mL, and the detection limit was estimated to be 0.14 U/mL. The selectivity and inhibitor screening ability were demonstrated as well.

Lastly, in Chapter 7, a portable M.SssI MTase activity biosensor was developed by using a personal glucose meter as the signal readout. Similar MTase/endonuclease couple employed in the last two MTase activity

biosensors was adopted. Invertase, which acts as the signal producer, was conjugated with the substrate DNA through a sulfo-SMCC chemical crosslinker. Streptavidin coated magnetic beads were used for the substrate DNA immobilization and for the separation after the methylation/cleavage step. Finally, the produced glucose in the invertase catalyzed hydrolysis of sucrose was monitored by the PGM. This simple, robust, and portable MTase activity biosensor showed good analytical performance as well.

## 8.2 Future outlook

In this dissertation, two types of mediated enzymatic glucose biosensors mainly aim at the improvement of anti-interference capability. Although the interference-free detection of glucose is remarkably realized, some other capabilities like the linear range, long-term storage stability, anti-biofouling capability of the sensing membrane are not up to the mark when compared with some other reported glucose biosensors. Further efforts are required to improve these aspects in order to apply them in real blood sample analysis. The third glucose biosensor based on the architectured gold is a nonenzymatic type of electrochemical glucose biosensor, its operation potential is relative high. Even though a wide linear range, high sensitivity, and a low LOD were achieved, the intrinsic drawbacks of the nonenzymatic methods, such as poor selectivity, may hinder the wide application of this glucose biosensor. Thus, further improvements are also needed.

The DNA MTase activity biosensors proposed in this dissertation targeted at M.SssI and Dam MTase that are separated from bacteria. Although they are

well established and may provide effective approaches for drug (e.g. MTase inhibitors) discovery, they are all restricted to the proof-of-concept study and no real sample analysis is performed. In fact, if the substrate DNA in these studies could be replaced by the hemi-methylated DNAs, these proposed biosensors could in principle be adapted to detect human MTase (Dnmt1) activity. As the work conducted by Barton's group,[250, 251] it will be of great significance if experiments based on human DNA MTases can be carried out in the future. Apart from the target MTase, another kind of endonuclease is involved in these proposed biosensors. So far, this kind of multiple-enzyme strategy is also the most popular one adopted for MTase activity detection. However, as we all know, enzymes are usually fragile, sensitive to environment, and/or unsuitable for long-term storage. Thus, further efforts to minimize the number of enzymes employed for the MTase activity detection will be of revolutionary significance.

# References


1. L. Guariguata, D. R. Whiting, I. Hambleton, J. Beagley, U. Linnenkamp and J. E. Shaw, *Diabetes Res. Clin. Practic.* 2014, **103**, 137-149.
2. K. G. M. M. Alberti and P. Z. Zimmet, *Diabet. Med*. 1998, **7**, 539-553.
3. X. Cheng and R. J. Roberts, *Nucleic Acids Res.* 2001, **29**, 3784-3795.
4. K. D. Robertson, E. Uzvolgyi, G. N. Liang, C. Talmadge, J. Sumegi, F. A. Gonzales and P. A. Jones, *Nucleic Acids Res.* 1999, **27**, 2291-2298.
5. B. F. Chen and W. Y. Chan, *Epigenetics* 2014, **9**, 669-677.
6. R. Monošík, M. Streďanský and E. Šturdík, *Acta Chimica Slovaca* 2012, **5**.
7. M. Zourob, *Recognition receptors in biosensors*, Springer, New York ; London, 2010.
8. M. Badihi-Mossberg, V. Buchner and J. Rishpon, *Electroanalysis* 2007, **19**, 2015-2028.
9. A. K. Wanekaya, W. Chen and A. Mulchandani, *J. Environ. Monit.* 2008, **10**, 703-712.
10. J. S. Van Dyk and B. Pletschke, *Chemosphere* 2011, **82**, 291-307.
11. N. Verma and M. Singh, *BioMetals* 2005, **18**, 121-129.
12. M. Nayak, A. Kotian, S. Marathe and D. Chakravortty, *Biosens. Bioelectron.* 2009, **25**, 661-667.
13. E. Eltzov, V. Pavluchkov, M. Burstin and R. S. Marks, *Sensor. Actuat. B-Chem.* 2011, **155**, 859-867.
14. L. A. Terry, S. F. White and L. J. Tigwell, *J. Agric. Food Chem*. 2005, **53**, 1309-1316.

15. R. G. Smith, N. D'Souza and S. Nicklin, *Analyst* 2008, **133**, 571-584.

16. J. J. Gooding, *Anal. Chim. Acta* 2006, **559**, 137-151.

17. P. D'Orazio, *Clin. Chim. Acta* 2011, **412**, 1749-1761.

18. J. Wang, *Chem. Rev*. 2008, **108**, 814-825.

19. M. Mascini and S. Tombelli, *Biomarkers* 2008, **13**, 637-657.

20. D. R. Thévenot, K. Toth, R. A. Durst and G. S. Wilson, *Biosens. Bioelectron.* 2001, **16**, 121-131.

21. M. N. Velasco-Garcia, *Semin. Cell Dev. Biol.* 2009, **20**, 27-33.

22. K. Ramanathan and B. Danielsson, *Biosens. Bioelectron.* 2001, **16**, 417-423.

23. K. A. Marx, *Biomacromolecules* 2003, **4**, 1099-1120.

24. N. V. Lavrik, M. J. Sepaniak and P. G. Datskos, *Rev. Sci. Instrum.* 2004, **75**, 2229.

25. V. Scognamiglio, *Biosens. Bioelectron.* 2013, **47**, 12-25.

26. A. American Diabetes, *Diabetes Care* 2013, **36 Suppl 1**, S67-74.

27. D. M. Nathan, *N. Engl. J. Med*. 1993, **328**, 1676-1685.

28. N. Poolsup, N. Suksomboon and S. Rattanasookchit, *Diabetes Technol. Ther*. 2009, **11**, 775-784.

29. J. Wang, *Electroanalysis* 2001, **13**, 983-988.

30. A. Heller and B. Feldman, *Chem. Rev.* 2008, **108**, 2482-1505.

31. A. Heller and B. Feldman, *Acc. Chem. Res*. 2010, **43**, 963-973.

32. R. J. McNichols and G. L. Coté, *J. Biomed. Optics* 2000, **5**, 5-16.

33. J. C. Pickup, F. Hussain, N. D. Evans, O. J. Rolinski and D. J. Birch, *Biosens. Bioelectron.* 2005, **20**, 2555-2565.

34. M. M. Rahman, A. J. Ahammad, J. H. Jin, S. J. Ahn and J. J. Lee, *Sensors* 2010, **10**, 4855-4886.

35. Z. Zhu, L. Garcia-Gancedo, A. J. Flewitt, H. Xie, F. Moussy and W. I. Milne, *Sensors* 2012, **12**, 5996-6022.

36. L. C. Clark and C. Lyons, *Ann. N. Y. Acad. Sci*. 1962, **102**, 29-45.

37. E. Kosela, H. Elzanowska and W. Kutner, *Anal. Bioanal. Chem.* 2002, **373**, 724-734.

38. H. Kang, R. Liu, H. Sun, J. Zhen, Q. Li and Y. Huang, *J. Phys. Chem. B*, 2012, **116**, 55-62.

39. M. E. Ghica and C. M. A. Brett, *Anal. Chim. Acta* 2005, **532**, 145-151.

40. B. K. Sohn, B. W. Cho, C. S. Kim and D. H. Kwon, *Sensor. Actuat. B-Chem.* 1997, **41**, 7-11.

41. A. Fulati, S. M. U. Ali, M. H. Asif, N. u. H. Alvi, M. Willander, C. Brännmark, P. Strålfors, S. I. Börjesson, F. Elinder and B. Danielsson, *Sensor. Actuat. B- Chem.* 2010, **150**, 673-680.

42. R. K. Shervedani, A. H. Mehrjardi and N. Zamiri, *Bioelectrochemistry* 2006, **69**, 201-208.

43. D. Zane, G. B. Appetecchi, C. Bianchini, S. Passerini and A. Curulli, *Electroanalysis* 2011, **23**, 1134-1141.

44. E. J. D'Costa, I. J. Higgins and A. P. F. Turner, *Biosensors* 1986, **2**, 71-87.

45. R. Wilson and A. P. F. Turner, *Biosens. Bioelectron.* 1992, **7**, 165-185.

46. S. B. Bankar, M. V. Bule, R. S. Singhal and L. Ananthanarayan, *Biotechnol. Adv.* 2009, **27**, 489-501.

47. S. J. Updike and G. P. Hicks, *Nature* 1967, **214**, 986-988.

48. G. G. Guilbault and G. J. Lubrano, *Anal. Chim. Acta* 1973, **64**, 439-455.

49. M. Shichiri, R. Kawamori, Y. Yamasaki, N. Hakui and H. Abe, *Lancet* 1982, **2**, 1129-1131.

50. A. E. G. Cass, G. Davis, G. D. Francis, H. A. O. Hill, W. J. Aston, I. J. Higgins, E. V. Plotkin, L. D. Scott and A. P. F. Turner, *Anal. Chem.* 1984, **56**, 667-671.

51. Y. Degani and A. Heller, *J. Phys. Chem*. 1987, **91**, 1285-1289.

52. Y. Degani and A. Heller, *J. Am. Chem. Soc.* 1988, **110**, 2615-2610.

53. C. Kurzawa, A. Hengstenberg and W. Schuhmann, *Anal. Chem.* 2002, **74**, 355-361.

54. R. L. Weinstein, S. L. Schwartz, R. L. Brazg, J. R. Bugler, T. A. Peyser and G. V. McGarraugh, *Diabetes Care*. 2007, **30**, 1125-1130.

55. A. Chaubey and B. D. Malhotra, *Biosens. Bioelectron.* 2002, **17**, 441-456.

56. Z. Q. Gao, F. Xie, M. Shariff, M. Arshad and J. Y. Ying, *Sensor. Actuat. B-Chem.* 2005, **111**, 339-346.

57. F. Ge, X. E. Zhang, Z. P. Zhang and X. M. Zhang, *Anal. Lett*. 1998, **31**, 383-394.

58. K. T. Lau, S. A. L. de Fortescu, L. J. Murphy and J. M. Slater, *Electroanalysis* 2003, **15**, 975-981.

59. A. Silber, N. Hampp and W. Schuhmann, *Biosens. Bioelectron.* 1996, **11**, 215-223.

60. B. A. Gregg and A. Heller, *Anal. Chem.* 1990, **62**, 258-263.

61. A. Riklin, E. Katz, I. Willner, A. Stocker and A. F. Bückmann, *Nature* 1995, **376**, 672-675.

62. Y. Lin, W. Yantasee and J. Wang, *Front. Biosci*. 2005, **10**, 492-505.

63. P. Palmisano, P. G. Zambonin, D. Centonze and M. Quinto, *Anal. Chem.* 2002, **74**, 5913-5918.

64. J. Rubio Retama, E. Lopez Cabarcos, D. Mecerreyes and B. Lopez-Ruiz, *Biosens. Bioelectron.* 2004, **20**, 1111-1117.

65. J. Wu and Y. Qu, *Anal. Bioanal. Chem.* 2006, **385**, 1330-1335.

66. F. Palmisano and P. G. Zambonin, *Anal. Chem.* 1993, **65**, 2690-2692.

67. L. J. Cartier, P. Leclerc, M. Pouliot, L. Nadeau, G. Turcotte and B. Fruteau-de-Laclos, *Clin. Chem*. 1998, **44**, 893-894.

68. T. Matsumoto, M. Furusawa, H. Fujiwara, Y. Matsumoto and N. Ito, *Sensor. Actuat. B-Chem.* 1998, **49**, 68-72.

69. D. Moatti-Sirat, V. Poitout, M. N. Gangnerau, Y. Zhang, Y. Hu, G. S. Wilson, F. Lemonnier, J. C. Klein and G. Reach, *Diabetologia* 1994, **37**, 610-616.

70. R. Vaidya, P. Atanasov and E. Wilkins, *Med. Eng. Phys*. 1995, **17**, 416-424.

71. C. Malitesta, F. Palmisano, L. Torsi and P. G. Zambonin, *Anal. Chem.* 1990, **62**, 2735-2740.

72. F. Palmisano, C. Malitesta, D. Centonze and P. G. Zambonin, *Anal. Chem.* 1995, **67**, 2207-2211.

73. S. K. Jung and G. S. Wilson, *Anal. Chem.* 1996, **68**, 591-596.

74. R. Sternberg, D. S. Bindra, G. S. Wilson and D. R. Thévenot, *Anal. Chem.* 1988, **60**, 2781-2786.

75. L. Jiang, H. Liu, J. Liu, Q. Yang and X. Cai, *J. Electroanal. Chem.* 2008, **619-620**, 11-16.

76. G. Cui, J. H. Yoo, B. W. Woo, S. S. Kim, G. S. Cha and H. Nam, *Talanta* 2001, **54**, 1105-1111.

77. R. Holliday, *Science* 1987, **238**, 163-170.

78. A. P. Feinberg and B. Tycko, *Nat. Rev. Cancer* 2004, **4**, 143-153.

79. R. Holliday and J. E. Pugh, *Science* 1975, **187**, 226-232.

80. A. D. Riggs, *Cytogenet. Cell Genet*. 1975, **14**, 9-25.

81. A. Jeltsch, *ChemBioChem.* 2002, **3**, 274-293.

82. G. G. Wilson and N. E. Murray, *Annu. Rev. Genet.* 1991, **25**, 585-627.

83. K. L. Tucker, *Neuron* 2001, **30**, 649-652.

84. E. Li, C. Beard and R. Jaenisch, *Nature* 1993, **366**, 362-365.

85. G. Csankovszki, A. Nagy and R. Jaenisch, *J. Cell Biol*. 2001, **153**, 773-784.

86. J. G. Herman, F. Latif, Y. Weng, M. I. Lerman, B. Zbar, S. Liu, D. Samid, D. R. Duan, J. R. Gnarra, W. M. Linehan and S. B. Baylin, *Proc. Natl. Acad. Sci. U.S.A.* 1994, **91**, 9700-9704.

87. M. Esteller, *N. Engl. J. Med*. 2008, **35**, 1148-1159.

88. K. D. Robertson, *Nat. Rev. Genet.* 2005, **6**, 597-610.

89. K. D. Robertson, *Oncogene* 2001, **20**, 3139-3155.

90. M. Ehrlich, *Oncogene* 2002, **21**, 5400-5413.

91. J. J. Issa, P. M. Vertino, J. Wu, S. Sazawal, P. Celano, B. D. Nelkin, S. R. Hamilton and S. B. Baylin, *J. Natl. Cancer Inst.* 1993, **85**, 1235-1240.

92. S. A. Belinsky, K. J. Nikula, S. B. Baylin and J. J. Issa, *Proc. Natl. Acad. Sci. U.S.A.* 1996, **93**, 4045-4050.

93. S. K. Patra, A. Patra, H. Zhao and R. Dahiya, *Mol. Carcinog*. 2002, **33**, 163-171.

94. Y. Kanai and S. Hirohashi, *Carcinogenesis* 2007, **28**, 2434-2442.

95. K. Mutze, R. Langer, F. Schumacher, K. Becker, K. Ott, A. Novotny, A. Hapfelmeier, H. Hofler and G. Keller, *Eur. J. Cancer* 2011, **47**, 1817-1825.

96. S. L. Samudio-Ruiz and L. G. Hudson, *Epigenetics* 2012, **7**, 216-224.

97. E. Boye, M. G. Marinus and A. Løbner-Olesen, *J. Bacteriol*. 1992, **174**, 1682-1685.

98. S. A. Belinsky, K. J. Nikula, S. B. Baylin and J. J. Issa, *Toxicol. Lett*. 1995, **82**, 335-340.

99. U. Hübscher, G. Pedrali-Noy, B. Knust-Kron, W. Doerfler and S. Spadari, *Anal. Biochem.* 1985, **150**, 442-448.

100. B. Y. Kim, O. S. Kwon, S. A. Joo, J. A. Park, K. Y. Heo, M. S. Kim and J. S. Ahn, *Anal. Biochem.* 2004, **326**, 21-24.

101. M. Roth and A. Jeltsch, *Biol. Chem*. 2000, **381**, 269-272.

102. T. Yokochi and K. D. Robertson, *Methods Mol. Biol.* 2004, **287**, 285-296.

103. M. E. Salyan, D. L. Pedicord, L. Bergeron, G. A. Mintier, L. Hunihan, K. Kuit, L. A. Balanda, B. J. Robertson, J. N. Feder, R. Westphal, P. A. Shipkova and Y. Blat, *Anal. Biochem.* 2006, **349**, 112-117.

104. J. Su, X. He, Y. Wang, K. Wang, Z. Chen and G. Yan, *Biosens. Bioelectron.* 2012, **36**, 123-128.

105. Z. Xu, M. Wang, T. Zhou, H. Yin and S. Ai, *Sensor. Actuat. B-Chem.* 2013, **178**, 412-417.

106. X. Jing, X. Cao, L. Wang, T. Lan, Y. Li and G. Xie, *Biosens. Bioelectron.* 2014, **58**, 40-47.

107. X. Wang, X. Liu, T. Hou, W. Li and F. Li, *Sensor. Actuat. B-Chem.* 2015, **208**, 575-580.

108. S. Liu, P. Wu, W. Li, H. Zhang and C. Cai, *Chem. Commun.* 2011, **47**, 2844-2846.

109. H. Yin, Z. Xu, M. Wang, X. Zhang and S. Ai, *Electrochim. Acta* 2013, **89**, 530-536.

110. G. L. Wang, L. Y. Zhou, H. Q. Luo and N. B. Li, *Anal. Chim. Acta* 2013, **768**, 76-81.

111. W. Li, P. Wu, H. Zhang and C. Cai, *Anal. Chem.* 2012, **84**, 7583-7590.

112. S. Baek, B. Y. Won, K. S. Park and H. G. Park, *Biosens. Bioelectron.* 2013, **49**, 542-546.

113. Q. Shen, L. Han, G. Fan, E. S. Abdel-Halim, L. Jiang and J. J. Zhu, *Biosens. Bioelectron.* 2015, **64**, 449-455.

114. H. Wu, S. Liu, J. Jiang, G. Shen and R. Yu, *Chem. Commun.* 2012, **48**, 6280-6282.

115. M. Wang, Z. Xu, L. Chen, H. Yin and S. Ai, *Anal. Chem.* 2012, **84**, 9072-9078.

116. H. Yin, Y. Zhou, Z. Xu, M. Wang and S. Ai, *Biosens. Bioelectron.* 2013, **49**, 39-45.

117. H. Yin, Y. Zhou, Z. Xu, L. Chen, D. Zhang and S. Ai, *Biosens. Bioelectron.* 2013, **41**, 492-497.

118. Z. Xu, H. Yin, L. Huo, Y. Zhou and S. Ai, *Sensor. Actuat. B-Chem.* 2014, **192**, 143-149.

119. Y. Zhou, Z. Xu, M. Wang, B. Sun, H. Yin and S. Ai, *Biosens. Bioelectron.* 2014, **53**, 263-267.

120. Y. H. Woo, P. T. Rajagopalan and S. J. Benkovic, *Anal. Biochem.* 2005, **340**, 336-340.

121. J. Song, C. Chen, J. Ren and X. QU, *ACS Nano* 2009, **3**, 1183-1189.

122. T. Liu, J. Zhao, D. Zhang and G. Li, *Anal. Chem.* 2010, **82**, 229-233.

123. Z. Wu, Z. K. Wu, H. Tang, L. J. Tang and J. H. Jiang, *Anal. Chem.* 2013, **85**, 4376-4383.

124. W. Li, Z. Liu, H. Lin, Z. Nie, J. Chen, X. Xu and S. Yao, *Anal. Chem.* 2010, **82**, 1935-1941.

125. C. Zhu, Y. Wen, H. Peng, Y. Long, Y. He, Q. Huang, D. Li and C. Fan, *Anal. Bioanal. Chem.* 2011, **399**, 3459-3464.

126. Y. Zhao, F. Chen, M. Lin and C. Fan, *Biosens. Bioelectron.* 2014, **54**, 565-570.

127. L. Schermelleh, F. Spada, H. P. Easwaran, K. Zolghadr, J. B. Margot, M. C. Cardoso and H. Leonhardt, *Nat. Methods* 2005, **2**, 751-756.

128. C. Frauer and H. Leonhardt, *Nucleic Acids Res.* 2009, **37**, e22.

129. J. Li, H. Yan, K. Wang, W. Tan and X. Zhou, *Anal. Chem.* 2007, **79**, 1050-1056.

130. R. J. Wood, J. C. McKelvie, M. D. Maynard-Smith and P. L. Roach, *Nucleic Acids Res.* 2010, **38**, e107.

131. T. Tian, H. Xiao, Y. Long, X. Zhang, S. Wang, X. Zhou, S. Liu and X. Zhou, *Chem. Commun.* 2012, **48**, 10031-10033.

132. X. H. Zhao, L. Gong, X. B. Zhang, B. Yang, T. Fu, R. Hu, W. Tan and R. Yu, *Anal. Chem.* 2013, **85**, 3614-3620.

133. Y. Zhao, F. Chen, Y. Wu, Y. Dong and C. Fan, *Biosens. Bioelectron.* 2013, **42**, 56-61.

134. F. Chen and Y. Zhao, *Analyst* 2013, **138**, 284-289.

135. X. W. Xing, F. Tang, J. Wu, J. M. Chu, Y. Q. Feng, X. Zhou and B. F. Yuan, *Anal. Chem.* 2014, **86**, 11269-11274.

136. J. Lee, Y. K. Kim and D. H. Min, *Anal. Chem.* 2011, **83**, 8906-8912.

137. L. Ji, Z. Cai, Y. Qian, P. Wu, H. Zhang and C. Cai, *Chem. Commun.* 2014, **0**, 10691-10694.

138. X. Ouyang, J. Liu, J. Li and R. Yang, *Chem. Commun.* 2012, **48**, 88-90.

139. G. L. Wang, H. Q. Luo and N. B. Li, *Analyst* 2014, **139**, 4572-4577.

140. P. A. Lay, A. M. Sargeson and H. Taube, *Inorg. Synth.* 1986, **24**, 291-306.

141. T. de Lumley-Woodyear, P. Rocca, J. Lindsay, D. Y., A. Freeman and A. Heller, *Anal. Chem.* 1995, **67**, 1332-1338.

142. Z. Gao, G. Binyamin, H. Kim, S. C. Barton, Y. Zhang and A. Heller, *Angew. Chem. Int. Ed.* 2002, **41**, 810-813.

143. A. J. Bard and L. R. Faulkner, *Electrochemical methods : fundamentals and applications*, Wiley, New York, 2001.

144. A. Heller, *Acc. Chem. Res*. 1990, **23**, 128-134.

145. N. Mano, F. Mao and A. Heller, *J. Electroanal. Chem.* 2005, **574**, 347-357.

146. A. Heller, *J. Phys. Chem*. 1992, **96**, 3579-3587.

147. B. N. Ames, R. Cathcart, E. Schwiers and P. Hochstein, *Proc. Natl. Acad. Sci. U.S.A.* 1981, **78**, 6858-6862.

148. Z. Gao and A. Ivaska, *Talanta* 1993, **40**, 399-403.

149. Z. Gao, B. Chen and M. Zi, *J. Electroanal. Chem*. 1994, **365**, 197-205.

150. T. Chen, K. A. Friedman, L. Lei and A. Heller, *Anal. Chem.* 2000, **72**, 3757-3763.

151. J. Fei, Y. Wu, X. Ji, J. Wang, S. Hu and Z. Gao, *Anal. Sci*. 2003, **19**, 1259-1263.

152. Z. L. Gui, J. W. Qian, Q. F. An, H. Xu and Q. Zhao, *Eur. Polym. J*. 2009, **45**, 1403-1411.

153. I. Willner, A. Lapidot and A. Riklin, *J. Am. Chem. Soc*. 1990, **112**, 6438-6439.

154. S. M. Mobin, B. J. Sanghavi, A. K. Srivastava, P. Mathur and G. K. Lahiri, *Anal. Chem.* 2010, **82**, 5983-5992.

155. B. J. Sanghavi, S. M. Mobin, P. Mathur, G. K. Lahiri and A. K. Srivastava, *Biosens. Bioelectron.* 2013, **39**, 124-132.

156. B. E. P. Swoboda and V. Massory, *J. Biol. Chem*. 1965, **240**, 2209-2215.

157. H. Deng, W. Shen and Z. Gao, *ChemPhysChem.* 2013, **14**, 2343-2347.

158. P.-C. Nien, T.-S. Tung and K.-C. Ho, *Electroanalysis* 2006, **18**, 1408-1415.

159. K. Yamamoto, H. Zeng, Y. Shen, M. M. Ahmed and T. Kato, *Talanta* 2005, **66**, 1175-1180.

160. D. Moatti-Sirat, G. Velho and G. Reach, *Biosens. Bioelectron.* 1992, **7**, 345-352.

161. M. Lindh, K. Lindgren, A. Carlström and P. Masson, *Clin. Chem*. 1982, **28**, 726.

162. I. Kaufmann-Raab, H. G. Jonen, E. Jähnchen, G. F. Kahl and U. Groth, *Clin. Chem*. 1976, **22**, 1729-1731.

163. Y. H. Won, K. Huh and L. A. Stanciu, *Biosens. Bioelectron.* 2011, **26**, 4514-4519.

164. W. A. Zhao, M. M. Ali, S. D. Aguirre, M. A. Brook and Y. F. Li, *Anal. Chem.* 2008, **80**, 8431-8437.

165. A. K. Singh, D. Senapati, S. G. Wang, J. Griffin, A. Neely, P. Candice, K. M. Naylor, B. Varisli, J. R. Kalluri and P. C. Ray, *Acs Nano* 2009, **3**, 1906-1912.

166. S. K. Dondapati, T. K. Sau, C. Hrelescu, T. A. Klar, F. D. Stefani and J. Feldmann, *Acs Nano* 2010, **4**, 6318-6322.

167. Y. Bai, W. W. Yang, Y. Sun and C. Q. Sun, *Sensor. Actuat. B-Chem.* 2008, **134**, 471-476.

168. L. Yang, Y. J. Zhang, M. Chu, W. F. Deng, Y. M. Tan, M. Ma, X. L. Su, Q. J. Xie and S. Z. Yao, *Biosens. Bioelectron.* 2014, **52**, 105-110.

169. Y. G. Zhou, S. Yang, Q. Y. Qian and X. H. Xia, *Electrochem. Commun*. 2009, **11**, 216-219.

170. Y. Li, Y. Y. Song, C. Yang and X. H. Xia, *Electrochem. Commun*. 2007, **9**, 981-988.

171. S. Park, H. Boo and T. D. Chung, *Anal. Chim. Acta* 2006, **556**, 46-57.

172. H. J. Qiu, L. Y. Xue, G. L. Ji, G. P. Zhou, X. R. Huang, Y. B. Qu and P. J. Gao, *Biosens. Bioelectron.* 2009, **24**, 3014-3018.

173. Y. E. Seidel, A. Schneider, Z. Jusys, B. Wickman, B. Kasemo and R. J. Behm, *Faraday Discuss*. 2008, **140**, 167-184.

174. A. Schneider, L. Colmenares, Y. E. Seidel, Z. Jusys, B. Wickman, B. Kasemo and R. J. Behm, *Phys. Chem. Chem. Phys*. 2008, **10**, 1931-1943.

175. X. M. Guo, H. Zhou, D. Zhang and T. X. Fan, *Rsc Adv*. 2014, **4**, 3748-3752.

176. N. L. Rosi and C. A. Mirkin, *Chem. Rev.* 2005, **105**, 1547-1562.

177. N. L. Rosi, C. S. Thaxton and C. A. Mirkin, *Angew. Chem. Int. Ed.* 2004, **43**, 5500-5503.

178. T. H. Galow, A. K. Boal and V. M. Rotello, *Adv. Mater.* 2000, **12**, 576-579.

179. F. W. Huo, A. K. R. Lytton-Jean and C. A. Mirkin, *Adv. Mater.* 2006, **18**, 2304-+.

180. X. Y. Xu, N. L. Rosi, Y. H. Wang, F. W. Huo and C. A. Mirkin, *J. Am. Chem. Soc.* 2006, **128**, 9286-9287.

181. S. Lou, X. M. Guo, T. X. Fan and D. Zhang, *Energ. Environ. Sci*. 2012, **5**, 9195-9216.

182. M. Sethi, G. Joung and M. R. Knecht, *Langmuir* 2009, **25**, 317-325.

183. B. Nikoobakht and M. A. El-Sayed, *Chem. Mater*. 2003, **15**, 1957-1962.

184. T. K. Sau and C. J. Murphy, *Langmuir* 2004, **20**, 6414-6420.

185. Z. Li, S. W. Chung, J. M. Nam, D. S. Ginger and C. A. Mirkin, *Angew. Chem. Int. Ed.* 2003, **42**, 2306-2309.

186. A. R. Parker and H. E. Townley, *Nat. Nanotechnol*. 2007, **2**, 347-353.

187. A. Sweeney, C. Jiggins and S. Johnsen, *Nature* 2003, **423**, 31-32.

188. P. Vukusic and I. Hooper, *Science* 2005, **310**, 1151-1151.

189. Y. W. Tan, J. J. Gu, X. N. Zang, W. Xu, K. C. Shi, L. H. Xu and D. Zhang, *Angew. Chem. Int. Ed.* 2011, **50**, 8307-8311.

190. D. Menshykau, I. Streeter and R. G. Compton, *J. Phys. Chem. C*. 2008, **112**, 14428-14438.

191. H. Tsunoyama, H. Sakurai, N. Ichikuni, Y. Negishi and T. Tsukuda, *Langmuir* 2004, **20**, 11293-11296.

192. D. V. Leff, L. Brandt and J. R. Heath, *Langmuir* 1996, **12**, 4723-4730.

193. S. Tanwar, J. A. A. Ho and E. Magi, *Talanta* 2013, **117**, 352-358.

194. H. Kita and H. Nakajima, *Electrochim. Acta*. 1986, **31**, 193-200.

195. L. Y. Chen, X. Y. Lang, T. Fujita and M. W. Chen, *Scripta Mater*. 2011, **65**, 17-20.

196. X. Y. Lang, H. Y. Fu, C. Hou, G. F. Han, P. Yang, Y. B. Liu and Q. Jiang, *Nat. Commun*. 2013, **4**, 2169.

197. D. Menshykau and R. G. Compton, *Electroanalysis* 2008, **20**, 2387-2394.

198. Y. N. Zhang, Y. B. Hu, G. S. Wilson, D. Moattisirat, V. Poitout and G. Reach, *Anal. Chem.* 1994, **66**, 1183-1188.

199. Q. Y. Yan, B. Peng, G. Su, B. E. Cohan, T. C. Major and M. E. Meyerhoff, *Anal. Chem.* 2011, **83**, 8341-8346.

200. Y. Peng, C. W. Wei, Y. N. Liu and J. Li, *Analyst* 2011, **136**, 4003-4007.

201. M. J. Sims, N. V. Rees, E. J. F. Dickinson and R. G. Compton, *Sensor. Actuat. B-Chem.* 2010, **144**, 153-158.

202. R. N. Goyal, V. K. Gupta and S. Chatterjee, *Sensor. Actuat. B-Chem.* 2010, **149**, 252-258.

203. R. S. Nicholson and I. Shain, *Anal. Chem.* 1964, **36**, 706-723.

204. I. Streeter, G. G. Wildgoose, L. D. Shao and R. G. Compton, *Sensor. Actuat. B-Chem.* 2008, **133**, 462-466.

205. N. C. Tansil, H. Xie, F. Xie and Z. Gao, *Anal. Chem.* 2006, **77**, 126-134.

206. W. Ma, Y. L. Ying, L. X. Qin, Z. Gu, H. Zhou, D. W. Li, T. C. Sutherland, H. Y. Chen and Y. T. Long, *Nat. Protoc.* 2013, **8**, 439-450.

207. B. Y. Chang and S. M. Park, *Annu. Rev. Anal. Chem.* 2010, **3**, 207-229.

208. F. Lyko and R. Brown, *J. Natl. Cancer Inst.* 2005, **97**, 1498-1506.

209. J. K. Christman, *Oncogene* 2002, **21**, 5483-5495.

210. Y. Wang, X. He, K. Wang, J. Su, Z. Chen, G. Yan and Y. Du, *Biosens. Bioelectron.* 2013, **41**, 238-243.

211. H. S. Matte, A. Gomathi, A. K. Manna, D. J. Late, R. Datta, S. K. Pati and C. N. Rao, *Angew. Chem. Int. Ed.* 2010, **49**, 4059-4062.

212. J. N. Coleman, M. Lotya, A. O'Neill, S. D. Bergin, P. J. King, U. Khan, K. Young, S. Gaucher, S. De, R. J. Smith, I. V. Shvets, S. K. Arora, G. Stanton, H. Y. Kim, K. Lee, G. T. Kim, G. S. Duesberg, T. Hallam, J. J. Boland, J. Wang, J. F. Donegan, J. C. Grunlan, G. Moriarty, A. Shmeliov, R. J. Nicholls, J. M. Perkins, E. M. Grieveson, K. Theuwissen, D. W. McComb, P. D. Nellist and V. Nicolosi, *Science* 2011, **331**, 568-571.

213. J. Xie, J. Zhang, S. Li, F. Grote, X. Zhang, H. Zhang, R. Wang, Y. Lei, B. Pan and Y. Xie, *J. Am. Chem. Soc.* 2013, **135**, 17881-17888.

214. K. Chang and W. Chen, *ACS Nano* 2011, **5**, 4720-4728.

215. K. Lee, R. Gatensby, N. McEvoy, T. Hallam and G. S. Duesberg, *Adv. Mater.* 2013, **25**, 6699-6702.

216. C. Zhu, Z. Zeng, H. Li, F. Li, C. Fan and H. Zhang, *J. Am. Chem. Soc.* 2013, **135**, 5998-6001.

217. Q. Xi, D. M. Zhou, Y. Y. Kan, J. Ge, Z. K. Wu, R. Q. Yu and J. H. Jiang, *Anal. Chem.* 2014, **86**, 1361-1365.

218. Y. Yuan, R. Li and Z. Liu, *Anal. Chem.* 2014, **86**, 3610-3615.

219. J. Z. Ou, A. F. Chrimes, Y. Wang, S. Y. Tang, M. S. Strano and K. Kalantar-zadeh, *Nano lett.* 2014, **14**, 857-863.

220. L. Wang, Y. Wang, J. I. Wong, T. Palacios, J. Kong and H. Y. Yang, *Small* 2014, **10**, 1101-1105.

221. H. Song, Y. Ni and S. Kokot, *Biosens. Bioelectron.* 2014, **56**, 137-143.

222. K. G. Zhou, N. N. Mao, H. X. Wang, Y. Peng and H. L. Zhang, *Angew. Chem. Int. Ed.* 2011, **50**, 10839-10842.

223. P. G. Moses, J. J. Mortensen, B. I. Lundqvist and J. K. Norskov, *The J. Chem. Phys.* 2009, **130**, 104709.

224. W. M. Heckl, D. P. E. Smith, G. Binnig, H. Klagges, T. W. Hänsch and J. Maddocks, *Proc. Natl. Acad. Sci. U.S.A.* 1991, **88**, 8003-8005.

225. D. M. Heithoff, *Science* 1999, **284**, 967-970.

226. C. G. Moertel, S. Frytak, R. G. Hahn, M. J. M.J. O'Connell, R. J. R.J. Reitemeier, J. J. Rubin, A. J. Schutt, L. H. Weiland, D. S. Childs, M. A. Holbrook, P. T. Lavin, E. Livstone, H. Spiro, A. Knowlton, M. Kalser, J. Barkin, H. Lessner, R. Mann-Kaplan, K. Ramming, H. O. J. Douglas,

P. Thomas, H. Nave, J. Bateman, J. Lokich, J. Brooks, J. Chaffey, J. M. Corson, N. Zamcheck and J. W. Novak, *Cancer* 1981, **48**, 1705-1710.

227. D. Salonga, K. D. Danenberg, M. Johnson, R. Metzger, S. Groshen, D. D. Tsao-Wei, H.-J. Lenz, C. G. Leichman, L. Leichman, R. B. Diasio and P. V. Danenberg, *Clin. Cancer Res*. 2000, **6**, 1322-1327.

228. A. E. Carroll, D. G. Marrero and S. M. Downs, *Diabetes Technol. Ther.* 2007, **9**, 158-164.

229. Y. Xiang and Y. Lu, *Nat. Chem*. 2011, **3**, 697-703.

230. Y. Xiang and Y. Lu, *Anal. Chem.* 2012, **84**, 1975-1980.

231. Y. Xiang and Y. Lu, *Anal. Chem.* 2012, **84**, 4174-4178.

232. Y. Xiang and Y. Lu, *Chem. Commun.* 2013, **49**, 585-587.

233. N. N. P. and J. O. Lampen, *Biochemistry* 1967, **6**, 468-475.

234. J. Xu, B. Jiang, J. Xie, Y. Xiang, R. Yuan and Y. Chai, *Chem. Commun.* 2012, **48**, 10733-10735.

235. X. T. Xu, K. Y. Liang and J. Y. Zeng, *Biosens. Bioelectron.* 2015, **64**, 671-675.

236. Q. Wang, H. Wang, X. Yang, K. Wang, F. Liu, Q. Zhao, P. Liu and R. Liu, *Chem. Commun.* 2014, **50**, 3824-3826.

237. X. Ma, Z. Chen, J. Zhou, W. Weng, O. Zheng, Z. Lin, L. Guo, B. Qiu and G. Chen, *Biosens. Bioelectron.* 2014, **55**, 412-416.

238. X. Zhu, H. Xu, R. Lin, G. Yang, Z. Lin and G. Chen, *Chem. Commun.* 2014, **50**, 7897-7899.

239. J. Su, J. Xu, Y. Chen, Y. Xiang, R. Yuan and Y. Chai, *Chem. Commun.* 2012, **48**, 6909-6911.

240. X. Fu, X. Feng, K. Xu and R. Huang, *Anal. Methods* 2014, **6**, 2233.

241. J. Joo, D. Kwon, H. H. Shin, K.-H. Park, H. J. Cha and S. Jeon, *Sensor. Actuat. B-Chem.* 2013, **188**, 1250-1254.

242. J. Chen, W. Wu and L. Zeng, *Anal. Methods* 2014, **6**, 4840.

243. J. Su, J. Xu, Y. Chen, Y. Xiang, R. Yuan and Y. Chai, *Biosens. Bioelectron.* 2013, **45**, 219-222.

244. J. Zhou, K. Xu, P. Zhou, O. Zheng, Z. Lin, L. Guo, B. Qiu and G. Chen, *Biosens. Bioelectron.* 2014, **51**, 386-390.

245. L. Yan, Z. Zhu, Y. Zou, Y. Huang, D. Liu, S. Jia, D. Xu, M. Wu, Y. Zhou, S. Zhou and C. J. Yang, *J. Am. Chem. Soc.* 2013, **135**, 3748-3751.

246. R. Chavali, N. S. K. Gunda, S. Naicker and S. K. Mitra, *Anal. Methods* 2014, **6**, 6223-6227.

247. L. Hou, C. Zhu, X. Wu, G. Chen and D. Tang, *Chem. Commun.* 2014, **50**, 1441-1443.

248. Z. Gao, D. Tang, M. Xu, G. Chen and H. Yang, *Chem. Commun.* 2014, **50**, 6256-6258.

249. Y. Wang, M. Lu, J. Zhu and S. Tian, *J. Mater. Chem*. 2014, **2**, 5874-5880.

250. N. B. Muren and J. K. Barton, *J. Am. Chem. Soc.* 2013, **135**, 16632-16640.

251. A. L. Furst, N. B. Muren, M. G. Hill and J. K. Barton, *Proc. Natl. Acad. Sci. U.S.A.* 2014, **111**, 14985-14989.